How to cite: Angew. Chem. Int. Ed. 2024, e202400350
doi.org/10.1002/anie.202400350

Macrocycles Hot Paper

Large Libraries of Structurally Diverse Macrocycles Suitable for Membrane Permeation

*Alexander L. Nielsen, Zsolt Bognar[+], Ganesh K. Mothukuri[+], Anne Zarda[+], Mischa Schüttel, Manuel L. Merz, Xinjian Ji, Edward J. Will, Monica Chinellato, Christian R. O. Bartling, Kristian Strømgaard, Laura Cendron, Alessandro Angelini, and Christian Heinis**

Abstract: Macrocycles offer an attractive format for drug development due to their good binding properties and potential to cross cell membranes. To efficiently identify macrocyclic ligands for new targets, methods for the synthesis and screening of large combinatorial libraries of small cyclic peptides were developed, many of them using thiol groups for efficient peptide macrocyclization. However, a weakness of these libraries is that invariant thiol-containing building blocks such as cysteine are used, resulting in a region that does not contribute to library diversity but increases molecule size. Herein, we synthesized a series of structurally diverse thiol-containing elements and used them for the combinatorial synthesis of a 2,688-member library of small, structurally diverse peptidic macrocycles with unprecedented skeletal complexity. We then used this library to discover potent thrombin and plasma kallikrein inhibitors, some also demonstrating favorable membrane permeability. X-ray structure analysis of macrocycle-target complexes showed that the size and shape of the newly developed thiol elements are key for binding. The strategy and library format presented in this work significantly enhance structural diversity by allowing combinatorial modifications to a previously invariant region of peptide macrocycles, which may be broadly applied in the development of membrane permeable therapeutics.

Introduction

Traditional drug discovery methods have focused predominantly on small molecules and monoclonal antibodies; however, small molecules often are not able to engage with challenging biological targets such as proteins with flat and featureless protein surfaces, and antibodies are not membrane permeable, limiting the applicability of both classes in certain therapeutic areas. A molecule format that could potentially fill this gap are the macrocycles.[1] These ring-shaped structures have a high conformational stability that allows strong and specific binding to challenging targets. Their slightly larger size compared to classical small molecules also allows for more molecular contact with the target, increasing the overall interaction surface area.[2] Despite their size that typically falls outside the range of conventional druglikeness models such as Lipinski's rule of five (Ro5),[3] some macrocycles are membrane permeable and thus can reach intracellular targets, and some can even be applied orally.[4] Overall, their favorable binding properties and ability to cross membrane barriers offer enormous opportunities for macrocycles in drug development, such as for generating inhibitors of the numerous intracellular protein-protein interactions that have been difficult to target with classical modalities.

Most existing macrocyclic drugs are based on natural products or derivatives thereof,[1,5,6] though for the majority of disease targets, natural ligands do not exist and must therefore be developed de novo using synthetic approaches. However, this discovery process is currently

[*] A. L. Nielsen, Z. Bognar,[+] G. K. Mothukuri,[+] A. Zarda,[+] M. Schüttel, M. L. Merz, X. Ji, E. J. Will, C. Heinis
Institute of Chemical Sciences and Engineering, School of Basic Sciences, École Polytechnique Fédérale de Lausanne (EPFL), CH-1015 Lausanne, Switzerland
E-mail: christian.heinis@epfl.ch

M. Chinellato, L. Cendron
Department of Biology, University of Padova, 35131 Padova, Italy

C. R. O. Bartling, K. Strømgaard
Center for Biopharmaceuticals and Department of Drug Design and Pharmacology, Faculty of Health and Medical Sciences, University of Copenhagen, Jagtvej 162, DK-2100 Copenhagen, Denmark

A. Angelini
Department of Molecular Sciences and Nanosystems, Ca' Foscari University of Venice, Via Torino 155, Venezia Mestre, Venice 30172, Italy

A. Angelini
European Centre for Living Technologies (ECLT), Ca' Bottacin, Dorsoduro 3911, Calle Crosera, Venice 30124, Italy

[+] These authors contributed equally to this work

hindered by a lack of techniques for developing and screening libraries of permeable macrocyclic ligands to new targets. Cyclic peptide libraries screened by phage or mRNA display usually yield peptides longer than ten amino acids that typically are not membrane permeable, though an exception to this was recently reported being a heavily *N*-methylated cyclic peptide ligand of KRAS that is cell active.[7,8] DNA-encoding technologies have been applied to generate and screen macrocycles libraries and are promising, but the synthesis of good quality libraries is not trivial due to the large number of coupling and deprotection steps in the presence of DNA.[9] In recent years, collections of purified macrocyclic compounds were produced and are offered for classical high-throughput screening but such libraries are rather small. The generation of larger collections comprising ten-thousands of macrocyclic compounds is hindered by typically low-yielding cyclization reactions that necessitate chromatographic purifications of individual macrocycles prior to screening. Consequently, creating large numbers of macrocycles is extremely time-consuming and resource-intensive. Overall, the difficulty of generating these libraries has drastically limited the potential applicability of macrocyclic compounds as therapeutics.

To address these existing issues with macrocyclic drug development, methods for generating and screening large libraries comprising tens of thousands of small peptide-based macrocycles were developed.[10–12] The approaches are based on screening crude products without purification, which is made possible by high-throughput solid-phase peptide synthesis (SPPS) of short random peptides that can be efficiently cyclized via two thiol end groups[13,14] and combinatorial late-stage diversification of the peptides using efficient and selective reactions.[11,12,15] However, a major limitation of current macrocycle libraries is that they have a structurally identical region that is required for macrocyclization (colored groups in Figure 1a and 1b), which compromises the structural diversity of the library and impairs the chances of identifying good binders. Not surprisingly, ligands identified from such libraries were all binding via the variable region and the constant groups are pointing away from the targets.[10–12] The same structural limitation is also found in disulfide- or thioether-cyclized peptide collections produced by cyclizing peptides via thiol groups, where the random amino acids are flanked by two constant cysteines.[16–19] In macrocycle libraries produced most recently in our lab, we cyclized peptides via the two thiol building blocks, 3-mercaptopropionic acid (Mpa; at the N-terminal end) and 2-mercaptoethylamine (Mea; also named cysteamine).[11,12] They contribute 89 and 76 Da to the molecular mass, respectively, which is substantial considering that this comprises 33 % of the molecule weight target of <500 Da for the best chances of membrane permeability. Hence, to increase the structural diversity of our macrocyclic libraries while remaining within the realm of likely permeable compounds, it is essential to diversify one or both of these constant elements.

Accordingly, in this work, we developed a synthetic strategy to efficiently produce short peptides with altered C-terminal thiol-containing elements (Figure 1a and 1b) to contribute to the development of macrocyclic ligands with a high probability of being membrane-permeable. Adding six structurally different C-terminal thiol-containing elements increases the skeletal diversity of the generated libraries 7-fold compared to existing libraries, all without increasing the size of the macrocycles that could negatively affect membrane permeability. Several of the developed thiol-containing elements lack an H-bond donor, reducing the overall polarity of the macrocycles for even increased chances of membrane permeability. Synthesis and screening of structurally diverse libraries of 2,688 macrocycles containing varied C-terminal thiols yielded nanomolar inhibitors of thrombin and plasma kallikrein, of which several exhibited high cellular permeabilities. The herein-developed approach for synthesizing small and structurally diverse macrocycles suitable for membrane permeation is broadly applicable and may offer a solution for developing therapeutics that can be orally applied and/or reach intracellular disease targets.

Results and Discussion

To synthesize large libraries of short peptides with altered C-terminal thiol-containing elements, we build on a recently established procedure in which peptides are synthesized by SPPS via a disulfide linker that can be reduced to release the peptides.[13,14] In this strategy, peptides are obtained in high purity without a purification step because we can first deprotect all side-chains on-resin using trifluoroacetic acid (TFA) and then release the washed and deprotected peptides from the resin via a disulfide reduction with 1,4-butanedithiol (BDT). BDT is volatile and can be removed under reduced pressure by rotary vacuum concentration (RVC) to afford only the remaining dithiol peptides in good crude purity (typically 80 % or higher). The C-terminal peptide building block used for this synthesis so far was the aminothiol group **1** (Mea; Figure 1a) that was conjugated to thiol-functionalized resin in a disulfide exchange reaction using pyridyldithioethylamine.[11,13,14] To generate peptides having different thiol-containing groups at the C-terminus (Figure 1b), our initial plan was to use analogous pyridylthiol-activated aminothiols, but we soon realized that their synthetic access was restricted due to the lack of commercial availability of structurally diverse aminothiols or high costs of the material. As an alternative approach, we conjugated different aminothiols onto thiol resin using aminothiols with phenylsulfone as leaving group that is equally suited for disulfide exchange reactions.[20–22] Such building blocks can easily be accessed by reacting thiosulfonates with halogenated *N*-Boc protected amines that are commercially available and cheap (Figure 2a). Importantly, the thiosulfonate precursors were separated from the excess thiosulfonate by extraction without the need of chromatographic purification, which enormously facili-

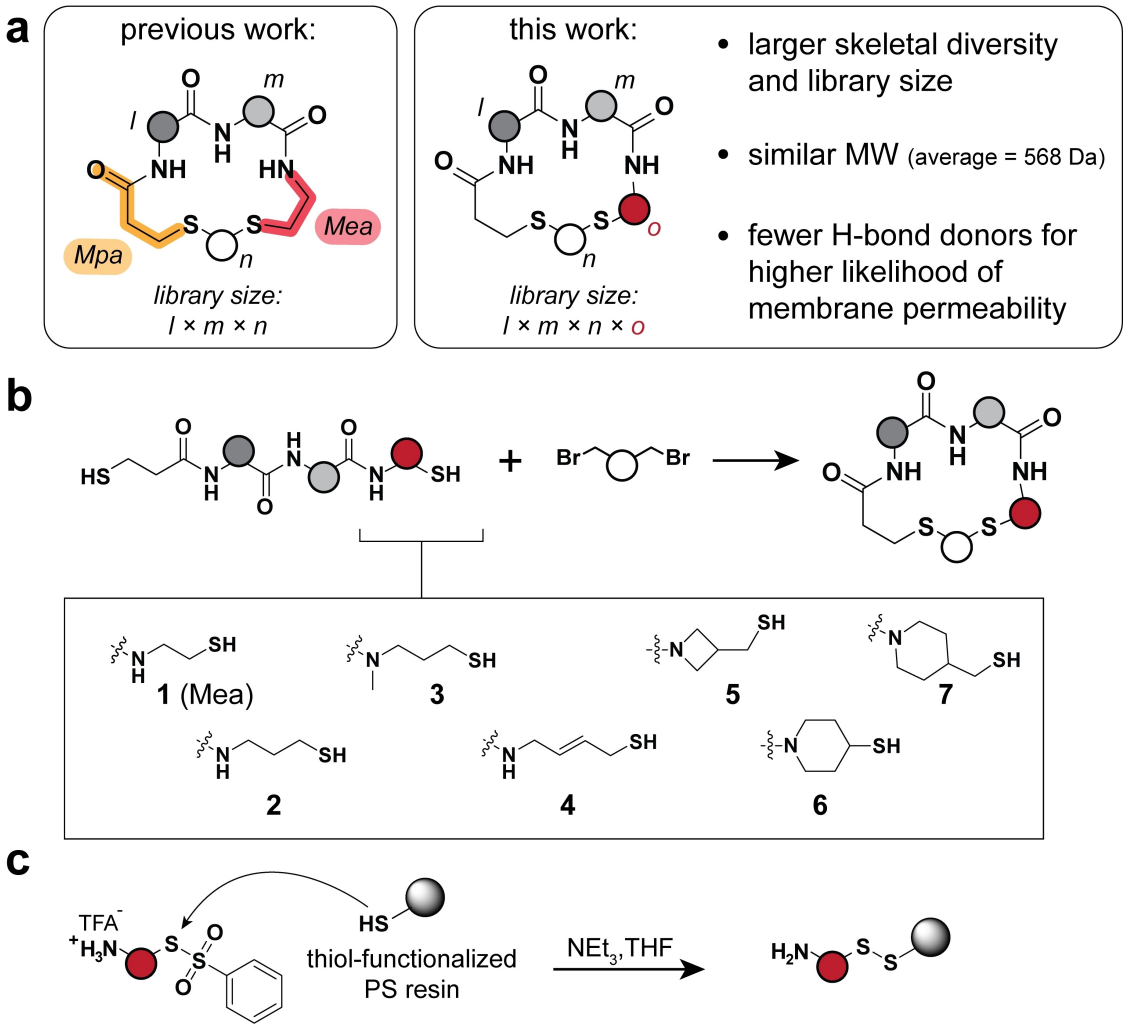

Figure 1. Macrocycle format and synthesis strategy. a) Macrocycle structures and building blocks that can be varied combinatorially to generate large libraries. Gray circles indicate amino acids, Mea and Mpa are the thiol-containing building blocks, and white circles are cyclization linkers. The red circle indicates the herein-developed varied C-terminal aminothiol element. In the chemical structures, standard amide bonds are shown for simplicity although some of them are *N*-methylated. b) Schematic representation of the thiol-thiol cyclization strategy. Chemical structures of diverse aminothiols are shown. c) Schematic representation of the linkage of aminothiols to resin via a disulfide bridge using thiosulfonate building blocks. PS = polystyrene.

tated the preparation of such reagents. Through nucleophilic substitution with sodium benzenethionosulfonate in DMF at 80 °C, we prepared six new *N*-Boc thiosulfonate building blocks on a gram-scale, ready for testing under library-synthesis conditions (Supporting Figure S1; see Supporting Information for the synthesis).

To immobilize the aminothiols **2**–**7** onto the solid support, we first performed Boc deprotection of the *N*-Boc thiosulfonate building blocks and then conjugated the crude mixtures to thiol-resin via a disulfide exchange reaction (Figure 1c and Supporting Scheme S1). To test the new aminothiol-functionalized resins, we synthesized on them the model peptide Mpa-Trp-Ala by SPPS and liberated the resulting dithiol peptides using the reducing agent BDT (Figure 2b). HPLC-MS analysis showed purities ranging between 85 and 98 % (Figure 2c and Supporting Figure S2), indicating the new aminothiol building blocks generate sufficiently pure crude products for the preparation and screening of macrocycle libraries.

To test whether target-specific macrocycles could be identified using the new diversification elements, we designed a library of 2,688 macrocycles that would be generated by cyclizing 384 dithiol peptides with seven bis-electrophilic linker reagents (Figure 3a). The 384 dithiol peptides were designed to each contain: one aminothiol derivative (**1**–**7**), an amino acid that binds the S1 pocket (chosen from three motifs known from literature to improve targeting to trypsin-like serine proteases),[11] a random amino acid (from 27 diverse α, β, γ, and *N*-methylated amino acids), and Mpa as the N-terminal thiol element (Figure 3a and 3b; see Supporting Table S1 for list of synthesized peptides). Primarily due to the variation of the aminothiol building blocks, this library contains a high number of diverse macrocycle backbones (2,107) that

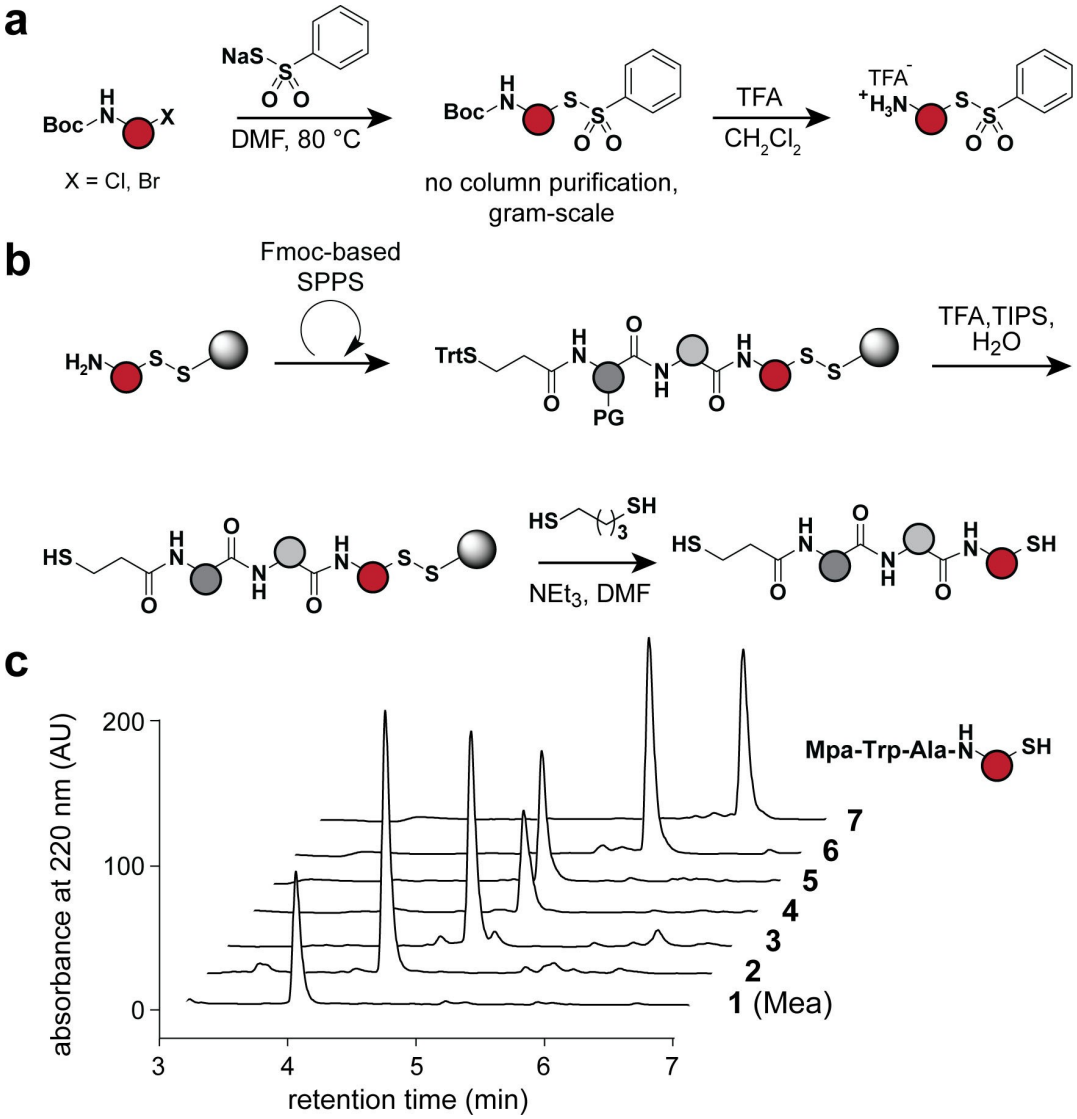

Figure 2. Preparation of aminothiol building blocks. a) Strategy for the "no purification" synthesis of aminothiol compounds activated with a phenylsulfone leaving group. b) SPPS of dithiol peptides using resin carrying a disulfide-linked aminothiol group. c) Stacked HPLC chromatograms of the quality of crude model peptides (Mpa-Trp-Ala-aminothiol X) synthesized with aminothiols **1**–**7**.

are counted by considering only the macrocyclic ring structure and ignoring side chains. This makes the skeletal diversity of the library >4-fold larger than that of the most diverse libraries developed previously (144 and 432 backbones).[10,12] We computationally predicted the physicochemical properties of the generated macrocycles and found that the average molecular weight (568 Da) and other key properties such as polar surface area are well inside the range where macrocyclic compounds are typically able to cross membranes. Overall, this suggested that hits from this library have a good chance of being cell-permeable (Figure 3c and Supporting Table S2), so we proceeded with the library synthesis.

We synthesized the 384 dithiol peptides by automated SPPS in 4×96-well plates using the seven different aminothiols and BDT for peptide release (see workflow in Supporting Figure S3). We determined the peptide yields using Ellman's reagent, which showed an even concentration distribution of compounds prepared with the different aminothiol building blocks (24.9 ± 10.7 mM average concentration; Supporting Figure S4) and a yield of ~60 % based on resin loading. An analysis of 20 randomly chosen peptides by HPLC-MS showed a greater than 80 % average purity, with most impurities stemming from incomplete couplings with challenging Fmoc amino acids during SPPS. This shows that the structurally diverse C-terminal thiol elements are fully compatible with the established SPPS library synthesis, deprotection and reductive release method. More specifically, the results also meant that the disulfide bridges formed by the new aminothiols were sufficiently stable for Fmoc deprotection and on-resin side chain deprotection by TFA, and enough accessible for efficient reductive cleavage with BDT.

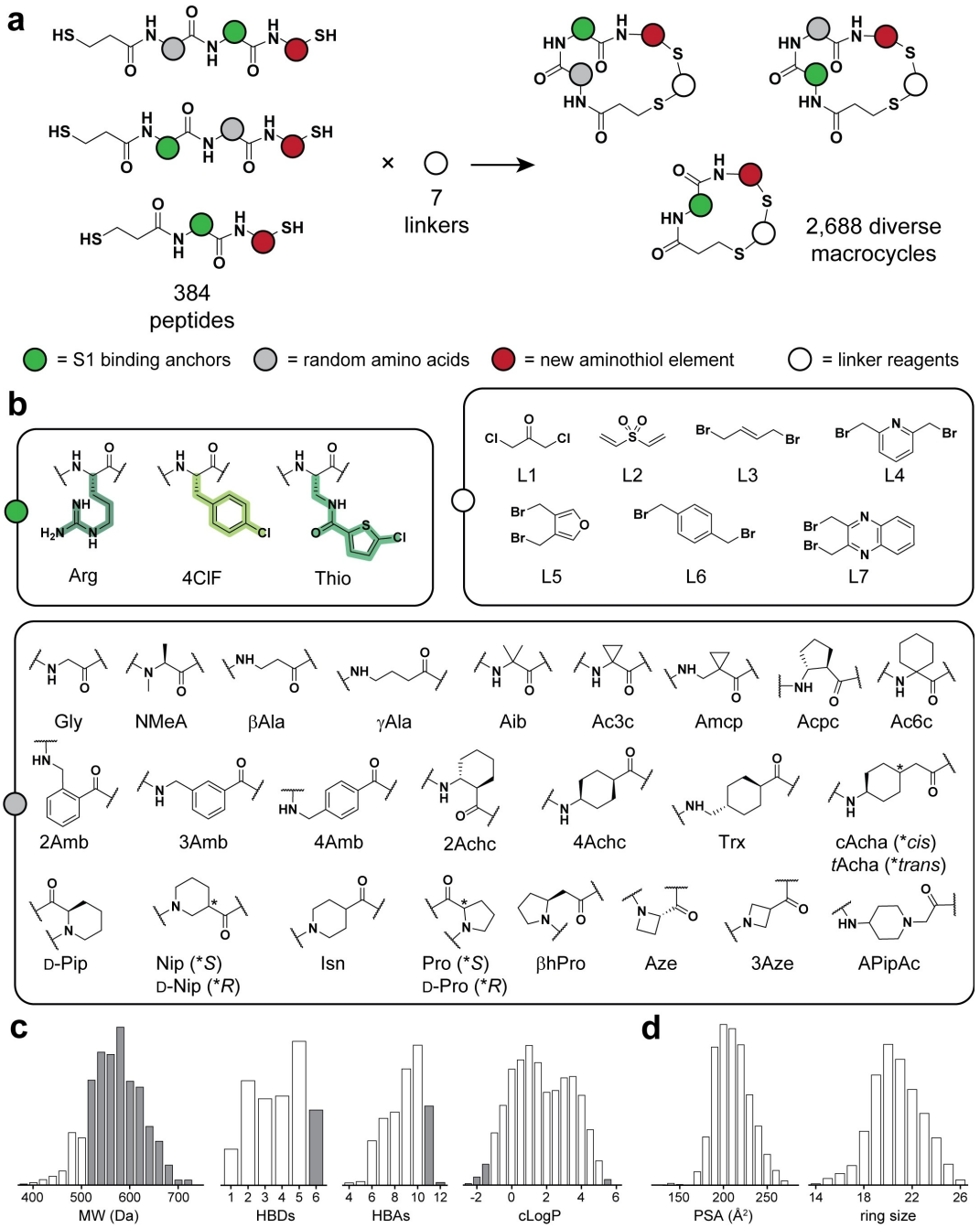

Figure 3. Macrocycle library designed for the inhibition of trypsin-like serine proteases. a) Format of linear peptides before and after cyclization by bis-electrophilic reagents. In the chemical structures, standard amide bonds are shown for simplicity although some of them are *N*-methylated. b) Amino acids and linkers used for library synthesis. The colored dots indicate the four groups of building blocks. c) Histograms of selected physicochemical properties of the macrocyclic library calculated using DataWarrior.[31] Marked in white is the area in accordance with the Ro5.[3] d) Additional library properties not belonging to the Ro5.

Next, we cyclized the dithiol peptides using bis-electrophilic linker reagents. We applied seven linkers having different lengths and shapes to impose different conformations onto the peptide backbones.[10] To limit side products stemming from oxidation such as disulfide cyclized or oligomerized peptide observed in previous work, we introduced a new procedure in which we freshly reduced the thiol groups by incubation with BDT, removed the reducing agent by RVC, and added the linker reagents to the fully reduced and dried peptide (Figure 4a). We performed the cyclization reactions at a 40 nmol scale, distributing the peptides into 384-well polypropylene source plates by acoustic liquid transfer. HPLC-MS analysis of two random peptides cyclized with the seven different linkers showed nearly quantitative cyclization with all linkers (Supporting Figure S5). Thus, we were able to minimize disulfide oxidation

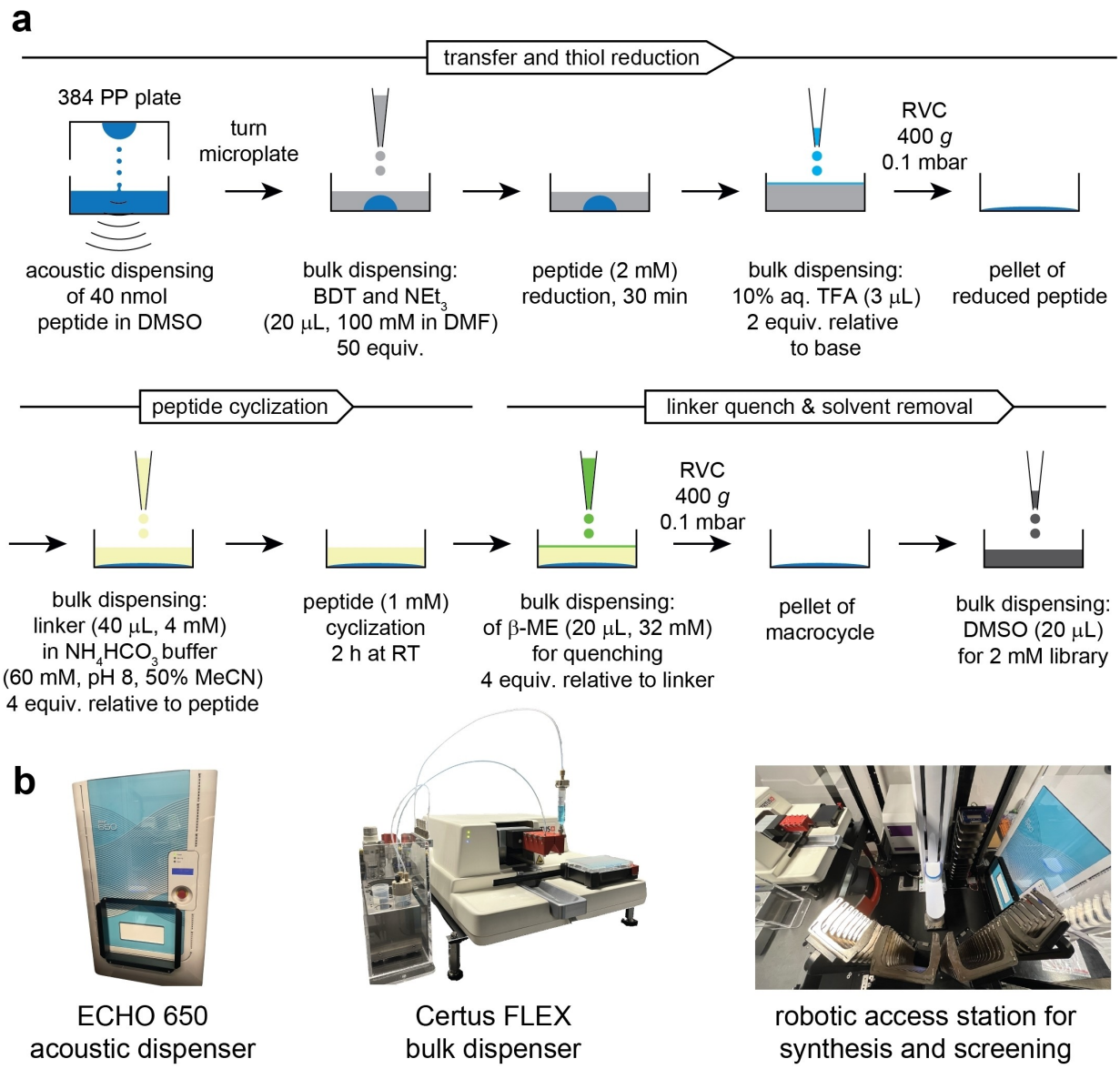

Figure 4. Workflow for the combinatorial cyclization of dithiol peptides in microtiter plates. a) Workflow for the reduction, cyclization, and quenching of the linker reagent in 384-well plates. b) Robotic instrumentation used for the full automation and tip-less peptide library cyclization and activity screening.

side products by developing a procedure to dispense bis-electrophiles to reduced and dried rather than dissolved peptides. Our workflow generated macrocyclic compounds at a larger scale than previously (40 nmol vs. 160 pmol),[11] producing material for more than 100 screens and thus allowing screening of the same library against multiple targets, as shown herein. While we synthesized the macrocyclic molecules in 384-well plates in this work, we have preliminary data showing that the same procedures are applicable in 1,536-well plates, allowing us to further increase the library size and throughput by 4-fold with an equivalent effort. As final quality check, we analyzed by LC-MS 28 randomly picked library members wherein we ensured that all seven aminothiol building blocks and cyclization linkers were represented. While some reactions showed major side products such as truncated peptide or non-identified species, and some products were difficult to detect due to low UV absorbance of the chemical structures, the desired products could be detected in 27 of the 28 samples and for 16 of them, the desired macrocycle was the main product (Supporting Figure S5).

We screened the crude library against five trypsin-like serine proteases, namely thrombin, kallikrein 5 (KLK5), human coagulation factor XI (FXI), human coagulation factor XII (FXII), and plasma kallikrein (PK) using a final concentration of 10 µM (thrombin) or 20 µM (other proteases) crude compounds. To identify hit compounds based on activity and not just binding, we measured the ability of the macrocycles to inhibit enzymatic cleavage of fluorogenic 7-amino-4-methylcoumarin (AMC) substrates. The entire

screen was fully automated using a robotic access station (Figure 4b) so that the high-throughput screen for all targets, comprising a total of >15,000 assay wells (1,536-well plates), was performed in only a few hours. Pleasingly, the screens against two of the targets, thrombin and PK, showed many hits with high activities (Figure 5a). Given the much stronger inhibition seen for these two targets than for KLK5, FXI and FXII (Supporting Figure S6) we focused in our analysis and the characterization on hits form the thrombin and PK screens. Structure-activity analysis showed that all aminothiol building blocks generated hits in the thrombin screen (Supporting Figure S7), wherein the hits for PK were found only for macrocycles based on aminothiols **1**, **4**, and **7**, underscoring the importance of skeletal diversity in libraries.

We next analyzed whether hits of the crude macrocycle screens were based on the anticipated macrocycles or potential side-products that can occasionally give rise to activity in crude product screens.[10] HPLC-MS analysis showed that the predominant peptide was the desired

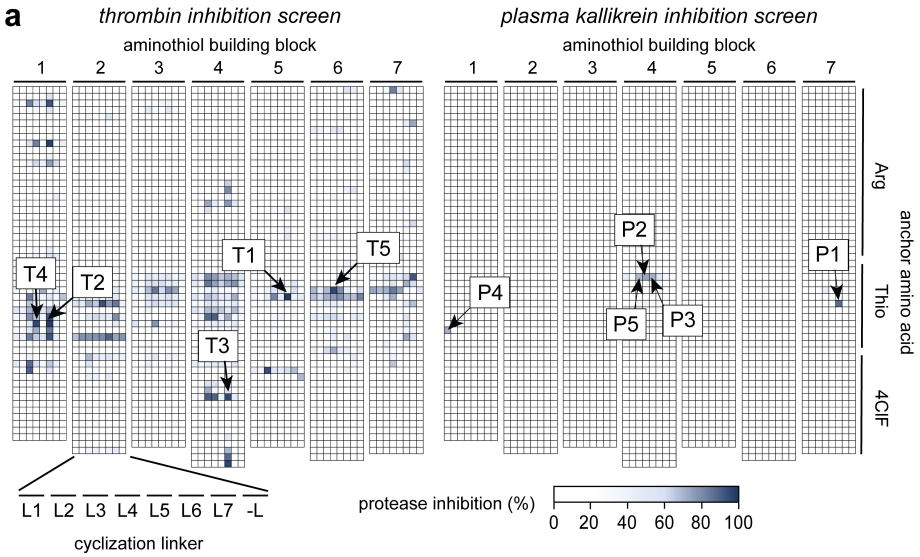

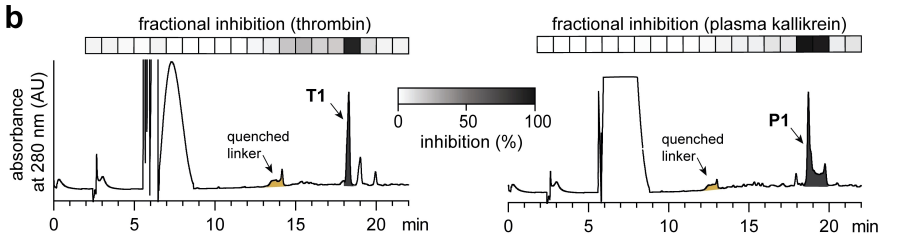

c

macrocycle	% inhibition in screen	K_i (nM)	sequence
T1	95.3	19.5 ± 3.2	Mpa Thio Nip **5** (L6)
T2	94.6	10.9 ± 5.6	Mpa *t*Acha Thio **1** (L6)
T3	92.5	123 ± 47	Mpa 4ClF Nip **4** (L6)
T4	92.5	26 ± 1	Mpa *t*Acha Thio **1** (L4)
T5	92.3	81 ± 5	Mpa Thio βAla **6** (L4)

macrocycle	% inhibition in screen	K_i (μM)	sequence
P1	85	0.51 ± 0.04	Mpa Thio Pro **7** (L6)
P2	72	6.5 ± 0.5	Mpa Thio Gly **4** (L4)
P3	70	12.3 ± 1.1	Mpa Thio Gly **4** (L5)
P4	70	13.6 ± 2.6	Mpa Thio APipAc **1** (L1)
P5	68	3.8 ± 0.2	Mpa Thio Gly **4** (L3)

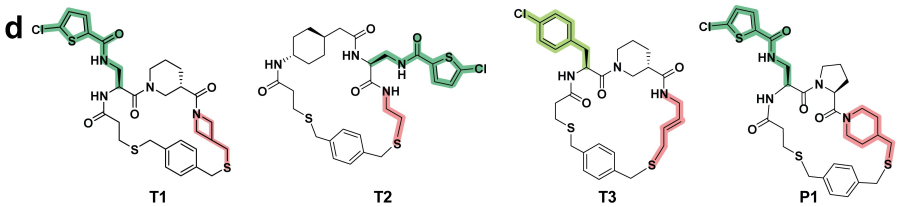

Figure 5. Macrocyclic library screening. a) Heatmap showing residual protease inhibition of thrombin (10 μM macrocycle) and PK (20 μM macrocycle). A non-linear color scale was chosen to emphasize compounds with higher activity (dark blue) and hide inhibition below 30% (all white) as shown by scale bar. Arrows indicate and label macrocycles that were purified and showed the highest protease inhibitory activity. b) Identification of active species in crude cyclization reaction of **T1** and **P1**. Fractional inhibition shows the extent of protease inhibition found for indicated HPLC fractions, each one corresponding to the indicated 1-minute elution times. c) Activities of purified macrocycles. Average values and SDs are based on four independent experiments (**T1**–**T3**), or two (**T4**) or four (**T5, P1**–**P5**) replicate measurements performed in one experiment. d) Chemical structures of selected hits. The group binding to the S1 pocket is highlighted in green and the aminothiol element in red.

macrocycle in all crude DMSO stocks of the top seven thrombin hits (**T1**–**T7**) and top five PK hits (**P1**–**P5**) (Supporting Figure S8). To confirm that the inhibitory effect stemmed from the macrocyclic species as opposed to the presence of excess quenched linkers, side products, or peptide aggregates, we repeated the cyclization of **T1** and **P1** at 40 nmol scales, fractionated the crude cyclization mixture using preparative reversed-phase (RP) HPLC, and measured the activity of all collected fractions. In both cases, strong inhibition was observed only for fractions containing the desired macrocycle (Figure 5b). To determine IC_{50} and K_i values, we re-synthesized all 12 hits on a larger scale (25 μmol) and purified them by preparative RP-HPLC (Figure 5c and 5d, Supporting Figures S9–S12). Of the seven thrombin hits that showed 92 % or greater inhibition in the crude screen, five (**T1**–**T5**) were nanomolar binders, and the one with the highest affinity (**T2**) had a measured K_i of 10.9 ± 5.6 nM (Figure 5c). **T2** was around 4-fold more potent than inhibitors identified previously by screening of other random libraries (best $K_i = 42$ nM),[10,11] suggesting that the higher structural diversity directly translated into the isolation of better inhibitors. For PK, we confirmed the inhibition for all top five hits (**P1**–**P5**) and determined the best inhibitor to be **P1** ($K_i = 0.51 \pm 0.04$ μM). For PK, previous screening of other synthetic libraries performed in our lab had not yielded any binders (not published), so the sub-micromolar inhibitor was likely found as a result of the larger structural diversity in this screen. Testing the five thrombin inhibitors in the PK activity assay showed that they are all highly specific for thrombin with a selectivity of over 1,000-fold. In contrast, the five PK inhibitors blocked thrombin to a similar extent, with the exception of **P1** that showed more than 50-fold selectivity for PK over thrombin (Supporting Figure S13).

To determine the importance of the size and shape of the newly introduced aminothiol elements in the binding interaction, we used X-ray crystallography to analyze the macrocycles bound to thrombin. We obtained diffraction-quality crystals of thrombin co-crystallized with compounds **T1** (PDB 8ASF, 2.57 Å resolution) and **T3** (PDB 8ASE, 2.55 Å resolution). From the structures, we see that the macrocycles perfectly occupy the enzyme's active site, with the S1-binding chlorothiophene and 4-chlorophenylalanine groups pointing directly into the S1 pocket (Figure 6a and 6b; see Supporting Results and Supporting Figures S14–S16 for additional discussion of the structures). An overlay of the two inhibitors showed an overall similar binding orientation, though the positions of the α-carbons of the S1-binding groups differ greatly due to the different lengths but identical binding modes of these groups (Figure 6c). The different shapes and dimensions of the aminothiol groups seem to thus accommodate the structural differences of the S1-binding groups. Taken together, the structural results showed that the larger structural diversity in the backbones of the macrocycles enabled the discovery of perfectly fitting inhibitors.

Finally, to measure the membrane permeability of these compounds, we first determined the passive permeability of the thrombin inhibitors **T1**–**T5** using the parallel artificial membrane permeability assay (PAMPA).[23] Two macrocycles, **T1** and **T3**, displayed an effective permeability coefficient (P_e) of greater than 1×10^{-6} cm/s (Figure 7a,

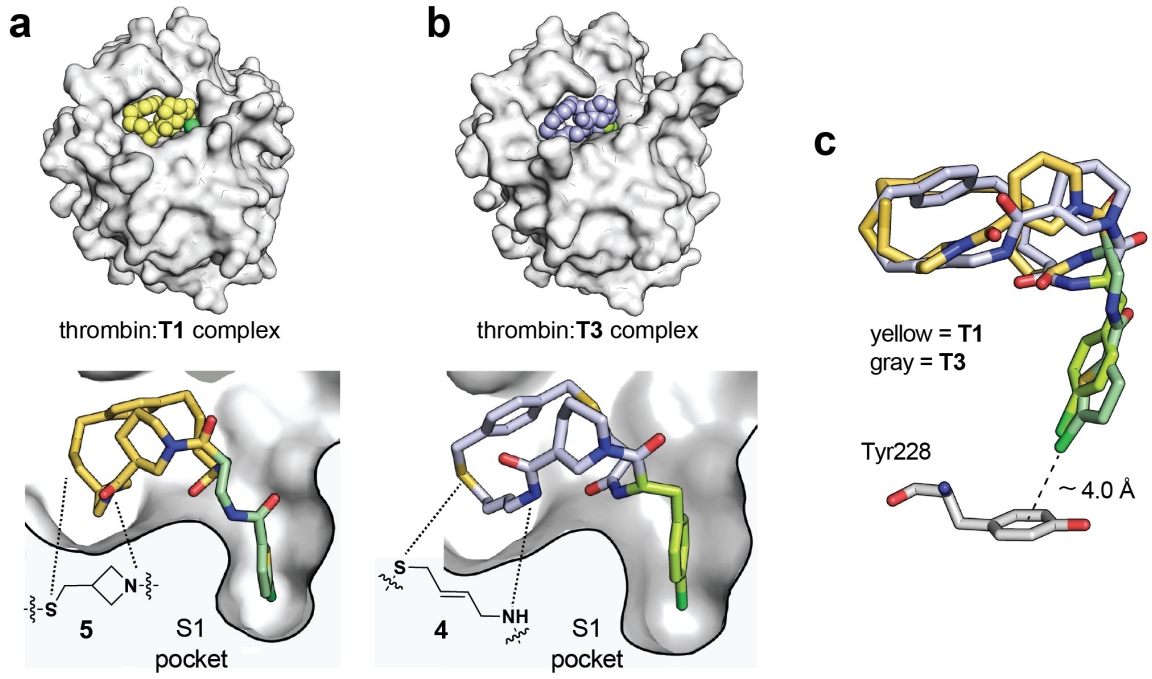

Figure 6. X-ray structures of thrombin:macrocycle complexes. a,b) Surface view of thrombin (grey) with bound **T1** (a) or **T3** (b). The lower parts of the panels show the macrocycles as sticks, wherein the S1 binding anchor is highlighted in green. The regions of the aminothiol building blocks are indicated. c) Superposition of **T1** and **T3** in the active site and highlighting of the halogen-π interaction with Tyr228.

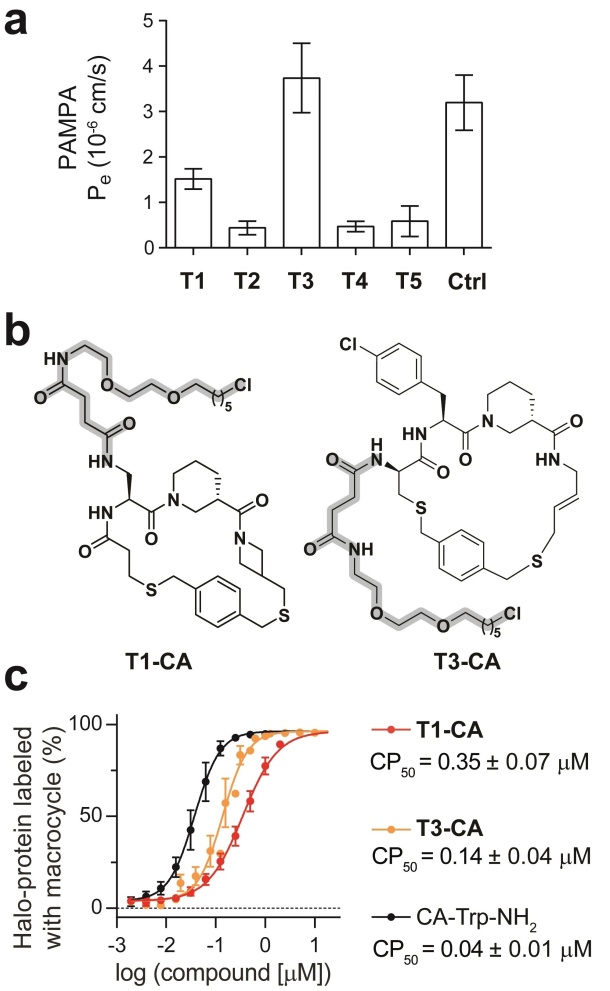

Figure 7. Macrocycle membrane permeability. a) PAMPA permeability after 12 h incubation at 50 μM concentration. Ctrl = previously reported membrane permeable macrocycle **15** (see Supporting Figure S17 for structure) was used as positive control. Mean values and SDs of three replicates done in the same PAMPA plate are shown. b) Structures of macrocycles **T1** and **T3** containing a chloroalkane (CA) tag (gray shaded) for quantification of compound that reaches the cell cytosol by the CAPA assay. c) CAPA results after exposure of cells to macrocycles for 4 hrs. The percent of HaloTag occupied by macrocycle-CA was quantified by reaction of free HaloTag with fluorescent TAMRA-CA and flow cytometry. Mean CP_{50} values ± SD from four experiments performed on different days. CA-Trp-NH_2 was used as positive control.

Supporting Table S3), which is in the range of the macrocycle-based drug cyclosporin that has a good membrane permeability ($P_e = 2\times10^{-6}$ cm/s).[24] To evaluate if **T1** and **T3** were also able to penetrate the plasma membranes of live cells, we applied the chloroalkane penetration assay (CAPA).[25,26] In this assay, compounds bearing a chloroalkane (CA) group are added to cultured cells that express HaloTag[27] protein in the cytosol and CA-tagged compounds that enter the cell react covalently with HaloTag. The %-HaloTag occupied with compound-CA, being proportional to the amount that crossed the membrane, is quantified with a cell-permeable fluorescent chase and flow cytometric analysis. To prepare for the assay, we therefore synthesized macrocycle analogs bearing a CA group by either replacing the chlorothiophene group in **T1** with an amino acid having CA as side chain to obtain the comparably sized macrocycle **T1-CA**, or by appending the CA to the N-terminus of **T3** to generate **T3-CA**, for the latter molecule risking that the larger size might reduce the permeability compared to the non-tagged macrocycle (Figure 7b and Supporting Figures S18–S20). After incubating cells for four hours with different concentrations of **T1-CA** and **T3-CA** (2-fold dilutions) we observed sub-micromolar half-maximal cellular penetration (CP_{50}) values of 0.35 ± 0.07 μM and 0.14 ± 0.04 μM, respectively (Figure 7b), which are found in CAPA for passively permeable compounds such as the highly permeable CA-Trp-NH_2 used as a control (0.04 ± 0.01 μM). This result effectively validated the strategy of diversifying a previously constant element in macrocycle libraries, which yielded more potent inhibitors that are also membrane-permeable. Notably, some of the identified binders showed good membrane permeability in artificial membranes (PAMPA) and live cells because the size of the macrocycles was maintained small, close to 500 Da.

Conclusion

In this work, we developed a strategy for efficiently synthesizing large libraries of peptide macrocycles that have a more than 4-fold higher structural diversity than previous libraries, important for identifying binders to targets, and yet are sufficiently small sized to achieve good membrane permeability. We achieved this by diversifying elements of macrocyclic peptides that are typically kept constant in library formation such as the cysteines or cysteamines used for cyclizing peptides via thioether or disulfide linkages. This diversification became possible via the development of an efficient synthesis pathway for generating structurally diverse, phenylsulfone-activated aminothiol building blocks that could be incorporated into peptides by SPPS. We tested our strategy in a proof-of-concept study, making a library of 2,688 compounds that culminated in the discovery of nanomolar inhibitors of two proteases, including some that displayed good membrane permeability.

The high structural diversity directly translated into the isolation of better binders from random libraries, with the best thrombin inhibitor ($K_i = 10.9$ nM) identified being 4-fold more potent than those isolated previously from other libraries (best $K_i = 42$ nM),[10] and the library is the first one in which we found inhibitors for plasma kallikrein. The importance of the expanded structural diversity is supported by the X-ray structural analysis of two of the macrocycles bound to thrombin, which showed that the specific size and shape of the aminothiol groups are needed to optimally accommodate the neighboring macrocycle building blocks for forming optimal contacts with the thrombin's active site. Importantly, several of the identified binders showed good membrane permeability in artificial membranes (PAMPA) and in live cells (CAPA), which was likely a result of keeping the size of the macrocycles rather small, close to 500 Da. Such a result would likely not have been possible if

the library diversity had been increased through adding an additional amino acid position for diversification due to the increase in size and the addition of an extra amide bond, the latter typically much reducing the membrane permeability due to its polar nature.

While we synthesized a rather small library of only 2,688 macrocycles in this study, much larger libraries can be generated with the applied methods. We recently modified a commercial 96-well plate peptide synthesizer to make peptides in 384-well plates.[28] The instrument holds four 384-well reactor plates allowing us to synthesize 1,536 peptides in one run and in less than three days. As mentioned above, we also have preliminary data that shows that the cyclization reactions and procedures established herein for 384-well plates are applicable to 1,536-well plates, allowing the synthesis of ten-thousands or even over hundred-thousand macrocyclic compounds with the described expanded skeletal diversity. Such larger libraries may be beneficial for developing macrocycle-based ligands to more challenging targets than the herein-applied proteases, such as protein-protein interactions.

We had used in this work seven different aminothiol building blocks, but this number may be grown further by synthesizing additional ones as for example aminothiol groups containing side chains. In addition, the *N*-terminal thiol-containing building block Mpa, which was kept constant in this work, may be diversified in the future too. Building blocks analogous to Mpa, may be prepared by reacting halogenated carboxylic acids with trityl mercaptan. Together with a set of diverse aminothiols, even greater macrocycles diversities for generating membrane permeable ligands could be generated. Finally, the macrocycle backbones may additionally be varied by introducing building blocks that add ester or thioamide bonds, that are also suited to improve membrane permeability.[29,30] We are optimistic that the herein developed new approach for synthesizing small and structurally highly diverse, membrane permeable macrocycles will be broadly applicable to many proteins and may offer a solution to develop therapeutics to some of the most challenging intracellular disease targets.

Abbreviations

AMC	7-amino-4-methyl coumarin
BDT	1,4-butanedithiol
CA	chloroalkane
CAPA	chloroalkane penetration assay
Mea	2-mercaptoethylamine
P_e	effective permeability coefficient
FXI	factor XI
FXII	factor XII
CP_{50}	half-maximal cellular penetration
HBD	hydrogen bond donors
HTS	high-throughput screening
KLK5	tissue kallikrein 5
Mpa	3-mercaptopropionic acid
PAMPA	parallel artificial membrane permeability assay
PK	plasma kallikrein
PP	polypropylene
PS	polystyrene
RVC	rotary vacuum concentration
RP	reversed-phase
Ro5	rule of five
SPPS	solid-phase peptide synthesis
β-ME	β-mercaptoethanol

Author Contributions

A.L.N, G.K.M and C.H. conceptualized the study; G.K.M innovated the synthetic strategy for synthesizing aminothiol reagents; Z.B. established the synthesis of aminothiols and testing in SPPS; A.L.N., Z.B., A.Z., and M.S. performed the chemical synthesis; A.L.N. A.Z., M.M., X.J. and E.J.W. conducted the biochemical experiments; M.C., L.C. and A.A. generated the co-crystals and solved the X-ray structures; C.R.O.B and K.S. performed the CAPA studies, A.L.N. and C.H. wrote the original draft of the manuscript, and all authors reviewed the final version.

Acknowledgements

We thank Peter M. F. Panzar, Elena Covato, Bo Fu, and Violaine Chirat for technical assistance and building block synthesis. Prof. Joshua Kritzer is acknowledged for providing the HaloTag-expressing HeLa cell line. Kaycie Butler and Mark D. Nolan are recognized for proofreading the manuscript. This project has received funding from the European Research Council (ERC) under the European Union's Horizon 2020 research and innovation programme (grant agreement No. 101020521-TARGET. This work was also supported by the Swiss National Science Foundation (grant 192368) and the BactiVax European Training Network (ETN), funded under the H2020-MSCA-ITN-2019 call (grant agreement ID: 860325). Open Access funding provided by École Polytechnique Fédérale de Lausanne.

Conflict of Interest

The authors declare the following competing financial interest(s): A.L.N., Z.B., G.K.M., M.S., M.M., and C.H. are inventors of a patent that covers aspects of this work. C.H. is a co-founder of Orbis Medicines. M.S. is an employee of Orbis Medicines. The remaining authors declare no competing interests.

Data Availability Statement

Supporting Information accompanies this paper and includes: Supporting results, Figures, and tables as well as experimental procedures, compound characterization data, and copies of HPLC chromatograms and NMR spectra. Raw data of results shown in figures is provided in an Excel

file. X-ray diffraction data, coordinates, and structure factors for the X-ray crystal structures are deposited with the PDB under the accession numbers 8ASF and 8ASE.

Keywords: cell permeability · cyclization · high-throughput screening · macrocycle · protease inhibitor

[1] E. M. Driggers, S. P. Hale, J. Lee, N. K. Terrett, *Nat. Rev. Drug Discovery* **2008**, *7*, 608–624.
[2] D. Garcia Jimenez, V. Poongavanam, J. Kihlberg, *J. Med. Chem.* **2023**, *66*, 5377–5396.
[3] C. A. Lipinski, F. Lombardo, B. W. Dominy, P. J. Feeney, *Adv. Drug Delivery Rev.* **2001**, *46*, 3–26.
[4] B. Over, P. Matsson, C. Tyrchan, P. Artursson, B. C. Doak, M. A. Foley, C. Hilgendorf, S. E. Johnston, M. D. Lee, R. J. Lewis, P. McCarren, G. Muncipinto, U. Norinder, M. W. D. Perry, J. R. Duvall, J. Kihlberg, *Nat. Chem. Biol.* **2016**, *12*, 1065–1074.
[5] M. R. Naylor, A. T. Bockus, M.-J. Blanco, R. S. Lokey, *Curr. Opin. Chem. Biol.* **2017**, *38*, 141–147.
[6] X. Ji, A. L. Nielsen, C. Heinis, *Angew. Chem. Int. Ed.* **2023**, *63*, e202308251, DOI 10.1002/anie.202308251.
[7] A. Ohta, M. Tanada, S. Shinohara, Y. Morita, K. Nakano, Y. Yamagishi, R. Takano, S. Kariyuki, T. Iida, A. Matsuo, K. Ozeki, T. Emura, Y. Sakurai, K. Takano, A. Higashida, M. Kojima, T. Muraoka, R. Takeyama, T. Kato, K. Kimura, K. Ogawa, K. Ohara, S. Tanaka, Y. Kikuchi, N. Hisada, R. Hayashi, Y. Nishimura, K. Nomura, T. Tachibana, M. Irie, H. Kawada, T. Torizawa, N. Murao, T. Kotake, M. Tanaka, S. Ishikawa, T. Miyake, M. Tamiya, M. Arai, A. Chiyoda, S. Akai, H. Sase, S. Kuramoto, T. Ito, T. Shiraishi, T. Kojima, H. Iikura, *J. Am. Chem. Soc.* **2023**, *145*, 24035–24051.
[8] M. Tanada, M. Tamiya, A. Matsuo, A. Chiyoda, K. Takano, T. Ito, M. Irie, T. Kotake, R. Takeyama, H. Kawada, R. Hayashi, S. Ishikawa, K. Nomura, N. Furuichi, Y. Morita, M. Kage, S. Hashimoto, K. Nii, H. Sase, K. Ohara, A. Ohta, S. Kuramoto, Y. Nishimura, H. Iikura, T. Shiraishi, *J. Am. Chem. Soc.* **2023**, *145*, 16610–16620.
[9] L. Plais, J. Scheuermann, *RSC Chem Biol* **2022**, *3*, 7–17.
[10] S. S. Kale, M. Bergeron-Brlek, Y. Wu, M. G. Kumar, M. V. Pham, J. Bortoli, J. Vesin, X.-D. Kong, J. F. Machado, K. Deyle, P. Gonschorek, G. Turcatti, L. Cendron, A. Angelini, C. Heinis, *Sci. Adv.* **2019**, *5*, eaaw2851.
[11] S. Habeshian, M. L. Merz, G. Sangouard, G. K. Mothukuri, M. Schüttel, Z. Bognár, C. Díaz-Perlas, J. Vesin, J. Bortoli Chapalay, G. Turcatti, L. Cendron, A. Angelini, C. Heinis, *Nat. Commun.* **2022**, *13*, 3823.
[12] M. L. Merz, S. Habeshian, B. Li, J.-A. G. L. David, A. L. Nielsen, X. Ji, K. Il Khwildy, M. M. Duany Benitez, P. Phothirath, C. Heinis, *Nat. Chem. Biol.* **2024**, *20*, 624–635 .
[13] S. Habeshian, G. A. Sable, M. Schüttel, M. L. Merz, C. Heinis, *ACS Chem. Biol.* **2022**, *17*, 181–186.
[14] Z. Bognar, G. K. Mothukuri, A. L. Nielsen, M. L. Merz, P. M. F. Pânzar, C. Heinis, *Org. Biomol. Chem.* **2022**, *20*, 5699–5703.
[15] M. D. Nolan, M. Schüttel, E. M. Scanlan, A. L. Nielsen, *Pept. Sci.* **2024**, *116*, e24310.
[16] D. P. Fairlie, A. Dantas de Araujo, *Pept. Sci.* **2016**, *106*, 843–852.
[17] R. A. Roof, K. Sobczyk-Kojiro, A. J. Turbiak, D. L. Roman, I. D. Pogozheva, L. L. Blazer, R. R. Neubig, H. I. Mosberg, *Chem. Biol. Drug Des.* **2008**, *72*, 111–119.
[18] L. E. J. Smeenk, D. Timmers-Parohi, J. J. Benschop, W. C. Puijk, H. Hiemstra, J. H. van Maarseveen, P. Timmerman, *ChemBioChem* **2015**, *16*, 91–99.
[19] F. F. Faucher, D. Abegg, P. Ipock, A. Adibekian, S. Lovell, M. Bogyo, *Isr. J. Chem.* **2023**, *63*, DOI 10.1002/ijch.202300020.
[20] N. S. Zefirov, N. V. Zyk, E. K. Beloglazkina, A. G. Kutateladze, *Sulfur Rep.* **1993**, *14*, 223–240.
[21] L. Lin, M. E. Olson, T. Sugane, L. D. Turner, M. A. Tararina, A. L. Nielsen, E. K. Kurbanov, S. Pellett, E. A. Johnson, S. M. Cohen, K. N. Allen, K. D. Janda, *J. Med. Chem.* **2020**, *63*, 11100–11120.
[22] E. A. Stura, L. Le Roux, K. Guitot, S. Garcia, S. Bregant, F. Beau, L. Vera, G. Collet, D. Ptchelkine, H. Bakirci, V. Dive, *J. Biol. Chem.* **2012**, *287*, 33607–33614.
[23] M. Kansy, F. Senner, K. Gubernator, *J. Med. Chem.* **1998**, *41*, 1007–1010.
[24] D. Lee, S. Lee, J. Choi, Y.-K. Song, M. J. Kim, D.-S. Shin, M. A. Bae, Y.-C. Kim, C.-J. Park, K.-R. Lee, J.-H. Choi, J. Seo, *J. Med. Chem.* **2021**, *64*, 8272–8286.
[25] L. Peraro, Z. Zou, K. M. Makwana, A. E. Cummings, H. L. Ball, H. Yu, Y.-S. Lin, B. Levine, J. A. Kritzer, *J. Am. Chem. Soc.* **2017**, *139*, 7792–7802.
[26] L. Peraro, K. L. Deprey, M. K. Moser, Z. Zou, H. L. Ball, B. Levine, J. A. Kritzer, *J. Am. Chem. Soc.* **2018**, *140*, 11360–11369.
[27] G. V. Los, L. P. Encell, M. G. McDougall, D. D. Hartzell, N. Karassina, C. Zimprich, M. G. Wood, R. Learish, R. F. Ohana, M. Urh, D. Simpson, J. Mendez, K. Zimmerman, P. Otto, G. Vidugiris, J. Zhu, A. Darzins, D. H. Klaubert, R. F. Bulleit, K. V. Wood, *ACS Chem. Biol.* **2008**, *3*, 373–382.
[28] M. Schüttel, E. Will, G. Sangouard, A. Zarda, S. Habeshian, A. L. Nielsen, C. Heinis, *J. Pept. Sci.* **2024**, *4*, e3555.
[29] P. Ghosh, N. Raj, H. Verma, M. Patel, S. Chakraborti, B. Khatri, C. M. Doreswamy, S. R. Anandakumar, S. Seekallu, M. B. Dinesh, G. Jadhav, P. N. Yadav, J. Chatterjee, *Nat. Commun.* **2023**, *14*, 6050.
[30] Y. Hosono, S. Uchida, M. Shinkai, C. E. Townsend, C. N. Kelly, M. R. Naylor, H.-W. Lee, K. Kanamitsu, M. Ishii, R. Ueki, T. Ueda, K. Takeuchi, M. Sugita, Y. Akiyama, S. R. Lokey, J. Morimoto, S. Sando, *Nat. Commun.* **2023**, *14*, 1416.
[31] T. Sander, J. Freyss, M. Von Korff, C. Rufener, *J. Chem. Inf. Model.* **2015**, *55*, 460–473.

Manuscript received: January 5, 2024
Accepted manuscript online: April 11, 2024
Version of record online: ■■, ■■

Research Articles

Macrocycles

A. L. Nielsen, Z. Bognar, G. K. Mothukuri, A. Zarda, M. Schüttel, M. L. Merz, X. Ji, E. J. Will, M. Chinellato, C. R. O. Bartling, K. Strømgaard, L. Cendron, A. Angelini, C. Heinis* e202400350

Large Libraries of Structurally Diverse Macrocycles Suitable for Membrane Permeation

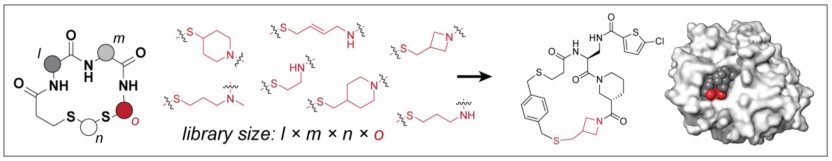

Macrocycles are promising for drug development due to their good binding properties and the potential to cross membranes. A synthetic strategy and chemical building blocks are developed to produce and screen thousands of small, structurally highly diverse peptidic macrocycles. HTS identifies potent thrombin inhibitors with good membrane permeability. The strategy may be broadly applied in the development of membrane permeable therapeutics.

Angewandte Chemie
Eine Zeitschrift der Gesellschaft Deutscher Chemiker

Supporting Information

Large Libraries of Structurally Diverse Macrocycles Suitable for Membrane Permeation

*A. L. Nielsen, Z. Bognar, G. K. Mothukuri, A. Zarda, M. Schüttel, M. L. Merz, X. Ji, E. J. Will, M. Chinellato, C. R. O. Bartling, K. Strømgaard, L. Cendron, A. Angelini, C. Heinis**

Supporting Information

Large Libraries of Structurally Diverse Macrocycles Suitable for Membrane Permeation

Alexander L. Nielsen,[a] Zsolt Bognar,[a,†] Ganesh K. Mothukuri,[a,†] Anne Zarda,[a,†] Mischa Schüttel,[a] Manuel Merz,[a] Xinjian Ji,[a] Edward J. Will,[a] Monica Chinellato,[b] Christian R.O. Bartling,[c] Kristian Strømgaard,[c] Laura Cendron,[b] Alessandro Angelini[d,e] and Christian Heinis[a,*]

[a]Institute of Chemical Sciences and Engineering, School of Basic Sciences, École Polytechnique Fédérale de Lausanne (EPFL), CH-1015 Lausanne, Switzerland

[b]Department of Biology, University of Padova, 35131 Padova, Italy

[c]Center for Biopharmaceuticals and Department of Drug Design and Pharmacology, Faculty of Health and Medical Sciences, University of Copenhagen, Jagtvej 162, DK-2100 Copenhagen, Denmark

[d]Department of Molecular Sciences and Nanosystems, Ca' Foscari University of Venice, Via Torino 155, Venezia Mestre, Venice 30172, Italy

[e]European Centre for Living Technologies (ECLT), Ca' Bottacin, Dorsoduro 3911, Calle Crosera, Venice 30124, Italy

[†]These authors contributed equally to this work

*Corresponding author: christian.heinis@epfl.ch

TABLE OF CONTENTS

SUPPORTING RESULTS

Overall structure of human α-thrombin in complex with T1

Human α-thrombin consists of two polypeptide chains of 36 (light chain) and 259 amino acid residues (heavy chain) covalently linked via a disulfide bridge (Cys122 of heavy-chain with Cys1 of light-chain). X-ray structure analysis of crystals formed by α-thrombin (light- and heavy-chain) and macrocycle **T1** (PDB 8ASF; Table S4) showed two nearly identical copies of heavy- and light-chains of human α-thrombin in the asymmetric unit with the catalytic site of each enzyme that point in opposite directions. The two light/heavy chains of α-thrombin are named A/B and H/L. The structure of H/L was used for all calculations and for preparing the structure figures. The light chain of human α-thrombin can be traced unambiguously from Glu1C to Ile14K. The amino terminal residues (Thr1H to Gly1D) and the carboxyl-terminal residues Asp14L to Arg15 are undefined and not visible in the Fourier map. The electron density of the heavy chain is clearly visible for all residues except for few amino acids that are part of the surface flexible autolysis loop (Trp148 to Lys149E). The carboxy-terminal residue Glu247 lacks adequate electron density. Minor differences occur at the level of flexible and less defined loops or in the orientation of exposed peripheral side chains. The overall structure of human α-thrombin bound to **T1** does not show any striking rearrangements of the main backbone if compared to other human α-thrombin structures, neither in the apo-form, nor in complex with inhibitors.

Overall structure of macrocycle T1

The electron density of the macrocycle **T1** is well-defined allowing an unambiguous assignment of group orientations for the two protein complexes present in the asymmetric unit. The numbering of the atoms in **T1** is shown in Figure S14. No classical secondary structure elements and no non-covalent intramolecular interactions are found in the macrocycle. The molecule appears to adopt a boat-like conformation that fits well the shape of the catalytic pocket with the 5-chlorothiophene functional group pointing toward the opposite site and filling the S1 sub-site.

Interactions between human α-thrombin and T1

The **T1** macrocycle fits well into the cleft formed by the active site and the surrounding substrate pockets covering a surface area on protein and on macrocycle of 395 $Å^2$ and 608 $Å^2$, respectively (Table S5). The macrocycles in the two active sites of the two-thrombin molecules present in the asymmetric unit superimpose well, except for the thioether linker connecting the azetidine to the benzyl group that appear to adopt slightly different conformations. A large portion of interactions of **T1** with human α-thrombin are mediated by the 5-chlorothiophene functional group that accommodates in the primary specificity S1 pocket. This group is trapped in the pocket by hydrogen bonding with the main chain of Gly216 (**T1** N33 with Gly216 O) and a molecule of H_2O that bridges

the oxygen O40 of **T1** with the main chain oxygen of Cys191 (Cys191 O), the main chain nitrogen of Gly193 (Gly193 N) and both the main chain nitrogen and the side chain oxygen of Ser195 (Gly195 N, Gly195 OG). 5-chlorothiophene-2-carboxamide is further involved in a network of polar contacts with the main chain of the nearby Cys191 (**T1** O40 with Cys191 O), Glu192 (**T1** O40 with Glu192 N), Trp215 (**T1** S36 with Trp215 N), Gly216 (**T1** N33 with Gly216 N and Gly216 O, and **T1** S36 with Gly216 N) and Gly219 (**T1** N33 with Gly219 O). The chlorine atom of the 5-chlorothiophene functional group points toward the bottom of the S1 pocket, where it likely forms a halogen-aromatic π interaction (~4.0 Å) with the aromatic ring of Tyr228. The main chain oxygen O31 of **T1** forms hydrogen bonds with the main chain nitrogen of Gly216 (Gly216 N). Additionally, the main chain sulfur S22 and oxygen O31 of **T1** can form polar contacts with the main chain oxygen of Glu97A (Glu97A O) and oxygen of Gly216 (Gly216 O), respectively. Importantly, the binding of **T1** to human α-thrombin is mediated by multiple hydrophobic contacts by main and side chains of adjacent enzyme residues (Table S6). The phenyl ring (C15–C20) of the macrocycle backbone lays towards the hydrophobic cage shaped by the side chains of residues His57, Tyr60A, Trp60D (proximal S2 pocket) and Leu99 (distal S3 pocket) where it forms a π-stacking interaction with Tyr60A side chain ring. The azetidine four-member heterocycle ring (C24–C27) explores the opposite hydrophobic pocket formed by Leu99, Ile174 and Trp215. Finally, the piperidine six-member heterocycle ring (C1–C6) point towards the solvent while the remaining backbone (C8–C12), including the amide moiety, establishes multiple interaction with residues of the thrombin loop (Gly216–Cys220; Table S6).

Overall structure of human α-thrombin in complex with T3

X-ray structure analysis of crystals formed by α-thrombin (light and heavy chain) and macrocycle **T3** (PDB 8ASE; Table S7) also showed two nearly identical copies of heavy- and light chains of human α-thrombin in the asymmetric unit with the catalytic site of each enzyme that face each other. The two light/heavy chains of α-thrombin are named A/B and H/L. The structure of H/L was used for all calculations and for preparing the structure figures. The light chain of human α-thrombin can be traced unambiguously from Glu1C to Ile14K. The amino terminal residues (Thr1H to Gly1D) and the carboxyl-terminal residues Asp14L to Arg15 are undefined and not visible in the Fourier map. The electron density of the heavy chain is clearly visible for all residues except for few amino acids that are part of a flexible loop (Ser72 to Arg75). Differently from the X-ray structure of human α-thrombin in complex with macrocycle **T1**, the electron density of the surface flexible autolysis loop (Trp148 to Lys149E) of human α-thrombin in complex with **T3** is clearly visible. This might be the result of the peculiar crystal packing of this complex with the two catalytic sites facing each other. The carboxyl-terminal residues Gly246 and Glu247 lack adequate electron density. Again, minor differences occur at the level of flexible and less defined loops or in the orientation of exposed peripheral side chains.

However, the overall structure of human α-thrombin bound to **T3** does not show any striking rearrangements of the main backbone if compared to other human α-thrombin structures, neither in the apo form, nor in complex with inhibitors.

Overall structure of macrocycle T3

The electron density of the macrocycle **T3** is well-defined allowing an unambiguous assignment of group orientations for all the four protein complexes present in the asymmetric unit. The numbering of the atoms in **T3** is shown in Figure S15. No classical secondary structure elements are found in the macrocycle. Notably, an intramolecular hydrogen bond is established between O3 and N1 of **T3** macrocycle (2.77 Å). Analogously to **T1**, the macrocycle **T3** appears to adopt a boat-like conformation that fits well to the shape of the catalytic pocket, with the 4-chlorobenzyl functional group pointing toward the opposite site and filling the S1 sub-site.

Interactions between human α-thrombin and T3

The **T3** macrocycle fits well into the cleft formed by the active site and the surrounding substrate pockets, covering a surface area on the protein and on the macrocycle of 368 $Å^2$ and 558 $Å^2$, respectively (Table S5). The macrocycles' conformations and interactions are equivalent in the two active sites of the two-thrombin molecules present in the asymmetric unit. The chlorine atom of the 4-chlorobenzyl functional group points toward the bottom of the primary specificity S1 pocket, where it likely forms a halogen-aromatic π interaction (~4.0 Å) with the aromatic ring of Tyr228. Notably, the 4-chlorobenzyl ring stacks on top the Trp15 – Gly216 peptide bond. Most of the polar interaction of **T3** with human α-thrombin are mediated by the backbone of **T3** including the amide moiety (N3-C19-O3) and both main chain oxygen O1 and sulfur S1 of **T3** (Table S8). The main chain nitrogen N1 and N3 of **T3** form hydrogen bonds with the main chain oxygen of Gly216 (Gly216 O). Additional polar contacts are established between the main chain oxygen of the nearby Glu97A (**T3** S1 with Glu97A O) and both the main chain nitrogen and oxygen of Gly216 (**T3** O3 with Gly216 N and Gly216 O, and **T3** N3 with Gly216 N). The binding of **T3** to human α-thrombin is further mediated by multiple hydrophobic contacts by main and side chains of adjacent enzyme residues (Table S8). Analogously to **T1**, the phenyl ring (C1, C23–C27) of the macrocycle backbone lays towards the hydrophobic cage shaped by the side chains of residues Tyr60A and Trp60D (proximal S2 pocket) as well as Leu99 (distal S3 pocket) where it forms an offset π-stacking interaction with Tyr60A side chain. An additional offset π-stacking interaction is established by the *trans*-alkene aminothiol element (C4–C5) with the Trp215 side chain. Again, the piperidine six-member heterocycle ring (C1–C6) of **T3** point towards the solvent. Finally, intermolecular interactions are observed between atoms of **T3** and the side chain of the Arg173 of the opposite human α-thrombin molecule present in the asymmetric unit. This contact is favored by the presence of sulfate ion (SO_4^{2-}) closed to the macrocycle that

appear to promote the formation of few non polar contacts with side chain atoms of Arg173 and Glu271 as well as a hydrogen bond between the side chain nitrogen of Arg173 (Arg173 NH1) and the O2 of **T3**.

MATERIALS AND METHODS

Chemical synthesis of building blocks and amino acids

All reagents and solvents were of analytical grade and used without further purification as obtained from commercial suppliers. Reactions were monitored by thin-layer chromatography (TLC) using silica gel coated plates (analytical SiO_2-60, F-254) and/or by HPLC-MS analysis. TLC plates were visualized under UV light or by dipping into a solution of potassium permanganate (10 g/L in water) followed by visualization with a heatgun. Rotary evaporation of solvents was carried out under reduced pressure at a temperature below 40 °C. HPLC-MS analyses were performed with a UHPLC and single quadrupole MS system (Shimadzu LCMS-2020) using a C18 reversed phase (RP) column (Phenomenex Kinetex 2.1×50 mm C18 column, 100 Å pore, 2.6 µm particle). A linear gradient of solvent B (0.05% HCOOH in MeCN) over solvent A (0.05% HCOOH in water) rising from 0% to 60% during t = 1.00–6.00 min was applied at a flow rate of 1.00 mL/min. Nuclear magnetic resonance (NMR) spectra were recorded on a Bruker Avance III (^{1}H NMR and ^{13}C NMR recorded at 400 and 101 MHz, respectively) equipped with a cryogenically cooled probe. All spectra were recorded at 298 K. Chemical shifts are reported in ppm relative to deuterated solvent as internal standard (δ_H DMSO-d_6 2.50 ppm; δ_C DMSO 39.52 ppm; δ_H $CDCl_3$ 7.26 ppm; δ_C $CDCl_3$ 77.16 ppm). High-resolution mass spectrometry (HRMS) measurements were recorded on a Xevo G2-XS QTof time-of-flight (TOF) mass spectrometer.

<u>*S*-(3-((tert-butoxycarbonyl)amino)propyl) benzenesulfonothioate (**S1**)</u>

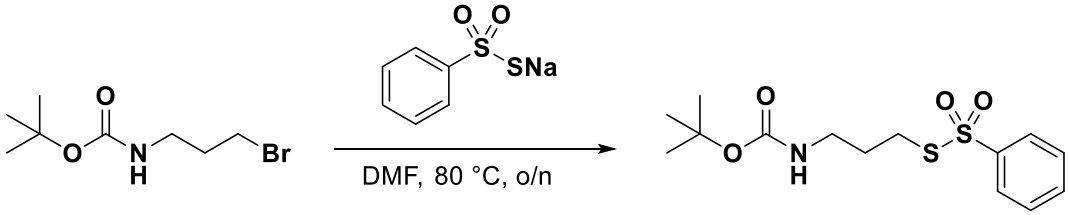

To a stirring solution of 3-(Boc-amino)propyl bromide (6.02 g, 25.3 mmol, 1.0 equiv.) in DMF (120 mL) was added sodium benzenethionosulfonate (7.48 g, 38.0 mmol, 1.5 equiv.; tech. 85%) and the solution was stirred overnight at 80 °C. After cooling down, the reaction mixture was concentrated under reduced pressure, resuspended in water (100 mL) and extracted with EtOAc:hexanes (2×150 mL, 10:1, v/v). The combined organic layers were washed with water (3×150 mL) and brine (150 mL), dried over anhydrous Na_2SO_4 and concentrated under reduced pressure to afford crude **S1** (8.21 g, 24.8 mmol, 98%) as a yellow-tainted oil. The applied extraction procedure would co-purify also the starting material 3-(Boc-amino)propyl bromide but this molecule was not detected in the extracted product. TLC (25% EtOAc in hexanes): R_f = 0.25 ($KMnO_4$ stain). ^{1}H NMR (400 MHz, $CDCl_3$) δ 7.98–7.90 (m, 2H), 7.70–7.61 (m, 1H), 7.60–7.52 (m, 2H), 3.16 (q, J = 6.4 Hz, 2H), 3.02 (t, J = 7.2 Hz, 2H), 1.83 (p, J = 6.8 Hz, 2H), 1.43 (s, 9H).

tert-butyl (3-chloropropyl)(methyl)carbamate (**S2**)

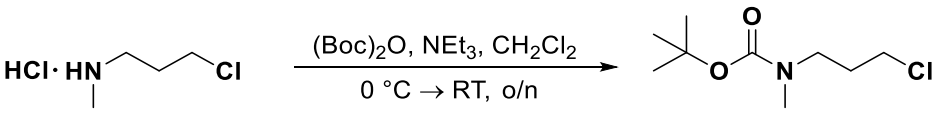

S2 (quant.)

A stirring solution of 3-chloropropyl-*N*-methylamine hydrochloride (4.32 g, 30.0 mmol, 1.0 equiv.) and di-*tert*-butyl dicarbonate (6.54 g, 30.0 mmol, 1.0 equiv.) in CH_2Cl_2 (150 mL) was cooled to 0 °C under argon atmosphere. NEt_3 (4.18 mL, 30.0 mmol, 1.0 equiv.) was added dropwise over 5 min and the solution was stirred overnight going towards ambient temperature. The reaction mixture was concentrated under reduced pressure and resuspended in EtOAc (120 mL). The solution was washed with aq. HCl (1 M, 2×120 mL), sat. $NaHCO_3$ (120 mL) and brine (120 mL), dried over anhydrous Na_2SO_4 and concentrated under reduced pressure to afford crude **S2** (6.22 g, 30.0 mmol, quant.) as a colorless oil.* TLC (25% EtOAc in hexanes): R_f = 0.45 ($KMnO_4$ stain). ^{1}H NMR (400 MHz, $CDCl_3$) δ 3.55 (t, *J* = 6.5 Hz, 2H), 3.36 (t, *J* = 6.8 Hz, 2H), 2.87 (s, 3H), 2.06–1.91 (m, 2H), 1.46 (s, 9H). CAS RN: 114326-14-6. *Product is volatile, so limit time under low pressure.

S-(3-((tert-butoxycarbonyl)(methyl)amino)propyl) benzenesulfonothioate (**S3**)

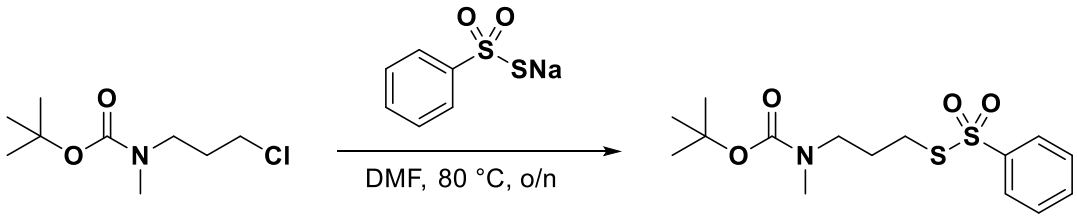

S2 **S3** (87%)

To a stirring solution of **S2** (3.51 g, 16.9 mmol, 1.0 equiv.) in DMF (25 mL) was added sodium benzenethionosulfonate (5.47 g, 27.9 mmol, 1.65 equiv.; tech. 85%) and the solution was stirred overnight at 80 °C. After cooling down, the reaction mixture was concentrated under reduced pressure, resuspended in water (100 mL) and extracted with EtOAc:hexanes (2×75 mL, 10:1, v/v). The combined organic layers were washed with water (3×75 mL) and brine (75 mL), dried over anhydrous Na_2SO_4 and concentrated under reduced pressure to afford crude **S3** (5.07 g, 14.7 mmol, 87%) as a yellow-tainted oil. The applied extraction procedure would co-purify also the starting material **S2** but this molecule was not detected in the extracted product. TLC (12.5% EtOAc in hexanes): R_f = 0.30 ($KMnO_4$ stain). ^{1}H NMR (400 MHz, $CDCl_3$) δ 8.01–7.88 (m, 2H), 7.69–7.50 (m, 3H), 3.24 (t, *J* = 6.7 Hz, 2H), 2.96 (t, *J* = 7.3 Hz, 2H), 2.77 (s, 3H), 1.85 (p, *J* = 6.8 Hz, 2H), 1.42 (s, 9H).

tert-butyl (*Z*)-(4-chlorobut-2-en-1-yl)carbamate (**S4**)

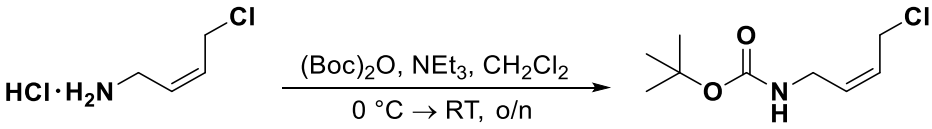

S4 (98%)

A stirring solution of *cis*-4-chloro-2-butenylamine hydrochloride (2.50 g, 17.6 mmol, 1.0 equiv.) and di-*tert*-butyl dicarbonate (3.84 g, 17.6 mmol, 1.0 equiv.) in CH_2Cl_2 (75 mL) was cooled to 0 °C under argon atmosphere. NEt_3 (2.45 mL, 17.6 mmol, 1.0 equiv.) was added dropwise over 5 min and the solution was stirred overnight going towards ambient temperature. The reaction mixture was concentrated under reduced pressure and resuspended in CH_2Cl_2 (100 mL). The solution was washed with aq. HCl (1 M, 2×100 mL), sat. $NaHCO_3$ (100 mL) and brine (100 mL), dried over anhydrous Na_2SO_4 and concentrated under reduced pressure to afford crude **S4** (3.55 g, 17.3 mmol, 98%) as a light-brown solid. TLC (25% EtOAc in hexanes): R_f = 0.30 ($KMnO_4$ stain). ^{1}H NMR (400 MHz, $CDCl_3$) δ 5.82–5.70 (m, 1H), 5.63 (dt, *J* = 10.8, 6.9 Hz, 1H), 4.59 (br s, 1H), 4.12 (d, *J* = 7.8 Hz, 2H), 3.83 (t, *J* = 6.6 Hz, 2H), 1.44 (s, 9H). CAS RN: 123642-28-4. Spectral data is in agreement with literature.[1]

(*Z*)-*S*-(4-((tert-butoxycarbonyl)amino)but-2-en-1-yl) benzenesulfonothioate (**S5**)

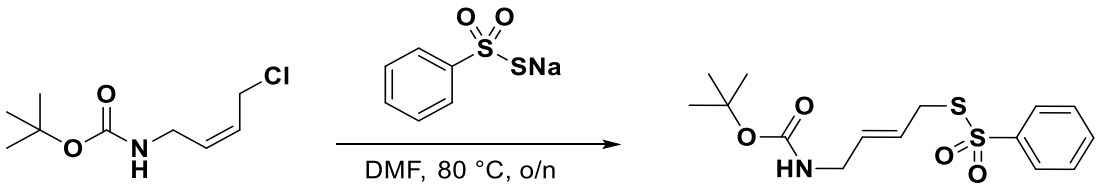

S4 **S5** (85%)

To a stirring solution of **S4** (3.55 g, 17.3 mmol, 1.0 equiv.) in DMF (70 mL) was added sodium benzenethionosulfonate (6.77 g, 34.5 mmol, 2.0 equiv.; tech. 85%) and the solution was stirred overnight at 80 °C. After cooling down, the reaction mixture was concentrated under reduced pressure, resuspended in water (400 mL) and extracted with EtOAc (3×100 mL). The combined organic layers were washed with water (3×200 mL) and brine (200 mL), dried over anhydrous Na_2SO_4 and concentrated under reduced pressure to obtain crude **S5** (5.03 g, 14.6 mmol, 85%*) as a brown oil. The applied extraction procedure would co-purify also the starting material **S4** but this molecule was not detected in the extracted product. TLC (25% EtOAc in hexanes): R_f = 0.20 ($KMnO_4$ stain). ^{1}H NMR (400 MHz, $CDCl_3$) δ 7.94–7.87 (m, 2H), 7.68–7.60 (m, 1H), 7.60–7.49 (m, 2H), 5.62 (dt, *J* = 15.4, 5.6 Hz, 1H), 5.46 (dtt, *J* = 15.4, 7.0, 1.5 Hz, 1H)**, 4.43 (br s, 1H), 3.67 (dq, *J* = 7.0, 1.1 Hz, 2H), 3.60 (t, *J* = 6.1 Hz, 2H), 1.43 (s, 9H). *The crude compound purity is lower than for other thiosulfonate building blocks, but still provides excellent resin quality in the subsequent resin loading steps (see chromatogram in Figure S2). Albeit not necessary prior to resin loading, the crude product

can be purified by silica column chromatography.**During the reaction, the *cis*-alkene converts into the *trans*-alkene. This is confirmed by the increase in the coupling constant between the two alkene protons (from 10.8 to 15.4 Hz), and was also observed from the observed X-ray co-crystal structure of macrocycle **T3** in complex with thrombin (Figures 6b and S15).

tert-butyl 3-(((phenylsulfonyl)thio)methyl)azetidine-1-carboxylate (**S6**)

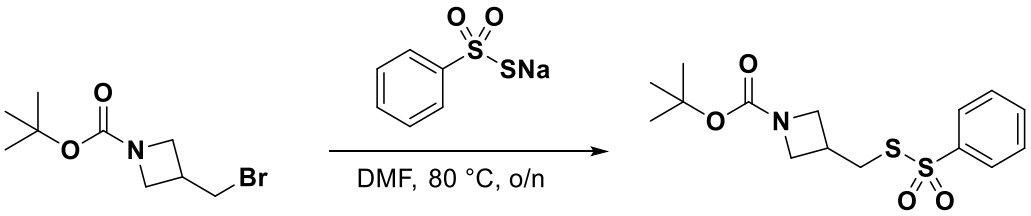

S6 (quant.)

To a stirring solution of 1-Boc-3-bromomethylazetidine (1.93 g, 7.71 mmol, 1.0 equiv.) in DMF (25 mL) was added sodium benzenethionosulfonate (2.41 g, 12.3 mmol, 1.6 equiv.; tech. 85%) and the solution was stirred overnight at 80 °C. After cooling down, the reaction mixture was concentrated under reduced pressure, resuspended in water (100 mL) and extracted with EtOAc:hexanes (2×75 mL; 10:1, v/v). The combined organic layers were washed with water (2×75 mL), sat. $NaHCO_3$ (75 mL) and brine (75 mL), dried over anhydrous Na_2SO_4 and concentrated under reduced pressure to obtain crude **S6** (2.65 g, 7.71 mmol, quant.) as a yellow-tainted oil. The applied extraction procedure would co-purify also the starting material 1-Boc-3-bromomethylazetidine but this molecule was not detected in the extracted product. TLC (33% EtOAc in hexanes): R_f = 0.30 ($KMnO_4$ stain). ^{1}H NMR (400 MHz, $CDCl_3$) δ 7.93 (d, *J* = 7.5 Hz, 2H), 7.66 (t, *J* = 7.4 Hz, 1H), 7.58 (t, *J* = 7.6 Hz, 2H), 3.96 (t, *J* = 8.6 Hz, 2H), 3.52 (dd, *J* = 9.0, 5.3 Hz, 2H), 3.23 (d, *J* = 7.8 Hz, 2H), 2.85–2.70 (m, 1H), 1.41 (s, 9H).

tert-butyl 4-((phenylsulfonyl)thio)piperidine-1-carboxylate (**S7**)

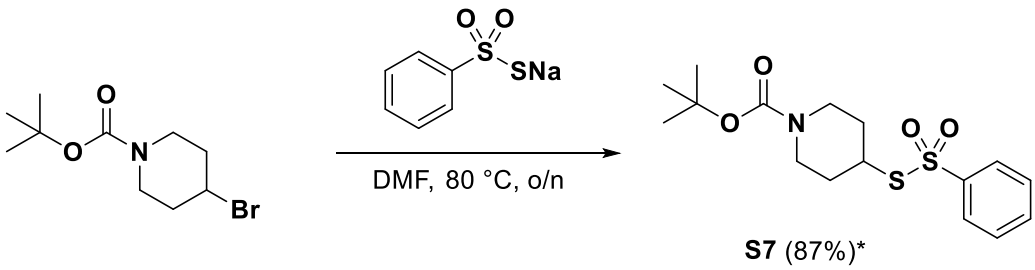

S7 (87%)*

To a stirring solution of 1-*N*-Boc-4-bromopiperidine (2.25 g, 8.51 mmol, 1.0 equiv.) in DMF (25 mL) was added sodium benzenethionosulfonate (2.75 g, 14.0 mmol, 1.65 equiv.; tech. 85%) and the solution was stirred overnight at 80 °C. Due to incomplete overnight reaction (monitored by TLC), additional sodium benzenethionosulfonate (1.38 g, 7.00 mmol, 0.83 equiv.; tech. 85%) was added and the reaction was stirred another 24 h at 80 °C. After cooling down, the reaction mixture was concentrated under reduced pressure, resuspended in water (100 mL) and extracted with EtOAc:hexanes (2×75 mL; 10:1, v/v). The combined organic layers were washed with water (2×75 mL), sat. $NaHCO_3$ (75 mL) and brine (75 mL), dried over anhydrous Na_2SO_4 and concentrated under reduced pressure to obtain crude **S7** (2.65 g, 7.41 mmol, 87%*) as a yellow-tainted oil. The applied extraction procedure would co-purify also the starting material 1-*N*-Boc-4-bromopiperidine but this molecule was not detected in the extracted product. TLC (33% EtOAc in hexanes): R_f = 0.44 ($KMnO_4$ stain). ^{1}H NMR (400 MHz, $CDCl_3$) δ 8.01–7.89 (m, 2H), 7.71–7.61 (m, 1H), 7.60–7.50 (m, 2H), 3.89–3.63 (m, 2H), 3.55–3.39 (m, 1H), 3.11–2.91 (m, 2H), 1.96–1.86 (m, 2H), 1.64–1.51 (m, 2H), 1.42 (s, 9H). *The substitution reaction progresses significantly slower than for the preparation of the other thiosulfonate building blocks. Additionally, the crude purity is lower, but still provides good resin quality in the subsequent resin loading steps (see chromatogram in Figure S2). Albeit not necessary prior to resin loading, the crude product can be purified by silica column chromatography.

tert-butyl 4-(((phenylsulfonyl)thio)methyl)piperidine-1-carboxylate (**S8**)

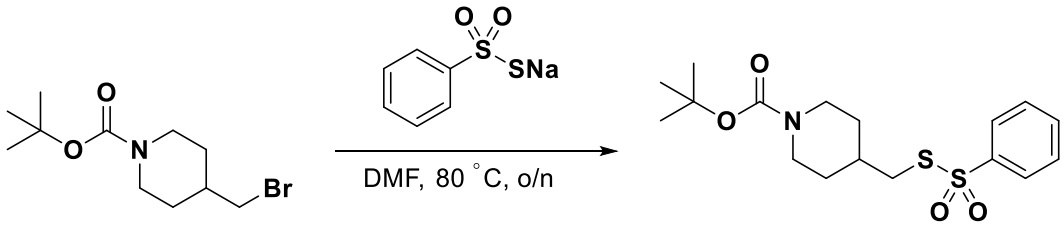

S8 (96%)

To a stirring solution of 1-*N*-Boc-4-(bromomethyl)piperidine (2.16 g, 7.76 mmol, 1.0 equiv.) in DMF (50 mL) was added sodium benzenethionosulfonate (2.52 g, 12.8 mmol, 1.65 equiv.; tech. 85%) and the solution was stirred overnight at 80 °C. After cooling down, the reaction mixture was concentrated under reduced pressure, resuspended in water (100 mL) and extracted with EtOAc:hexanes (2×75 mL; 10:1, v/v). The combined organic layers were washed with water

(2×75 mL), sat. $NaHCO_3$ (75 mL) and brine (75 mL), dried over anhydrous Na_2SO_4 and concentrated under reduced pressure to obtain crude **S8** (2.76 g, 7.42 mmol, 96%) as a clear oil. The applied extraction procedure would co-purify also the starting material 1-*N*-Boc-4-(bromomethyl)piperidine but this molecule was not detected in the extracted product. TLC (25% EtOAc in hexanes): R_f = 0.30 ($KMnO_4$ stain). ^{1}H NMR (400 MHz, $CDCl_3$) δ 8.01–7.87 (m, 2H), 7.70–7.61 (m, 1H), 7.61–7.51 (m, 2H), 4.20–3.94 (m, 2H), 2.91 (d, *J* = 6.5 Hz, 2H), 2.58 (t, *J* = 12.8 Hz, 2H), 1.73–1.57 (m, 3H), 1.43 (s, 9H), 1.14–0.98 (m, 2H).

(*S*)-2-((((9*H*-fluoren-9-yl)methoxy)carbonyl)amino)-3-(5-chlorofuran-2-carboxamido) propanoic acid (Fmoc-Thio-OH)

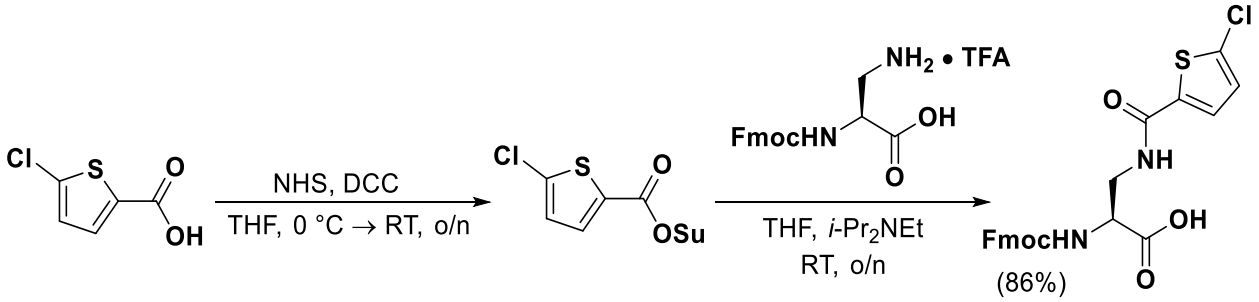

The synthesis was adapted from a previous procedure of similar amino acids:[2] 5-chlorothiophene-2-carboxylic acid (2.44 g, 15.0 mmol, 1.5 equiv.) and *N*-hydroxysuccinimide (NHS; 1.61 g, 14.0 mmol, 1.4 equiv.) were dissolved in THF (100 mL) and stirred under argon atmosphere. The solution was cooled to 0 °C after which a solution of *N*,*N*'-dicyclohexylcarbodiimide (DCC; 2.89 g, 14.0 mmol, 1.4 equiv.) dissolved in THF (30 mL) was added slowly to the reaction mixture. The solution slowly became turbid and was allowed to stir overnight going towards ambient temperature, after which the solution was filtered. Meanwhile, Fmoc-Dap(Boc)-OH (4.26 g, 10.0 mmol, 1.0 equiv.) was stirred in CH_2Cl_2 (20 mL; turbid solution) and TFA (20 mL) was added slowly to the solution. The solution immediately became yellowish clear and bubbles were forming. After bubbling had stopped the solution was stirred an additional 30 min at ambient temperature after which solvent was removed under a stream of nitrogen. Excess TFA was removed by co-evaporation with CH_2Cl_2:toluene (50 mL, 1:1, v/v). The residue was resuspended in THF (40 mL) followed by addition of *i*-Pr_2NEt (5.75 mL, 33.0 mmol, 3.3 equiv.). The solution was then poured into the mother liquour containing the NHS-activated thiophene and stirred overnight at ambient temperature. After completion, the solution was concentrated under reduced pressure, redissolved in EtOAc:hexane (300 mL, 10:1, v/v) and washed twice with water (100 mL) and brine (100 mL). The organic layer was dried over anhydrous Na_2SO_4 and concentrated under reduced pressure. The crude product was purified by silica column chromatography to obtain the Fmoc-protected amino acid building block **Fmoc-Thio-OH** (4.06 g, 8.62 mmol, 86%) as an off-white solid.* TLC (5% MeOH and 0.5% AcOH in CH_2Cl_2): R_f = 0.2 (UV). ^{1}H NMR (400 MHz, DMSO-d_6) δ 12.74 (br s, 1H), 8.68 (t, *J* = 5.8

Hz, 1H), 7.89 (d, *J* = 7.5 Hz, 2H), 7.70 (d, *J* = 7.4 Hz, 2H), 7.65 (d, *J* = 8.2 Hz, 1H), 7.61 (d, *J* = 4.1 Hz, 1H), 7.41 (t, *J* = 7.4 Hz, 2H), 7.30 (q, *J* = 7.6 Hz, 2H), 7.18 (d, *J* = 4.0 Hz, 1H), 4.43–4.11 (m, 4H), 3.68–3.50 (m, 2H, overlap with residual water). ^{13}C NMR (101 MHz, DMSO) δ 171.9, 160.5, 156.0, 143.80, 143.77, 140.7, 138.7, 133.1, 128.2, 128.1, 127.6, 127.1, 125.24, 125.21, 120.1, 65.7, 53.5, 46.6, 40.3 (overlap with solvent peak). HRMS *m/z* calcd for $C_{23}H_{20}ClN_2O_5S^+$ $[M+H]^+$, 471.0776; found 471.0786. *To remove residual acetic acid, we recommend to resuspend and freeze the compound in MeCN:H_2O followed by lyophilization.

Resin preparation

Preparation of thiol resin

The following procedure described the protocol to generate thiol resin applied in this work. In later experiments, we found that commercially offered thiol-functionalized PS (e.g. Polystyrene A SH from Rapp Polymere GmbH, Cat. #HA40004.0; ~0.85 mmol/g and 200–400 mesh) is equally suited, and we recommend the latter one as it can be purchased.

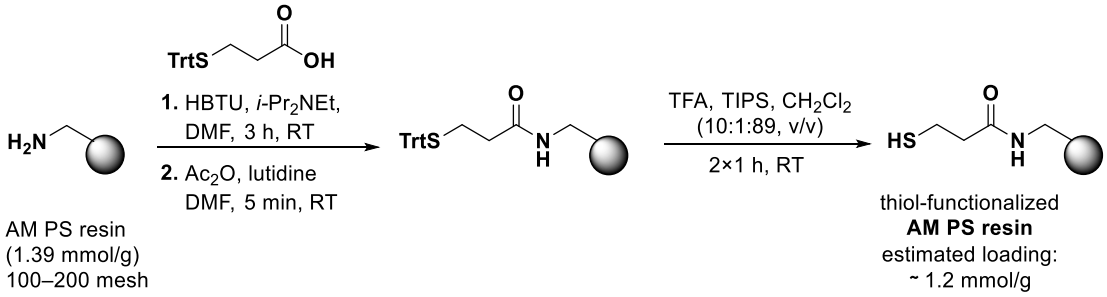

Pre-washing: Each 25 mL-fritted syringe was loaded with ~0.8 g (1.11 mmol) aminomethyl)polystyrene resin (AM PS resin; 1.39 mmol/g, 100–200 mesh; Aapptec, cat. #RAZ001) and pre-washed using MeOH (2×10 mL), CH_2Cl_2 (3×10 mL), 1% (v/v) TFA in CH_2Cl_2 (2×10 mL), *i*-Pr_2NEt in CH_2Cl_2 (1.2 M; 2×10 mL for 5 min), CH_2Cl_2 (2×10 mL) and DMF (2×10 mL).

Coupling: A solution of 3-(tritylthio)propionic acid (1.16 g, 3.33 mmol, 3.0 equiv.) and 2-(1*H*-benzotriazol-1-yl)-1,1,3,3-tetramethyluronium hexafluorophosphate (HBTU; 1.27 g, 3.33 mmol, 3.0 equiv.) in DMF (10 mL) was activated with *i*-Pr_2NEt (1.16 mL, 6.66 mmol, 6.0 equiv.) and added to the fritted syringe and agitated for 3 h at ambient temperature. The resin was filtered and washed with DMF (3×10 mL) and CH_2Cl_2 (3×10 mL) followed by drying the beads (first under mild suction and then under reduced pressure overnight (<0.5 mbar)). The loading of the Mpa(Trt) resin was determined to ~1.2 mmol/g (weight based).

Capping: A solution of 5% Ac_2O and 6% lutidine in DMF (12 mL; v/v/v) was added to the resin and incubated it for 5 min at ambient temperature. The resin was drained and washed with DMF (3×10 mL) and CH_2Cl_2 (3×10 mL).

Deprotection: A solution of 10% TFA and 1% TIPS in CH_2Cl_2 (15 mL, v/v/v) was added to the resin and agitated for 1 h at ambient temperature. The resin was washed with CH_2Cl_2 (3×10 mL) and the

procedure was repeated once to afford high-loaded thiol-functionalized polystyrene resin that was utilized for subsequent disulfide exchange and loading of aminothiol derivatives (termed SH PS resin).

Immobilization of aminothiol **1** (Mea) onto resin

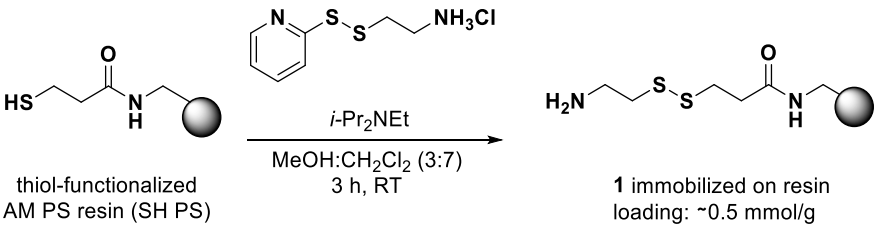

Dithiol exchange: Each 25 mL-fritted syringe was loaded with ~0.4 g (0.48 mmol). SH PS resin was swelled in CH_2Cl_2 (10 mL) and then drained. 2-pyridylthio cysteamine hydrochloride salt[3] (0.21 g, 0.96 mmol, 2.0 equiv.) was dissolved in MeOH:CH_2Cl_2 (19 mL, 3:7, v/v) followed by addition of *i*-Pr_2NEt (167 µL, 0.96 mmol, 2.0 equiv.). The solution was added to the resin and agitated for 3 h at ambient temperature. The resin was drained and washed with MeOH:CH_2Cl_2 (2×10 mL, 3:7, v/v), DMF (2×10 mL), *i*-Pr_2NEt in DMF (1.2 M; 10 mL for 5 min), DMF (3×10 mL) and CH_2Cl_2 (2×10 mL) followed by drying the beads (first under mild suction and then under reduced pressure overnight (<0.5 mbar). Average resin loading (free aminothiol derivative loaded onto resin) was determined to ~0.5 mmol/g by Fmoc-quantitation from coupling Fmoc-Gly-OH using litterature procedure.[4]

Qualitative controls: (1) Kaiser test: complete purple/blue coloration of the beads. (2) Ellman's reagent on beads: no coloration.

Immobilization of aminothiols **2**–**7** onto resin

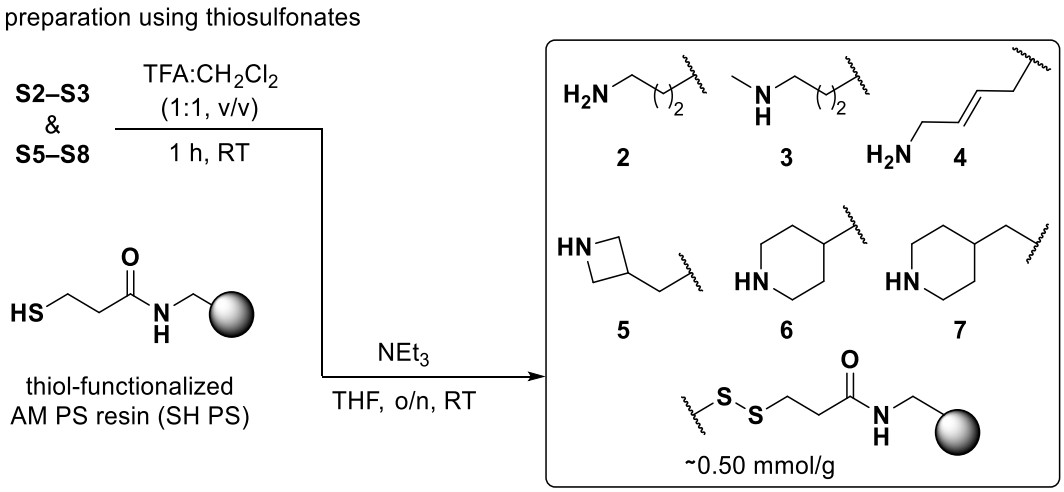

Deprotection: N-Boc protected thiosulfonate intermediate (**S2**, **S3**, **S5**, **S6**, **S7** or **S8**; ~7.0 mmol) was dissolved in CH_2Cl_2 (10 mL) followed by dropwise addition of TFA until CO_2 bubbling was observed (~10 mL). The solution was stirred for another 1 h at ambient temperature whereafter

solvent was removed under a stream of nitrogen. Excess TFA was removed under reduced pressure by co-evaporation with CH_2Cl_2:MeOH solution (1:1, v/v) to afford the TFA salts of the thiosulfonates.
Dithiol exchange: Each 25 mL-fritted syringe was loaded with ~0.8 g (0.96 mmol) SH PS. The resin was swelled in THF (15 mL) and then drained. The desired thiosulfonate TFA salt (2.40–2.88 mmol, 2.5–3.0 equiv.) was dissolved in THF (15 mL), and NEt_3 (803 µL, 5.76 mmol, 6.0 equiv.) was added. The solution was added to the resin and agitated overnight at ambient temperature. The resin was drained, washed with THF (3×15 mL) and CH_2Cl_2 (2×15 mL) followed by drying of the beads (first under suction and then under reduced pressure overnight (<0.5 mbar). Resin loading (free aminothiol derivative loaded onto resin) was even between the different aminothiol building blocks and averaged to ~0.5 mmol/g by Fmoc-quantitation from coupling Fmoc-Gly-OH using litterature procedure.[4] Due to sufficient yields to our application, optimization towards higher resin loading was not pursued in this work.
Qualitative controls: (1) Kaiser test: complete purple/blue coloration of the beads. (2) Ellman's reagent on beads: no coloration.

Automated solid-phase peptide synthesis (SPPS)

SPPS was performed on an Intavis Multipep RSi synthesizer using either plates or syringes:
Plates: Polypropylene (PP) 96-well filter plates were equipped with ~2 µmol/well of resin (**1**–**7** immobilised onto SH PS resin via a disulfide bridge), and washed with DMF (6×225 µL). Coupling was performed with 53 µL of amino acids (500 mM in DMF, 26.5 µmol, 13.3 equiv.), 50 µL of 1-[bis(dimethylamino)methylene]-1*H*-1,2,3-triazolo[4,5-b]pyridinium 3-oxide hexafluorophosphate (HATU; 500 mM in DMF, 25 µmol, 12.5 equiv), 13 µL of *N*-methylmorpholine (NMM; 4 M in DMF, 52 µmol, 26.0 equiv.), and 5 µL *N*-methylpyrrolidone (NMP). For couplings of expensive and/or synthesized amino acids (*t*-Acha, APipAc, 2Amb and Thio; consult Table S9 for information on amino acid abbreviations), 75 µL of amino acid (170 mM in DMF, 12.75 µmol, 6.4 equiv.), 25 µL HATU (500 mM in DMF, 12.5 µmol, 6.25 equiv.), 7 µL of *N*-methylmorpholine (4 M in DMF, 28 µmol, 14 equiv.), and 5 µL NMP were used. All components were pre-mixed for one minute, then added to the resin (two hour reaction, no shaking). Coupling was performed twice and resin was washed with DMF (6×225 µL). Fmoc deprotection was performed using 20% (v/v) piperidine in DMF (120 µL, 2×2 min) and the resin was washed with DMF (6×225 µL). At the end of the peptide synthesis, the resin was washed with CH_2Cl_2 (2×200 µL) and the resin beads were dried under suction.
Syringes: To a 5 mL syringe reactor was added resin (**1**–**7** immobilised onto SH PS resin via a disulfide bridge; 25 µmol/syringe), and washed with DMF (6×150 µL). Coupling was performed with 210 µL of amino acid (500 mM, 105 µmol, 4.2 equiv.), 200 µL HATU (500 mM, 100 µmol, 4.0 equiv.), 50 µL of NMM (4.0 M, 200 µmol, 8.0 equiv.) and 5 µL NMP. All components were pre-mixed for one minute, then added to the resin (two hour reaction, with shaking). Couplings were performed twice, then the resin was washed with DMF (2×600 µL). Fmoc deprotection was performed using using

20% piperidine in DMF (450 µL, 2×2 min), and the resin was washed with DMF (7×600 µL). At the end of the peptide synthesis, the resin was washed with CH_2Cl_2 (2×600 µL) and resin beads were dried under suction.

Exception: For synthesis of the chloroalkane (CA) containing macrocycles, synthesis was carried out manually. Each elongation step was performed by applying the relevant amino acid (3.0 equiv.), HATU (2.9 equiv.) and *i*-Pr_2NEt (6.0 equiv.) in DMF (~1 mL). For coupling of CA-building block (Halo-PEG(2)-Suc;[5] CAS RN 1488363) only 1.2 equiv. of reagent was used, together with HATU (1.2 equiv.) and *i*-Pr_2NEt (3.0 equiv.).

Reductive release procedure

Plates

Side-chain protecting group removal:

After automated SPPS, the bottom of a 96-well synthesis plate was sealed by pressing it onto a soft 6 mm thick ethylene-vinyl acetate pad (see Table S10 for catalogue and product numbers used in this work). The resin was incubated with TFA/TIPS/H_2O (300 µL, 95:2.5:2.5, v/v/v) for one hour covered by an adhesive PP plate lid. The TFA solution was discarded, and the resin was washed with CH_2Cl_2 (3×300 µL), and the procedure was repeated once.

Reductive release: After air drying for at least an hour, the plate was again sealed by presdsing it onto a soft 6 mm thick ethylene-vinyl acetate pad, and a solution of 1,4-butanedithiol (BDT) and NEt_3 in DMF (both 100 mM; 200 µL, 20 µmol, 10 equiv. relative to resin loading) was added to the resin, and plates were agitated overnight at ambient temperature. The following day, the DMF solutions were pushed into a 96-well deep well plate via centrifugation (1000 rpm) and the reductive release procedure was repeated once for 5 h and unified into the same 96-well deep well plate.

Removal of solvent, BDT and base: A solution of TFA in milliQ-water (10% (v/v); 62 µL, 2 equiv. relative to NEt_3) was added to the wells, and the peptides were dried by RVC (30 °C, 1750 rpm, 0.1 mbar).

Resolubilization and transfer: The dried peptide pellets were dissolved in DMSO (50 µL) and transferred to an Echo® qualified 384-well PP source plate.

Concentration determination: Ellman's assay was conducted to determine the concentrations of the di-thiol peptide stocks. Ellman's reagent (DTNB) was dissolved in assay buffer (150 mM NH_4HCO_3 in water:MeCN (90:10, v/v), pH 8) to a concentration of 10 mM. To a 384-well black microplate with transparent bottom was transferred dithiol peptide in DMSO (135 nL) by acoustic droplet ejection (ADE). Assay buffer (24 µL) was dispensed by bulk dispensing prior to addition of DTNB solution (6 µL). Plates were centrifuged (400 *g*, 2 min) and absorbance (412 nm) was measured on a TECAN M200 plate reader. Concentration of di-thiol peptides were calculated using the previously recorded calibration curve below:

Equation I

$$\text{abs} = 0.287\ \frac{\text{mAU}}{\text{nmol}} \cdot c + 0.0028$$

$$\text{where: abs} = \text{absorbance at 412 nm in mAU}$$

$$\text{c} = \text{concentration of dithiol peptide}$$

For concentration distribution of the S1-targeted library, please see Figure S4.

Syringes

Side-chain protecting group removal: After automated SPPS (25 µmol scale), the fritted syringe containing the resin was incubated with TFA/TIPS/H_2O (4 mL, 95:2.5:2.5, v/v/v) for 2 h at ambient temperature. The TFA solution was discarded, and the resin was washed with CH_2Cl_2 (5×4 mL) and DMF (4 mL).

Reductive release: After air drying for at least 1 h, a solution of BDT and NEt_3 in DMF (both 100 mM; 2.0 mL, 200 µmol, 8 equiv. relative to resin loading) was added to the syringe, which was agitated overnight at ambient temperature. The following day, the DMF solution was pushed into a 50 mL conical tube.

Removal of solvent, BDT and base: A solution of TFA in milliQ-water (10% (v/v); 312 µL, 2 equiv. relative to NEt_3) was added to peptide solution, which was dried by RVC (30 °C, 1750 rpm, 0.1 mbar) to afford the crude linear dithiol peptide ready for immediate cyclization in the next step.

Macrocyclization procedure

Plates

Transfer to microtiter plates: Based on the determined concentration of each di-thiol peptide in DMSO, 40 nmol of dithiol peptide in DMSO was transferred into 384-well PP plates (one plate per linker) using ADE.

Peptide reduction: As dithiol peptides oxidize in DMSO over time, we ensured that the peptides were fully reduced by adding a solution of BDT and NEt_3 in DMF (both 100 mM; 20 µL, 2 µmol, 50 equiv.) to each well, followed by incubation for 30 min at ambient temperature. A solution of TFA in milliQ-water (10% (v/v); 3 µL, 2 equiv. relative to NEt_3) was added and the peptides were dried by RVC (30 °C, 1750 rpm, 0.1 mbar) to afford the fully reduced dithiol peptides as dried pellets.

Cyclization: Biselectrophilic linkers (**L1**−**L7**, Table S9) were dissolved in a degassed 60 mM solution of NH_4HCO_3 in MeCN:H_2O (1:1, v/v, pH 8) to a final concentration of 4 mM. The prepared linker solutions (40 µL, 160 nmol, 4 equiv. relative to dithiol peptide) was added to the 384-well PP plates by bulk dispensing, which were sealed with adhesive PP lids and agitated for 2 h at ambient temperature.

Linker quenching: β-mercaptoethanol (β-ME) was dissolved in the cyclization buffer to a final concentration of 32 mM. The prepared solution (20 µL/well, 4 equiv. relative to linker) was added by bulk dispensing and incubated for 1 h at ambient temperature without plate lids.

Removal of solvent and β-ME, and resolubilization: Solvent was removed by RVC (40 °C, 1750 rpm, 0.1 mbar) to afford the peptide macrocycles as pellets, which were dissolved in DMSO (20 µL) to afford 2 mM macrocyclic peptide libraries that could immediately be applied in subsequent protease screening assays.

Conical tubes

Cyclization: Biselectrophilic linker were dissolved in a degassed 60 mM solution of NH_4HCO_3 in MeCN:H_2O (1:1 (v/v), pH 8) to a final concentration of 2 mM. The prepared linker solutions (12.5 mL, 2 equiv. relative to dithiol peptide assuming a 50% recovery after SPPS and reductive release) was added to a conical tube containing the desired dithiol peptide pellet, and the solution was agitated for approximately 2 h at ambient temperature monitored by HPLC-MS analysis.

Linker quenching: Upon reaction completion, excess linker was quenched by addition of β-ME (14 µL, 200 µmol, 4 equiv. relative to linker) and the solution was agitated for at least 30 min prior to subsequent purification.

Macrocycle purification: Samples were purified by preparative HPLC equipped with a C18 RP Waters OBD column. A linear gradient of solvent B (0.1% TFA in MeCN) over solvent A (0.1% TFA in water) rising linearly from 15% to 60% during t = 2.00–32.00 min was applied at a flow rate of 14.0 mL/min. Pure fractions containing the desired product were unified and lyophilized to afford the products as colorless fluffy materials.

DMSO stocks: Purified macrocycles were transferred into 2 mL centrifuge tubes and DMSO was added to afford 5 mM or 20 mM compound stocks. See Figures S9 and S20 for HPLC chromatograms, and Table S11 for HRMS data.

Protease screens of macrocyclic library

Enzyme inhibition of compound libraries was assessed by measuring the residual enzyme activity in presence of cyclic peptides (10 µM average concentration for thrombin, 20 µM average concentration for FXI, FXII, KLK5 and PK) at 1.0–1.2% final DMSO concentration. Compounds of the macrocyclic libraries (2 mM DMSO stocks in 384-well PP plates; 45 nL for thrombin, 90 nL for the other proteases) were transferred into black 1536-well microtiter OptiPlates via ADE. Applied buffered solutions (see next page) were prepared by filtration through PTFE syringe filters (0.22 µm). Assays were initiated by addition of protease (4.41 µL/well) in appropriate buffer (see list on next page) supplemented with bovine serum albumin (BSA; 0.1% w/v) and added by bulk dispensing. Plates were incubated for 10 min at ambient temperature before fluorogenic substrate (200 µM for

KLK5, 100 µM for the other proteases) in appropriate buffer (4.5 µL) was added by bulk dispensing. Plates were centrifugated (800 *g*, 2 min) and fluorescence intensity was measured using a PHERAstar plate reader (excitation 384 nm, emission 440 nm) in time increments of 150 s over 15 min. Slopes of fluorescence increase (m) were calculated with Microsoft Excel (vers. 16.56). Negative controls were prepared without macrocycle. An average of 12 negative controls was used to calculate residual activities using the following formula:

Equation II

$$\text{residual activity}\ (\%) = \frac{m_{sample}}{m_{DMSO\ control}} \cdot 100$$

Applied buffer compositions and enzyme concentrations

Enzymea and substrates in assays:

	Thrombin	**FXI**	**FXII**	**KLK5**	**PK**
Enzyme supplier	Innovative research (cat. #IHUTHRA)	Innovative research (cat. #IHUFXIA)	Innovative research (cat. #IHUFXIIAB)	From reference [6]	Innovative research (cat. #IHUKLK)
Enzyme conc.	4 nM	0.25 nM	4 nM	5 nM	0.25 nM
Substrate	Cbz-G-G-R-AMC	Boc-F-S-R-AMC	Boc-Q-G-R-AMC	Boc-V-P-R-AMC	Cbz-F-R-AMC
Bachem cat. #	4002155	4012340	4016429	4003460	4003379
Substrate conc.	50 µM	50 µM	50 µM	100 µM	50 µM
Substrate K_M	305 ± 46 µM[7]	n.d.	260 ± 40 µM[8]	200 ± 10 µM[9]	120 ± 28 µM[10]

n.d. = not determined

Buffer composition:

	Thrombin	**FXI**	**FXII**	**KLK5**	**PK**
Tris-HCl (pH 7.4)	50 mM	50 mM	50 mM	50 mM	50 mM
NaCl	150 mM	150 mM	150 mM	100 mM	150 mM
$MgCl_2$	10 mM	10 mM	10 mM	–	10 mM
$CaCl_2$	1 mM	1 mM	1 mM	10 mM	1 mM
Triton-X	0.01%	0.01%	0.01%	0.01%	0.01%

Identification of active species in crude macrocyclic products from hits

The top hits from the library screening (**T1** and **P1**) were re-synthesized and cyclized (40 nmol scale). Dried macrocyclic product was dissolved in MeCN:H_2O (1.5 mL, 1:1, v/v) and fractionated on a Thermo Fisher Dionex UltiMate 3000 system using a C18 NovaPak RP column (10×150 mm, 125 Å pore, 5 µm particle). A linear gradient of solvent B (0.1% TFA in MeCN) over solvent A (0.1% TFA in water) rising linearly from 0% to 80% (for thrombin hit **T1**) or 0% to 95% (for PK hit **P1**) during *t* = 2.00–22.0 min was applied at a flow rate of 4.00 mL/min. Fractions (one fraction/min) were collected in collection tubes and solvent was removed by RVC (30 °C, 1750 rpm, 0.1 mbar). The dried content was redissolved in DMSO (50 µL), transferred to a 384-well PP source plate and dried by RVC (30 °C, 1750 rpm, 0.1 mbar). Fractions were redissolved in DMSO (5 µL for thrombin, 2 µL for PK) and subsequent assays were conducted in black 384-well polystyrene plates with transparent bottom. DMSO fraction solution (0.5 µL) was pipetted to the microtiter plate and appropriate enzyme buffer solution (49.5 µL; similar composition as described above, but with 2 nM thrombin) was added and incubated for 10 min at ambient temperature. Substrate in buffer (25 µL) for a finaly concentration of 50 µM was added, plates were centrifuged (800 *g*, 2 min) and fluorescence intensity was measured using a PHERAstar plate reader (excitation 384 nm, emission 440 nm) in time increments of 150 s over 15 min. Slopes of fluorescence increase (m) were calculated with Microsoft Excel (vers. 16.56). Negative controls were prepared DMSO (0.5 µL) instead of fraction sample. An average of 6 negative controls was used to calculate residual activities using Equation II.

IC_{50} and K_i determination

The half maximal inhibitor concentration (IC_{50}) values were determined by measuring protease inhibition using a similar assay as for the library screening. A series of two-fold dilutions of purified macrocyclic compounds were prepared in 384-well LDV source plates and transferred into 1536-well OptiPlates by ADE (final volume: 45 nL macrocycle/DMSO). Enzyme solution in buffer (4.5 µL) was added by bulk dispensing and incubated for 10 min. Subsequently, substrate in buffer (4.5 µL) was added and plates were centrifuged (700 *g*, 2 min) and fluorescence intensity was measured using a PHERAstar plate reader (excitation 384 nm, emission 440 nm) in time increments of 150 s over 15 min. Slopes of fluorescence increase (m) were calculated with Microsoft Excel (vers. 16.56). Negative controls were prepared without macrocycle. An average of 12 negative controls was used to calculate residual activities using Equation II. IC_{50} values were obtained by fitting the resulting data to a variable slope (four parameters) concentration–response equation using GraphPad Prism (version 6.0.1) and K_i values were calculated based on the IC_{50} using the Cheng-Prusoff equation:

Equation III

$$K_{\mathrm{i}} = \frac{\mathrm{IC}_{50}}{1 + \frac{[S]_0}{K_M}}$$

where $[S]_0$ is the initial substrate concentration and K_M is the Michaelis−Menten constant for the enzyme and substrate.

Parallel artificial membrane permeability assay (PAMPA)

The PAMPA was performed using an adaptation of a previously described procedure: a solution of macrocycle (50 µM) in phosphate buffered saline (PBS; 137 mM NaCl, 2.7 mM KCl, 10 mM Na_2HPO_2, 1.8 mM KH_2PO_2 supplemented with 5% (v/v) DMSO) was prepared. PBS buffer (300 µL, also containing 5% DMSO) was added to a Teflon acceptor plate (Sigma-Millipore; cat. #MSSACCEPT0R), and compound solution (150 µL) was distributed into a 96-well pre-coated PAMPA plate (Corning; cat. #353015), then inserted into the acceptor plate. After overnight incubation (12 h), macrocycle concentration in the acceptor solution is determined by integration of the HPLC-MS spectra in positive ion mode over a mass of [M+0.5] to [M+3.5] Concentration in equilibrium was determined by integration of the MS trace as described for a 16.7 µM solution of macrocycle in PBS buffer containing 5% DMSO. All samples were prepared and measured in triplicates on the same plate.

Percent permeability was calculated using the formula below:

Equation IV

$$\text{permeability (\%)} = \frac{[\text{macrocycle}_{\text{acceptor}}]}{[\text{macrocycle}_{\text{equilibrated}}]} \cdot 100$$

where $[\text{macrocycle}_{\text{acceptor}}]$ represents the area under the curve (AUC) measured on the HPLC-MS for the acceptor wells and $[\text{macrocycle}_{\text{equilibrated}}]$ represents the AUC measured for the samples diluted to the theoretical equilibrium.

P_e values were calculated using the formula below:

Equation V

$$P_e = \frac{V_D \cdot V_A}{(V_D + V_A) \cdot A \cdot t} \cdot -\ln\left(1 - \frac{[\text{macrocycle}_{\text{acceptor}}]}{[\text{macrocycle}_{\text{equilibrated}}]}\right)$$

where V_D and V_A are the volumes of donor and acceptor wells respectively, A is the area of the membrane (0.3 cm^3) and t is the incubation time in seconds.

Compound mass retentions (R) were calculated using the formula below:

Equation VI

$$R = 1 - \frac{C_A(t) \cdot V_A + C_D(t) \cdot V_D}{C_D(t_0) \cdot V_D}$$

where V_D and V_A are the volumes of donor and acceptor wells respectively, C_A and C_D is the concentration in the donor and acceptor, respectively, and t is the incubation time in seconds.

Chloroalkane penetration assay (CAPA)

The CAPA assay[5,11] was done as previously described:[12] The HeLa cell line used for CAPA was generated by Chenoweth and co-workers to stably express HaloTag exclusively in the cytosol[13] and provided by Prof. Joshua A. Kritzer (Department of Chemistry, Tufts University, Medford, MA 02155, United States). Cells were seeded in a 96-well plate the day before the experiment at a density of 4×10^4 cells/well. On the day of the experiment the media was aspirated, and Opti-MEM (100 µL; Gibco, cat. #11058-021) was added to the cells. CA-tagged peptide stocks in DMSO were diluted in Opti-MEM and serial dilutions of the peptides (1:1) were performed in a separate 96-well plate, ensuring the final DMSO concentration was kept consistent at 1%. Next, peptide solution (25 µL) was added to each well (max. final concentration of 10 µM) and the plate was incubated for 4 h at 37 °C with 5% CO_2. The contents of the wells were aspirated off, and wells were washed using fresh Opti-MEM (80 µL) for 15 min. The wash was aspirated off, and cells were chased using CA-TAMRA (5 µM in Opti-MEM, 50 µL) for 15 min, except for no-CA-TAMRA control wells, which were incubated with Opti-MEM alone (50 µL). The contents of the wells were aspirated and washed with fresh Opti-MEM (80 µL) for 30 min. After aspiration, cells were trypsinized (20 µL; 0.5% Trypsin-EDTA; Gibco, cat. #15400-054), resuspended in PBS (100 mM; pH 7.4) containing 2% FBS (180 µL), and analyzed for red fluorescence using a benchtop flow cytometer counting 2000 events (singlet cells) gated for GFP+ expression in up to 240 s per well. Obtained mean red fluorescence intensity data was normalized based on no-CA-tag wells (high fluorescence, 100% penetration) and no-CA-TAMRA wells (low red fluorescence, 0% penetration). Either of two small molecule controls CA-Trp-OH (CP_{50} = 0.54 ± 0.06 µM, n = 4) and CA-Trp-NH_2 (CP_{50} = 0.04 ± 0.01 µM, n = 4) were included on each plate for referencing. Assay performance was controlled by Z' value determination resulting in Z' = 0.965 ± 0.003 (n = 4). Viability of HeLa cells was measured as % GFP+ cells and plotted along the normalized mean fluorescence intensity. Obtained raw data was processed in Microsoft Excel (vers. 16.56) and plotted in GraphPad Prism (version 9.4.1).

Crystallization of thrombin in complex with macrocycles T1 and T3

Human α-thrombin was purchased from Haematologic Technologies (cat. #HCT-0020). Protein-stabilizing agent was removed by using a PD-10 desalting column (GE Healthcare) equilibrated with 20 mM Tris-HCl, 200 mM NaCl, pH 8.0 and the same buffer as solvent. Buffer exchanged human α-thrombin was incubated with macrocycles (**T1** or **T3**) at a 1:3 molar ratio and subsequently concentrated to 8 mg/mL using a 5000 MWCO Vivaspin ultrafiltration device (Sartorius-Stedim Biotech GmbH). Additional **T1** and **T3** were added during the protein-macrocycle complexes

concentration to ensure that a 3-fold molar excess was preserved. Crystallization trials of the protein-macrocycle complexes were carried out at 293 K in a 96-well 2-drop MRC crystallization plate (Hampton Research, CA, USA) using the sitting-drop vapor-diffusion method and the Morpheus, LMB, and JCSG protein crystallization screen kits (Molecular Dimensions Ltd, Suffolk, UK). Droplets of 0.6 µL volume (with a 1:1 protein-macrocycle complex:precipitant ratio) were set up using an Oryx 8 crystallization robot (Douglas Instruments Ltd, Berkshire, UK) and equilibrated against 70 µL reservoir solution. Conditions optimization was performed by varying the protein-macrocycle complex's concentration, the drop volume and by applying seeding methods. The best crystals of α-thrombin in complex with **T1** were obtained after 2–3 days using the following mixture as precipitant agent: 100 mM sodium acetate, 50 mM magnesium chloride hexahydrate, PEG 3350 (8% w/v), pH 4.5. The best crystals of α-thrombin in complex with **T3** were also obtained after 2–3 days using the following mixture as precipitant agent: 100 mM Bis-Tris, 200 mM ammonium sulfate, PEG 3350 (25% w/v), pH 5.5.

X-ray diffraction data collection and processing

For X-ray data collection, crystals were mounted on LithoLoops (Molecular Dimensions Ltd, Suffolk, UK) soaked in a cryoprotectant solution (25% ethylene glycol, 100 mM sodium acetate, 50 mM magnesium chloride hexahydrate, PEG 3350 (8% w/v), pH 4.5 for human α-thrombin in complex with **T1** and 20% ethylene glycol, 100 mM Bis-Tris, 200 mM ammonium sulfate, PEG 3350 (25% w/v), pH 5.5 for human α-thrombin in complex with **T3**) and flash-cooled in liquid nitrogen. X-ray diffraction data of the protein-macrocycle complexes were collected at the ID23-1 beamline of the European Radiation Synchrotron Facility (ESRF, Grenoble, France). The best crystal of human α-thrombin in complex with **T1** diffracted to 2.58 Å maximum resolution. Crystals belong to the *P*1 space group, with unit cell parameters: a = 44.46 Å, b = 70.23 Å, c = 72.64 Å and α = 62.75°, β = 76.56°, γ = 75.83°). The asymmetric unit contains two molecules, corresponding to a Matthews coefficient of 2.55 $Å^3$/Da and a solvent content of about 51.7% of the crystal volume. The best crystal of human α-thrombin in complex with **T3** diffracted to 2.55 Å maximum resolution. Crystals belong to the $P2_12_12_1$ space group, with unit cell parameters: a = 44.20 Å, b = 120.31 Å, c = 128.81 Å and α = 90°, β = 90°, γ = 90°. The asymmetric unit contains two molecules, corresponding to a Matthews coefficient of 2.25 $Å^3$/Da and a solvent content of about 45.4% of the crystal volume. Frames were indexed and integrated with software XIA2, merged and scaled with Aimless (CCP4i2 crystallographic package).[14]

Structure determination and model refinement

Both protein-macrocycle complex structures were solved by molecular replacement with software Phaser[15] using as a template the model 6Z48.[16] Refinement was carried out using Refmac[17] and Phenix.[18] Building of the macrocycles was performed by Molview, restraint file generated and

optimized by Phenix eLBOW.[18] The macrocycle was fitted manually by graphic software Coot.[19] The electron densities corresponding to the bound macrocycles (**T1** and **T3**) were clearly visible in the differences maps since the first cycles of refinement. The final model of α-thrombin in complex with **T1** contains 4520 protein atoms, 110 ligand atoms (**T1** and *N*-acetyl-β-D-glucosamine (NAG)) and 58 atoms of water molecules. The final crystallographic *R* factor reached 0.19 (R_{free} 0.24). The final model α-thrombin in complex with **T3** contains 4553 protein atoms, 130 ligand atoms (**T3** and NAG) and 77 atoms of water molecules. The final crystallographic *R* factor reached 0.20 (R_{free} 0.25). Geometrical parameters of the two models are as expected or better for this resolution. The solvent excluded volumes and the corresponding buried surfaces were calculated using PISA software.[20] Intra- and intermolecular hydrogen bond interactions were analyzed by ProFunc,[21] LigPlot+ (vers. 2.2),[22] and PyMol.[23] The Protein Data Bank (PDB) identification code for α-thrombin in complex with **T1** is 8ASF and that of α-thrombin in complex with **T3** is 8ASE.

SUPPORTING TABLES

Supporting Table S1. List of generated linear dithiol peptides

P#	sequence				P#	sequence				P#	sequence				P#	sequence				P#	sequence			
1	Mpa	Arg	Gly	**1**	**78**	Mpa	βAla	Arg	**2**	**155**	Mpa	Gly	4ClF	**3**	**232**	Mpa	Isn	Arg	**5**	**309**	Mpa	Aib	Thio	**6**
2	Mpa	Arg	yAla	**1**	**79**	Mpa	Amcp	Arg	**2**	**156**	Mpa	βAla	4ClF	**3**	**233**	Mpa	D-Pro	Arg	**5**	**310**	Mpa	Ac3c	Thio	**6**
3	Mpa	Arg	Trx	**1**	**80**	Mpa	cAcha	Arg	**2**	**157**	Mpa	Amcp	4ClF	**3**	**234**	Mpa	3Aze	Arg	**5**	**311**	Mpa	4Achc	Thio	**6**
4	Mpa	Arg	tAcha	**1**	**81**	Mpa	4Amb	Arg	**2**	**158**	Mpa	cAcha	4ClF	**3**	**235**	Mpa	Arg	βAla	**5**	**312**	Mpa	D-Nip	Thio	**6**
5	Mpa	Arg	D-Pip	**1**	**82**	Mpa	Isn	Arg	**2**	**159**	Mpa	4Amb	4ClF	**3**	**236**	Mpa	Arg	Amcp	**5**	**313**	Mpa	3Aze	Thio	**6**
6	Mpa	Arg	APipAc	**1**	**83**	Mpa	D-Pro	Arg	**2**	**160**	Mpa	Nip	4ClF	**3**	**237**	Mpa	Arg	cAcha	**5**	**314**	Mpa	4ClF	Gly	**6**
7	Mpa	Arg	βhPro	**1**	**84**	Mpa	Thio	Aib	**2**	**161**	Mpa	Isn	4ClF	**3**	**238**	Mpa	Arg	4Amb	**5**	**315**	Mpa	4ClF	γAla	**6**
8	Mpa	Arg	-	**1**	**85**	Mpa	Thio	Ac3c	**2**	**162**	Mpa	D-Pro	4ClF	**3**	**239**	Mpa	Arg	Isn	**5**	**316**	Mpa	4ClF	Trx	**6**
9	Mpa	βAla	Arg	**1**	**86**	Mpa	Thio	3Amb	**2**	**163**	Mpa	Arg	βAla	**4**	**240**	Mpa	Arg	D-Pro	**5**	**317**	Mpa	4ClF	tAcha	**6**
10	Mpa	Amcp	Arg	**1**	**87**	Mpa	Thio	Pro	**2**	**164**	Mpa	Arg	Amcp	**4**	**241**	Mpa	Arg	3Aze	**5**	**318**	Mpa	4ClF	D-Pip	**6**
11	Mpa	cAcha	Arg	**1**	**88**	Mpa	Thio	3Aze	**2**	**165**	Mpa	Arg	cAcha	**4**	**242**	Mpa	Gly	Arg	**5**	**319**	Mpa	4ClF	D-Nip	**6**
12	Mpa	4Amb	Arg	**1**	**89**	Mpa	Thio	-	**2**	**166**	Mpa	Arg	4Amb	**4**	**243**	Mpa	Aib	Arg	**5**	**320**	Mpa	4ClF	APipAc	**6**
13	Mpa	Isn	Arg	**1**	**90**	Mpa	Ac6c	Thio	**2**	**167**	Mpa	Arg	Isn	**4**	**244**	Mpa	Ac3c	Arg	**5**	**321**	Mpa	4ClF	βhPro	**6**
14	Mpa	D-Pro	Arg	**1**	**91**	Mpa	2Amb	Thio	**2**	**168**	Mpa	Arg	D-Pro	**4**	**245**	Mpa	4Achc	Arg	**5**	**322**	Mpa	4ClF	-	**6**
15	Mpa	Arg	βAla	**1**	**92**	Mpa	Acpc	Thio	**2**	**169**	Mpa	Arg	-	**4**	**246**	Mpa	3Amb	Arg	**5**	**323**	Mpa	βAla	4ClF	**6**
16	Mpa	Arg	Amcp	**1**	**93**	Mpa	4ClF	Gly	**2**	**170**	Mpa	Aib	Arg	**4**	**247**	Mpa	D-Nip	Arg	**5**	**324**	Mpa	Amcp	4ClF	**6**
17	Mpa	Arg	cAcha	**1**	**94**	Mpa	4ClF	βAla	**2**	**171**	Mpa	Ac3c	Arg	**4**	**248**	Mpa	Pro	Arg	**5**	**325**	Mpa	cAcha	4ClF	**6**
18	Mpa	Arg	2Amb	**1**	**95**	Mpa	4ClF	Amcp	**2**	**172**	Mpa	4Achc	Arg	**4**	**249**	Mpa	Thio	Ac6c	**5**	**326**	Mpa	4Amb	4ClF	**6**
19	Mpa	Arg	4Amb	**1**	**96**	Mpa	4ClF	cAcha	**2**	**173**	Mpa	3Amb	Arg	**4**	**250**	Mpa	Thio	2Amb	**5**	**327**	Mpa	Isn	4ClF	**6**
20	Mpa	Arg	Isn	**1**	**97**	Mpa	4ClF	4Amb	**2**	**174**	Mpa	D-Nip	Arg	**4**	**251**	Mpa	Thio	Nip	**5**	**328**	Mpa	Acpc	4ClF	**6**
21	Mpa	Arg	D-Pro	**1**	**98**	Mpa	4ClF	Isn	**2**	**175**	Mpa	Pro	Arg	**4**	**252**	Mpa	Thio	Acpc	**5**	**329**	Mpa	D-Pro	4ClF	**6**
22	Mpa	Gly	Arg	**1**	**99**	Mpa	4ClF	D-Pro	**2**	**176**	Mpa	3Aze	Arg	**4**	**253**	Mpa	Thio	-	**5**	**330**	Mpa	Arg	NMeA	**7**
23	Mpa	Aib	Arg	**1**	**100**	Mpa	4ClF	-	**2**	**177**	Mpa	Arg	Aib	**4**	**254**	Mpa	Gly	Thio	**5**	**331**	Mpa	Arg	Ac6c	**7**
24	Mpa	Ac3c	Arg	**1**	**101**	Mpa	Aib	4ClF	**2**	**178**	Mpa	Arg	Ac3c	**4**	**255**	Mpa	Trx	Thio	**5**	**332**	Mpa	Arg	2Achc	**7**
25	Mpa	4Achc	Arg	**1**	**102**	Mpa	Ac3c	4ClF	**2**	**179**	Mpa	Arg	4Achc	**4**	**256**	Mpa	tAcha	Thio	**5**	**333**	Mpa	Arg	2Amb	**7**
26	Mpa	3Amb	Arg	**1**	**103**	Mpa	4Achc	4ClF	**2**	**180**	Mpa	Arg	3Amb	**4**	**257**	Mpa	D-Pip	Thio	**5**	**334**	Mpa	Arg	Nip	**7**
27	Mpa	D-Nip	Arg	**1**	**104**	Mpa	3Amb	4ClF	**2**	**181**	Mpa	Arg	D-Nip	**4**	**258**	Mpa	βhPro	Thio	**5**	**335**	Mpa	Arg	Acpc	**7**
28	Mpa	Pro	Arg	**1**	**105**	Mpa	D-Nip	4ClF	**2**	**182**	Mpa	Arg	Pro	**4**	**259**	Mpa	4ClF	Aib	**5**	**336**	Mpa	Arg	Aze	**7**
29	Mpa	3Aze	Arg	**1**	**106**	Mpa	APipAc	4ClF	**2**	**183**	Mpa	Arg	3Aze	**4**	**260**	Mpa	4ClF	Ac3c	**5**	**337**	Mpa	Arg	-	**7**
30	Mpa	Thio	NMeA	**1**	**107**	Mpa	Pro	4ClF	**2**	**184**	Mpa	NMeA	Arg	**4**	**261**	Mpa	4ClF	4Achc	**5**	**338**	Mpa	Gly	Arg	**7**
31	Mpa	Thio	2Achc	**1**	**108**	Mpa	3Aze	4ClF	**2**	**185**	Mpa	Ac6c	Arg	**4**	**262**	Mpa	4ClF	3Amb	**5**	**339**	Mpa	γAla	Arg	**7**
32	Mpa	Thio	Nip	**1**	**109**	Mpa	Arg	Aib	**3**	**186**	Mpa	2Achc	Arg	**4**	**263**	Mpa	4ClF	D-Nip	**5**	**340**	Mpa	Trx	Arg	**7**
33	Mpa	Thio	Aze	**1**	**110**	Mpa	Arg	Ac3c	**3**	**187**	Mpa	2Amb	Arg	**4**	**264**	Mpa	4ClF	Pro	**5**	**341**	Mpa	tAcha	Arg	**7**
34	Mpa	Thio	-	**1**	**111**	Mpa	Arg	4Achc	**3**	**188**	Mpa	Nip	Arg	**4**	**265**	Mpa	4ClF	3Aze	**5**	**342**	Mpa	D-Pip	Arg	**7**
35	Mpa	γAla	Thio	**1**	**112**	Mpa	Arg	3Amb	**3**	**189**	Mpa	Acpc	Arg	**4**	**266**	Mpa	4ClF	-	**5**	**343**	Mpa	APipAc	Arg	**7**
36	Mpa	tAcha	Thio	**1**	**113**	Mpa	Arg	D-Nip	**3**	**190**	Mpa	Aze	Arg	**4**	**267**	Mpa	NMeA	4ClF	**5**	**344**	Mpa	βhPro	Arg	**7**
37	Mpa	APipAc	Thio	**1**	**114**	Mpa	Arg	Pro	**3**	**191**	Mpa	Thio	Gly	**4**	**268**	Mpa	Ac6c	4ClF	**5**	**345**	Mpa	Arg	Gly	**7**
38	Mpa	βhPro	Thio	**1**	**115**	Mpa	Arg	3Aze	**3**	**192**	Mpa	Thio	γAla	**4**	**269**	Mpa	2Achc	4ClF	**5**	**346**	Mpa	Arg	γAla	**7**
39	Mpa	4ClF	Aib	**1**	**116**	Mpa	Arg	-	**3**	**193**	Mpa	Thio	Trx	**4**	**270**	Mpa	2Amb	4ClF	**5**	**347**	Mpa	Arg	Trx	**7**
40	Mpa	4ClF	Ac3c	**1**	**117**	Mpa	NMeA	Arg	**3**	**194**	Mpa	Thio	tAcha	**4**	**271**	Mpa	Nip	4ClF	**5**	**348**	Mpa	Arg	tAcha	**7**
41	Mpa	4ClF	4Achc	**1**	**118**	Mpa	Ac6c	Arg	**3**	**195**	Mpa	Thio	D-Pip	**4**	**272**	Mpa	Acpc	4ClF	**5**	**349**	Mpa	Arg	D-Pip	**7**
42	Mpa	4ClF	3Amb	**1**	**119**	Mpa	2Achc	Arg	**3**	**196**	Mpa	Thio	APipAc	**4**	**273**	Mpa	Aze	4ClF	**5**	**350**	Mpa	Arg	APipAc	**7**
43	Mpa	4ClF	D-Nip	**1**	**120**	Mpa	2Amb	Arg	**3**	**197**	Mpa	Thio	βhPro	**4**	**274**	Mpa	Arg	Gly	**6**	**351**	Mpa	Arg	βhPro	**7**
44	Mpa	4ClF	Pro	**1**	**121**	Mpa	Nip	Arg	**3**	**198**	Mpa	Thio	-	**4**	**275**	Mpa	Arg	Aib	**6**	**352**	Mpa	βAla	Arg	**7**
45	Mpa	4ClF	3Aze	**1**	**122**	Mpa	Acpc	Arg	**3**	**199**	Mpa	bAla	Thio	**4**	**276**	Mpa	Arg	Ac3c	**6**	**353**	Mpa	Amcp	Arg	**7**
46	Mpa	4ClF	-	**1**	**123**	Mpa	Aze	Arg	**3**	**200**	Mpa	Amcp	Thio	**4**	**277**	Mpa	Arg	4Achc	**6**	**354**	Mpa	cAcha	Arg	**7**
47	Mpa	NMeA	4ClF	**1**	**124**	Mpa	Arg	NMeA	**3**	**201**	Mpa	cAcha	Thio	**4**	**278**	Mpa	Arg	3Amb	**6**	**355**	Mpa	4Amb	Arg	**7**
48	Mpa	Ac6c	4ClF	**1**	**125**	Mpa	Arg	Ac6c	**3**	**202**	Mpa	4Amb	Thio	**4**	**279**	Mpa	Arg	D-Nip	**6**	**356**	Mpa	Isn	Arg	**7**
49	Mpa	2Achc	4ClF	**1**	**126**	Mpa	Arg	2Achc	**3**	**203**	Mpa	Isn	Thio	**4**	**280**	Mpa	Arg	Pro	**6**	**357**	Mpa	D-Pro	Arg	**7**
50	Mpa	2Amb	4ClF	**1**	**127**	Mpa	Arg	2Amb	**3**	**204**	Mpa	D-Pro	Thio	**4**	**281**	Mpa	Arg	3Aze	**6**	**358**	Mpa	Thio	Aib	**7**
51	Mpa	Nip	4ClF	**1**	**128**	Mpa	Arg	Nip	**3**	**205**	Mpa	4ClF	NMeA	**4**	**282**	Mpa	Arg	-	**6**	**359**	Mpa	Thio	4Achc	**7**
52	Mpa	Acpc	4ClF	**1**	**129**	Mpa	Arg	Acpc	**3**	**206**	Mpa	4ClF	Ac6c	**4**	**283**	Mpa	NMeA	Arg	**6**	**360**	Mpa	Thio	3Amb	**7**
53	Mpa	Aze	4ClF	**1**	**130**	Mpa	Arg	Aze	**3**	**207**	Mpa	4ClF	2Achc	**4**	**284**	Mpa	Ac6c	Arg	**6**	**361**	Mpa	Thio	D-Nip	**7**
54	Mpa	Arg	NMeA	**2**	**131**	Mpa	γAla	Arg	**3**	**208**	Mpa	4ClF	2Amb	**4**	**285**	Mpa	2Achc	Arg	**6**	**362**	Mpa	Thio	Pro	**7**
55	Mpa	Arg	Ac6c	**2**	**132**	Mpa	Trx	Arg	**3**	**209**	Mpa	4ClF	Nip	**4**	**286**	Mpa	2Amb	Arg	**6**	**363**	Mpa	Thio	-	**7**
56	Mpa	Arg	2Achc	**2**	**133**	Mpa	tAcha	Arg	**3**	**210**	Mpa	4ClF	Acpc	**4**	**287**	Mpa	Nip	Arg	**6**	**364**	Mpa	NMeA	Thio	**7**
57	Mpa	Arg	2Amb	**2**	**134**	Mpa	D-Pip	Arg	**3**	**211**	Mpa	4ClF	Aze	**4**	**288**	Mpa	Acpc	Arg	**6**	**365**	Mpa	2Achc	Thio	**7**
58	Mpa	Arg	Nip	**2**	**135**	Mpa	APipAc	Arg	**3**	**212**	Mpa	4ClF	-	**4**	**289**	Mpa	Aze	Arg	**6**	**366**	Mpa	Nip	Thio	**7**
59	Mpa	Arg	Acpc	**2**	**136**	Mpa	βhPro	Arg	**3**	**213**	Mpa	Gly	4ClF	**4**	**290**	Mpa	Arg	NMeA	**6**	**367**	Mpa	Aze	Thio	**7**
60	Mpa	Arg	Aze	**2**	**137**	Mpa	Thio	Amcp	**3**	**214**	Mpa	γAla	4ClF	**4**	**291**	Mpa	Arg	Ac6c	**6**	**368**	Mpa	4ClF	βAla	**7**
61	Mpa	Arg	-	**2**	**138**	Mpa	Thio	cAcha	**3**	**215**	Mpa	Trx	4ClF	**4**	**292**	Mpa	Arg	2Achc	**6**	**369**	Mpa	4ClF	Amcp	**7**
62	Mpa	Gly	Arg	**2**	**139**	Mpa	Thio	4Amb	**3**	**216**	Mpa	tAcha	4ClF	**4**	**293**	Mpa	Arg	2Amb	**6**	**370**	Mpa	4ClF	cAcha	**7**
63	Mpa	γAla	Arg	**2**	**140**	Mpa	Thio	D-Pro	**3**	**217**	Mpa	D-Pip	4ClF	**4**	**294**	Mpa	Arg	Nip	**6**	**371**	Mpa	4ClF	4Amb	**7**
64	Mpa	Trx	Arg	**2**	**141**	Mpa	Thio	-	**3**	**218**	Mpa	APipAc	4ClF	**4**	**295**	Mpa	Arg	Acpc	**6**	**372**	Mpa	4ClF	Isn	**7**
65	Mpa	tAcha	Arg	**2**	**142**	Mpa	Aib	Thio	**3**	**219**	Mpa	βhPro	4ClF	**4**	**296**	Mpa	Arg	Aze	**6**	**373**	Mpa	4ClF	D-Pro	**7**
66	Mpa	D-Pip	Arg	**2**	**143**	Mpa	Ac3c	Thio	**3**	**220**	Mpa	Arg	Gly	**5**	**297**	Mpa	Gly	Arg	**6**	**374**	Mpa	4ClF	3Aze	**7**
67	Mpa	APipAc	Arg	**2**	**144**	Mpa	3Amb	Thio	**3**	**221**	Mpa	Arg	γAla	**5**	**298**	Mpa	γAla	Arg	**6**	**375**	Mpa	4ClF	-	**7**
68	Mpa	βhPro	Arg	**2**	**145**	Mpa	D-Nip	Thio	**3**	**222**	Mpa	Arg	Trx	**5**	**299**	Mpa	Trx	Arg	**6**	**376**	Mpa	Aib	4ClF	**7**
69	Mpa	Arg	Gly	**2**	**146**	Mpa	Pro	Thio	**3**	**223**	Mpa	Arg	tAcha	**5**	**300**	Mpa	tAcha	Arg	**6**	**377**	Mpa	γAla	4ClF	**7**
70	Mpa	Arg	γAla	**2**	**147**	Mpa	4ClF	Gly	**3**	**224**	Mpa	Arg	D-Pip	**5**	**301**	Mpa	D-Pip	Arg	**6**	**378**	Mpa	Ac3c	4ClF	**7**
71	Mpa	Arg	Trx	**2**	**148**	Mpa	4ClF	γAla	**3**	**225**	Mpa	Arg	APipAc	**5**	**302**	Mpa	APipAc	Arg	**6**	**379**	Mpa	Trx	4ClF	**7**
72	Mpa	Arg	4Achc	**2**	**149**	Mpa	4ClF	Trx	**3**	**226**	Mpa	Arg	βhPro	**5**	**303**	Mpa	βhPro	Arg	**6**	**380**	Mpa	4Achc	4ClF	**7**
73	Mpa	Arg	tAcha	**2**	**150**	Mpa	4ClF	tAcha	**3**	**227**	Mpa	Arg	-	**5**	**304**	Mpa	Thio	βAla	**6**	**381**	Mpa	3Amb	4ClF	**7**
74	Mpa	Arg	D-Pip	**2**	**151**	Mpa	4ClF	D-Pip	**3**	**228**	Mpa	βAla	Arg	**5**	**305**	Mpa	Thio	Amcp	**6**	**382**	Mpa	D-Nip	4ClF	**7**
75	Mpa	Arg	APipAc	**2**	**152**	Mpa	4ClF	APipAc	**3**	**229**	Mpa	Amcp	Arg	**5**	**306**	Mpa	Thio	cAcha	**6**	**383**	Mpa	Pro	4ClF	**7**
76	Mpa	Arg	βhPro	**2**	**153**	Mpa	4ClF	βhPro	**3**	**230**	Mpa	cAcha	Arg	**5**	**307**	Mpa	Thio	Isn	**6**	**384**	Mpa	3Aze	4ClF	**7**
77	Mpa	NMeA	Arg	**2**	**154**	Mpa	4ClF	-	**3**	**231**	Mpa	4Amb	Arg	**5**	**308**	Mpa	Thio	-	**6**					

P# = peptide identifier for the 384 synthesized peptides sequences. **1**−**7** represents the different aminothiol diversification elements.

Supporting Table S2. Macrocycle compound library

Library size	
Number of macrocycles	2,688
Structural diversity	
Number of different peptide sequences	384
Different macrocycle backbones*	2,107
Chemical diversity	
Total number of building blocks	45
Different aminothiol derivatives	7
Different amino acids	30
Different bis-electrophilic linkers	7
Physicochemical properties (average)	
Molecular weight	568 Da
cLogP	1.71
Polar surface area	188 $Å^2$
H-bond acceptors	8.88
H-bond donors	3.79
Ring size (atoms)	20.7
Number of rotable bonds	3.23

*Different backbones are determined as distinctive macrocyclic skeletons, ignoring peptide side chains. Same atom ring structures with different conformational constrains imposed by peripheral groups (*e.g. N*-methylations, cyclic side chains) are included as different backbones.

Supporting Table S3. PAMPA data of thrombin inhibitors and compound controls

Passive permeability was measured using PAMPA at a compound concentration of 50 µM upon 12 h incubation. The results are provided as the mean ± SD. Data are based on each compound measurement performed in triplicate on the same plate.

Compound	Flux (%)	Pe (nm/s)	-logPe (cm/s)	Mass retention (%)
T1	18 ± 2	15 ± 2	5.82 ± 0.05	35 ± 3
T2	5.5 ± 1.5	4.4 ± 1.2	6.37 ± 0.12	61 ± 6
T3	38 ± 5	37 ± 6	5.43 ± 0.08	48 ± 2
T4	5.9 ± 1.1	4.7 ± 0.9	6.34 ± 0.09	39 ± 1
T5	7.3 ± 3.3	5.9 ± 2.7	6.30 ± 0.26	41 ± 1
Craik (Peptide 15)	34 ± 4	32 ± 5	5.50 ± 0.07	26 ± 3
Carbamazepine	74 ± 3	103 ± 8	4.99 ± 0.03	8 ± 1

Supporting Table S4. Data collection and refinement statistics for X-ray co-crystal structures
Statistics on X-ray diffraction data collection and refinement of α-thrombin in complex with macrocycle **T1** (PDB 8ASF). A single crystal was used to collect all diffraction data. Highest-resolution shell statistics are shown within brackets.

Data collection	
Wavelength (Å)	0.8856
Space group	*P*1
Cell parameters	
a, *b*, *c* (Å); *α*, *β*, *γ* (°)	44.46, 70.23, 72.64; 62.75, 76.56, 75.83
Resolution (Å)	38.06–2.58 (2.67–2.58)
Total observations	61731 (2653)
Unique observations	20556 (943)
Multiplicity	3.0 (2.8)
R_{merge}	0.084 (0.377)
<I / σ(I)>	5.3 (1.9)
CC1/2	0.989 (0.885)
Completeness (%)	86.9 (77.3)
Wilson B-factor	45.15
Refinement	
No. reflections (used for R_{free} calculation)	1140 (44)
R_{work} / R_{free}	0.19/0.24
Number non-hydrogen atoms	4688
protein (chains A, B, H, L)	4520
ligands (macrocycle T1, NAG)	110
solvent	58
Geometry	
RMSD values	
bond lengths (Å)	0.013
bond angles (°)	1.57
Ramachandran plot (%)	
most favored	94.51
additionally allowed	5.49
outliers	0.00
Average B-factor	41.46

Supporting Table S5. Buried surface areas in protein and macrocycle complexes

Buried surfaces were calculated using the software PISA[20] by the web server ProFunc[21] and are reported here for the human α-thrombin and the macrocycles **T1** and **T3**. The designation "buried" implies that the residues are at least partially inaccessible to bulk solvent because of the proximity of the interface surfaces of the protein and the macrocycles. The average calculated values for each monomer in the asymmetric unit are reported.

thrombin-macrocycle complex	thrombin-**T1**	thrombin-**T3**
Buried surface area on protein (Å^2)	395 Å^2	368 Å^2
Buried surface area on macrocycle (Å^2)	608 Å^2	558 Å^2

The difference of the sum in buried surface area of interaction (Δ, Å^2) between thrombin-**T1** and thrombin-**T3** complex (77 Å^2) has been determined by using the following formula:

Equation VII

$$\Delta\left(\text{Å}^2\right) = \left[(P^X + p^X) - (P^Y + p^Y)\right]$$

where P^X is the buried surface area on protein in the thrombin-**T1** complex (395 Å^2), p^X is the buried surface area on macrocycle in the in the thrombin-**T1** complex (608 Å^2), P^Y is the buried surface area on protein in the thrombin-**T3** complex (368 Å^2) and p^Y is the buried surface area on macrocycle in the in the thrombin-**T3** complex (558 Å^2).

Supporting Table S6. Interactions in X-ray structures, thrombin–T1

Atoms of the macrocycle of **T1** forming interactions with atoms and residues of human α-thrombin (chymotrypsin numbering). Interactions have distances shorter than 4.0 Å and were defined using the software LigPlot+ by the web server ProFunc.

Thrombin atom / residue	T1 atom	Distance (Å)	Interaction
O / Glu97A	S22	3.46	PI
O / Cys191	O40	3.65	PI
N / Glu192	O40	3.32	PI
N / Trp215	S36	3.81	PI
N / Gly216	O31	3.33	HB
N / Gly216	N33	3.89	PI
N / Gly216	S36	3.48	PI
O / Gly216	N33	3.20	HB
O / Gly216	O31	3.07	PI
O / Gly219	N33	3.41	PI
O / Cys191 (H_2O)*	O40	2.90 (2.78)	HB
N / Gly193 (H_2O)*	O40	3.10 (2.78)	HB
N / Ser195 (H_2O)*	O40	3.44 (2.78)	HB
OG / Ser195 (H_2O)*	O40	2.68 (2.78)	HB

Thrombin atom / residue	T1 atom	Distance (Å)
NE2 / His57	C11	3.87
NE2 / His57	C12	3.87
CD1 / Tyr60A	C16	3.73
CE1 / Tyr60A	C16	3.38
CE1 / Tyr60A	C17	3.43
CE2 / Tyr60A	C15	3.75
CZ / Tyr60A	C15	3.61
CZ / Tyr60A	C16	3.58

CZ / Tyr60A	C17	3.75
CZ / Tyr60A	C20	3.80
OH / Tyr60A	C15	3.90
OH / Tyr60A	C17	3.77
OH / Tyr60A	C18	3.45
OH / Tyr60A	C19	3.36
OH / Tyr60A	C20	3.61
CZ3 / Trp60D	S13	3.62
CZ3 / Trp60D	C14	3.57
CH2 / Trp60D	S13	3.49
CH2 / Trp60D	C14	3.65
O / Trp96	C21	3.71
O / Glu97A	C23	3.61
CA / Asn98	C23	3.87
CG / Leu99	C17	3.62
CD1 / Leu99	C17	3.81
CD1 / Leu99	C27	3.75
CD2 / Leu99	C17	3.83
CG1 / Ile174	C25	3.80
CD1 / Ile174	C25	3.83
CG / Asp189	C38	3.71
OD1 / Asp189	C38	3.26
OD2 / Asp189	C38	3.60
C / Ala190	C39	3.85
O / Ala190	C38	3.49
O / Ala190	C39	3.26
CB / Ala190	C37	3.86
C / Cys191	C34	3.87
C / Cys191	O40	3.39

CA / Glu192	O40	3.59
O / Ser214	C11	3.28
CA / Trp215	C11	3.77
CA / Trp215	O31	3.54
CA / Trp215	S36	3.62
C / Trp215	S36	3.51
C / Trp215	C37	3.49
O / Trp215	C37	3.59
O / Trp215	CL41	3.67
CB / Trp215	C11	3.76
CB / Trp215	C27	3.86
CB / Trp215	O31	3.42
CG / Trp215	C24	3.79
CD2 / Trp215	C24	3.63
CD2 / Trp215	C25	3.88
CE3 / Trp215	C24	3.65
CE3 / Trp215	C25	3.37
CZ3 / Trp215	C25	3.74
N / Gly216	C35	3.43
N / Gly216	C37	3.61
N / Gly216	C38	3.67
N / Gly216	C39	3.52
CA / Gly216	C38	3.71
CA / Gly216	C39	3.60
O / Gly216	C5	3.58
O / Gly216	C32	3.42
CG / Glu217	O29	3.70
N / Gly219	C32	3.81
O / Gly219	C32	3.84

O / Gly219	C39	3.49
CA / Gly226	CL41	3.59
C / Gly226	CL41	3.84
N / Phe227	CL41	3.42
O / Phe227	CL41	3.40
CZ / Tyr228	CL41	3.68
OH / Tyr228	CL41	3.83

Supporting Table S7. Data collection and refinement statistics for X-ray co-crystal structures
Statistics on X-ray diffraction data collection and refinement of α-thrombin in complex with macrocycle **T3** (PDB 8ASE). A single crystal was used to collect all diffraction data. Highest-resolution shell statistics are shown within brackets.

Data collection	
Wavelength (Å)	0.8856
Space group	$P2_12_12_1$
Cell parameters	
a, *b*, *c* (Å); *α*, *β*, *γ* (°)	44.20, 120.31 128.81; 90, 90, 90
Resolution (Å)	41.81–2.55 (2.66–2.55)
Total observations	224806 (28452)
Unique observations	23267 (2803)
Multiplicity	9.70 (10.20)
R_{merge}	0.18 (1.12)
<I / σ(I)>	10.00 (2.20)
CC1/2	0.996 (0.770)
Completeness (%)	100.00 (100.00)
Wilson B-factor	33.18
Refinement	
No. reflections (used for R_{free} calculation)	1097 (102)
R_{work} / R_{free}	0.20/0.25
Number non-hydrogen atoms	4760
protein (chains A, B, H, L)	4553
ligands (macrocycle T3, NAG, SO_4)	130
solvent	77
Geometry	
RMSD values	
bond lengths (Å)	0.011
bond angles (°)	1.57
Ramachandran plot (%)	
most favored	94.73
additionally allowed	5.27
outliers	0.00
Average B-factor	45.59

Supporting Table S8. Interactions in X-ray structures, thrombin–T3

Atoms of the macrocycle of **T3** forming interactions with atoms and residues of human α-thrombin (chymotrypsin numbering). Interactions have distances shorter than 4.0 Å and were defined using the software LigPlot+ by the web server ProFunc.

Thrombin atom / residue	T3 atom	Distance (Å)	Interaction
O / Glu97A	S1	3.44	PI
N / Gly216	O3	3.41	PI
N / Gly216	N3	3.79	PI
O / Gly216	N1	3.11	HB
O / Gly216	O3	3.62	PI
O / Gly216	N3	3.18	HB

Thrombin atom / residue	T3 atom	Distance (Å)
CD2 / His57	C21	3.88
NE2 / His57	C20	3.83
NE2 / His57	C21	3.68
CE1 / Tyr60A	C23	3.89
CE1 / Tyr60A	C26	3.30
CE1 / Tyr60A	C27	3.66
CE2 / Tyr60A	C22	3.80
CE2 / Tyr60A	C23	3.71
CZ / Tyr60A	C23	3.45
CZ / Tyr60A	C26	3.29
CZ / Tyr60A	C27	3.64
OH / Tyr60A	C1	3.28
OH / Tyr60A	C23	3.55
OH / Tyr60A	C24	3.58
OH / Tyr60A	C25	3.45

OH / Tyr60A	C26	3.38
OH / Tyr60A	C27	3.24
CH2 / Trp60D	C22	3.89
CH2 / Trp60D	C29	3.87
CH2 / Trp60D	C30	3.74
CH2 / Trp60D	S2	3.86
CA / Asn98	S1	3.76
CD1 / Leu99	C26	3.44
CD1 / Leu99	C27	3.32
CD2 / Leu99	C26	3.70
O / Ala190	C17	3.78
C / Cys191	C12	3.76
N / Glu192	C12	3.41
CA / Glu192	C12	3.71
CB / Glu192	O2	3.67
OG / Ser195	C14	3.44
OG / Ser195	C15	3.74
CG1 / Val213	C15	3.50
CG1 / Val213	C16	3.87
CG1 / Val213	CL1	3.49
C / Ser214	C15	3.83
N / Trp215	C15	3.49
N / Trp215	C16	3.79
N / Trp215	CL1	3.60
CA / Trp215	C15	3.42
CA / Trp215	C16	3.67
CA / Trp215	C19	3.80
CA / Trp215	O3	3.28
C / Trp215	C15	3.66

C / Trp215	C16	3.33
C / Trp215	C17	3.72
C / Trp215	O3	3.88
C / Trp215	CL1	3.57
O / Trp215	C16	3.50
O / Trp215	CL1	3.14
CB / Trp215	C19	3.88
CB / Trp215	O3	3.00
CD2 / Trp215	C4	3.80
CE3 / Trp215	C4	3.58
CE3 / Trp215	C5	3.64
CE3 / Trp215	C6	3.78
N / Gly216	C16	3.64
N / Gly216	C17	3.54
N / Gly216	C18	3.84
CA / Gly216	C17	3.83
O / Gly216	C6	3.82
O / Gly216	C7	3.76
O / Gly216	C9	3.41
O / Gly219	C18	3.72
CA / Gly226	CL1	3.84
N / Phe227	CL1	3.64
O / Phe227	CL1	3.71

Supporting Table S9. List of amino acids, thiols and linkers used in library preparation

Name	Abbreviation	CAS RN
Fmoc-Ala-OH	Ala	35661-39-3
Fmoc-Trp-OH	Trp	35737-15-6
Fmoc-Arg(Pbf)-OH	Arg	154445-77-9
Fmoc-Phe(4-Cl)-OH	4ClF	175453-08-4
(*S*)-2-Fmoc-3-(5-chlorothiophene-2-carboxamido)propanoic acid	Thio	–
Fmoc-Gly-OH	Gly	29022-11-5
Fmoc-*N*-Me-Ala-OH	NMeA	84000-07-7
Fmoc-β-Ala-OH	βAla	35737-10-1
Fmoc-Gaba-OH	γAla	116821-47-7
Fmoc-Aib-OH	Aib	94744-50-0
Fmoc-Ac3c-OH	Ac3c	126705-22-4
Fmoc-Amcp-OH	Amcp	1263045-62-0
(1*R*,2*R*)-Fmoc-2-aminocyclopentane carboxylic acid	Acpc	359586-69-9
1-(Fmoc-amino)cyclohexanecarboxylic acid	Ac6c	162648-54-6
2-(Fmoc-aminomethyl)-benzoic acid	2Amb	219640-94-5
Fmoc-3-aminomethylbenzoic acid	3Amb	155369-11-2
4-(Fmoc-aminomethyl)benzoic acid	4Amb	164470-64-8
Fmoc-1,2-*trans*-Achc-OH	2Achc	381241-08-3
Fmoc-1,4-*cis*-Achc-OH	4Achc	147900-45-6
Fmoc-tranexamic acid	Trx	167690-53-1
Fmoc-1,4-*cis*-Acha-OH	*c*Acha	1217675-84-7
Fmoc-1,4-*trans*-Acha-OH	*t*Acha	1217650-00-4
Fmoc-D-pipecolic acid	D-Pip	101555-63-9
Fmoc-Nip-OH	Nip	193693-68-4
Fmoc-D-Nip-OH	D-Nip	193693-67-3
Fmoc-Isn-OH	Isn	148928-15-8
Fmoc-Pro-OH	Pro	71989-31-6
Fmoc-D-Pro-OH	D-Pro	101555-62-8
Fmoc-β-homoproline	βhPro	193693-60-6
Fmoc-Aze-OH	Aze	136552-06-2
1-Fmoc-azetidine-3-carboxylic acid	3Aze	193693-64-0
Fmoc-4-amino-1-carboxymethyl-piperidine	APipAc	221352-82-5

3-(tritylthio)propionic acid	Mpa	27144-18-9
1,3-dichloroacetone	L1	534-07-6
divinylsulfone	L2	77-77-0
trans-1,4-dibromo-2-butene	L3	821-06-7
2,6-bis-(bromomethyl)pyridine	L4	7703-74-4
3,4-bis(bromomethyl)furan	L5	146604-80-0
α,α’-dibromo-p-xylene	L6	623-24-5
2,3-bis(bromomethyl)quinoxaline	L7	3188-86-1

Supporting Table S10. List of applied laboratory equipment and utilities

Equipment	Model and/or cat. #	Supplier
96-well deep well plates	Fisherbrand 96-well deepwell TM polypropylene microplates (2.0 mL)	Thermo Fisher Scientific (Waltham, MA, USA)
96-well cell culture plate	Greiner bio-one, CELLSTAR sterile, flat bottom, with lid (cat. #655 180)	Merck KGaA (Darmstadt, Germany)
96-well PCR plate	non-skirted, standard profile (cat. #732-2387)	VWR avantor (Radnor, PA, USA)
384-well assay plate	polystyrene, Fbottom, µClear, black (cat. #781096)	Greiner Bio-One GmbH (Frickenhausen, Germany)
384-well LDV plate	Echo qualified 384-well COC source plate (cat. #LP-0200)	Labcyte (San José, CA, USA)
384-well PP plate	Echo qualified 384-well polypropylene source plate (cat. #P-05525)	Labcyte (San José, CA, USA)
1536-well OptiPlate	OptiPlate-1536F, untreated (cat. #6004270)	PerkinElmer (Waltham, MA, USA)
Acoustic liquid transfer	Echo® 650 Liquid handler (cat. #001-16079)	Labcyte (San José, CA, USA)
Adhesive metal plate lids	Silverseal sealer, aluminum (cat. #676090)	Greiner Bio-One GmbH (Frickenhausen, Germany)
Adhesive PP plate lids	Adhesive polypropylene film (cat. #IST-125-080LS)	IST scientific (Farnham, United Kingdom)
Automated bulk dispenser	CERTUS Flex	Fritz Gyger AG (Gwatt, Switzerland)
Automated SPPS synthesizer	MultiPep 2 Rsi	Intavis AG (Tübingen, Germany)
Centrifuge	Sigma 4-16KHS centrifuge (equipped for plates or falcon tubes)	Sigma Laborzentrifugen GmbH (Osterode, Germany)
Flow cytometer	Guava EasyCyte	EMD Millipore (Darmstadt, Germany)
HPLC-MS system	Single quadrupole MS system (Shimadzu LCMS-2020)	Shimadzu (Kyoto, Japan)
HRMS system	Quadrupole time-of-flight MS system (Xevo G2-XS QTof)	Waters (Milford, MA, USA)
Lyophilizer	Alpha 2-4 LDplus freeze dryer	Martin Christ Gefriertrocknungs-anlagen GmbH (Osterode, Germany)
PAMPA plates	96-well pre-coated PAMPA plate system (cat. #353015)	Corning (Glendale, AZ, USA)
PAMPA teflon acceptor plate	Teflon acceptor plate (cat. #MSSACCEPT0R) ,	Merck KGaA (Darmstadt, Germany)
pH meter	Mettler Toldeo FiveEasy pH meter	Mettler (Columbus, OH, USA)
Plate reader	PHERAstar FSX	BMG Labtech (Ortenberg, Germany)
Plate reader	TECAN M200	Tecan (Männedorf, Switzerland)
Preparative HPLC	Waters system (2489 UV detector, 2535 pump, fraction Collector III)	Waters AG (Baden, Switzerland)
Rotary vacuum concentration	Maxi concentrator RVC 2-33 CDplus attached to Alpha 2-4 LSCbasic freeze dryer	Martin Christ Gefriertrocknungs-anlagen GmbH (Osterode, Germany)
RP column (PrepHPLC)	C18 Xterra OBD column (19×250 mm, 125 Å, 10 µm, cat. #186002259)	Waters AG (Baden, Switzerland)
RP column (Semi-prepHPLC)	C18 NovaPak CSH column (10×150 mm, 125 Å, 5 µm, cat. #186008238)	Waters AG (Baden, Switzerland)
Seal pad for filter plate	6 mm ethylen-vinyl acetate pad (cat. #7826301)	Rayher GmbH (Laupheim, Germany)

Semi-preparative HPLC	Dionex UltiMate 3000 UHPLC	Thermo Fisher Scientific (Waltham, MA, USA)
SPPS reactor syringes	5 mL BD syringe, polypropylene with 25 µm PE frit	Carl Roth GmbH (Karlsruhe, Germany)
SPPS 96-well synthesis plates	Polypropylene 96-well filter plates (cat. #OF1100)	Orochem (Naperville, IL, USA)
Tissue-culture dish	10 cm, sterile (cat. #83.3902)	Hounisen (Skanderborg, Denmark)

Supporting Table S11. Peptide purity and high-resolution mass spectrometry (HRMS)

Peptide purity measured by integration of HPLC chromatograms at 220 nm. Please find the HPLC chromatograms in Supplementary Figures S9 and S20. Retention times (t_R) correspond to linear gradients of eluent A (0.05% HCOOH in water) and eluent B (0.05% HCOOH in MeCN), rising linearly from 0% to 60% of B during t = 1.00−6.00 min. *broad peak shape was observed due to rotational conformers.

macro-cycle	peptide identifier	purity	t_R (min)	formula	HRMS (*m/z*)	found	(calcd)
T1	251_L6	>95%	4.86	$C_{29}H_{35}ClN_4O_4S_3$	$[M+H]^+$	635.1599	635.1582
T2	36_L6	>95%	4.62	$C_{29}H_{37}ClN_4O_4S_3$	$[M+H]^+$	637.1746	637.1738
T3	206_L6	>95%	5.36	$C_{30}H_{36}ClN_3O_3S_2$	$[M+H]^+$	586.1964	586.1959
T4	36_L4	>95%	3.77	$C_{28}H_{36}ClN_5O_4S_3$	$[M+H]^+$	638.1697	638.1691
T5	304_L4	>95%	4.06	$C_{26}H_{32}ClN_5O_4S_3$	$[M+H]^+$	610.1393	610.1378
T6	9_L6	>95%	3.37	$C_{22}H_{34}N_6O_3S_2$	$[M+H]^+$	495.2207	495.2207
T7	219_L6	>95%	5.17	$C_{30}H_{36}ClN_3O_3S_2$	$[M+H]^+$	586.1978	586.1959
P1	362_L6	>95%*	5.47*	$C_{30}H_{37}ClN_4O_4S_3$	$[M+H]^+$	649.1755	649.1738
P2	191_L4	>95%	4.13	$C_{24}H_{28}ClN_5O_4S_3$	$[M+H]^+$	582.1078	582.1065
P3	191_L5	>95%	4.62	$C_{23}H27ClN_4O_5S_3$	$[M+H]^+$	571.0914	571.0905
P4	37_L1	>88%	3.07	$C_{23}H_{32}ClN_5O_5S_3$	$[M+H]^+$	590.1340	590.1327
P5	191_L3	>95%	4.51	$C_{21}H_{27}ClN_4O_4S_3$	$[M+H]^+$	531.0967	531.0956
T1-CA	N/A	>92%	5.14	$C_{38}H_{58}ClN_5O_7S_2$	$[M+H]^+$	796.3562	796.3539
T1-CA2	N/A	>95%	5.70	$C_{43}H_{60}Cl_2N_6O_8S_3$	$[M+H]^+$	955.3059	955.3085
T3-CA	N/A	>95%	6.06	$C_{44}H_{61}Cl_2N_5O_7S_2$	$[M+Na]^+$	928.3269	928.3288

SUPPORTING SCHEMES

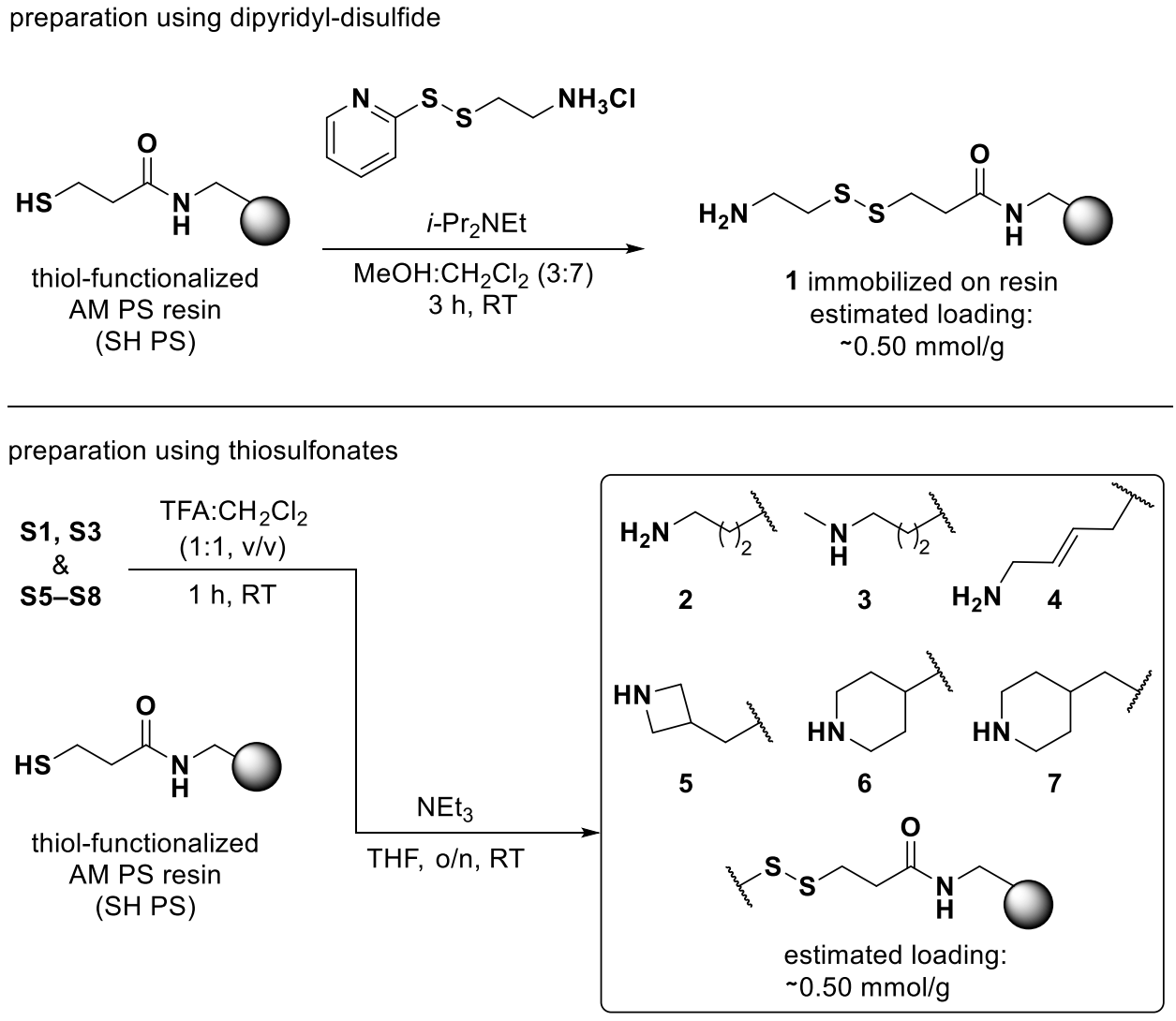

Supporting Scheme S1. Preparation of activated aminothiols (1–7) and their immobilization onto resin via a disulfide bridge. Method for functionalizing aminothiol derivatives via a disulfide linker onto solid support.

SUPPORTING FIGURES

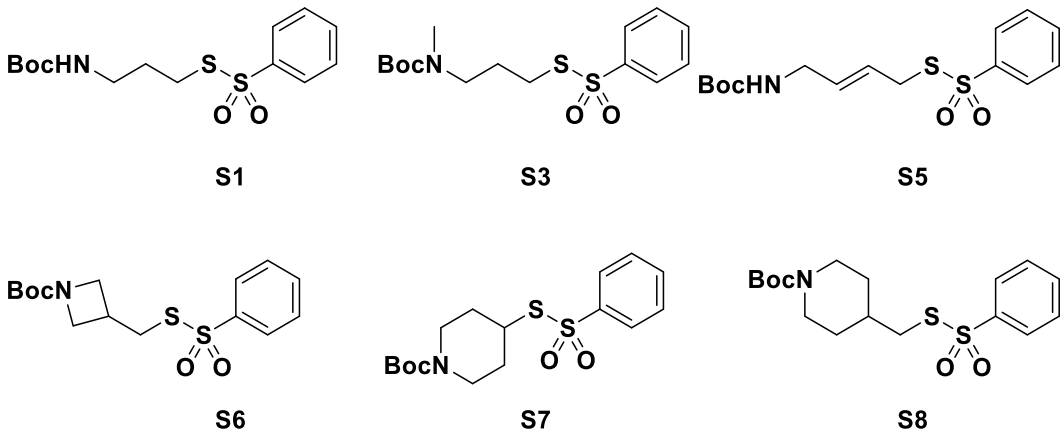

Supporting Figure S1. Synthesized thiosulfonate building blocks.

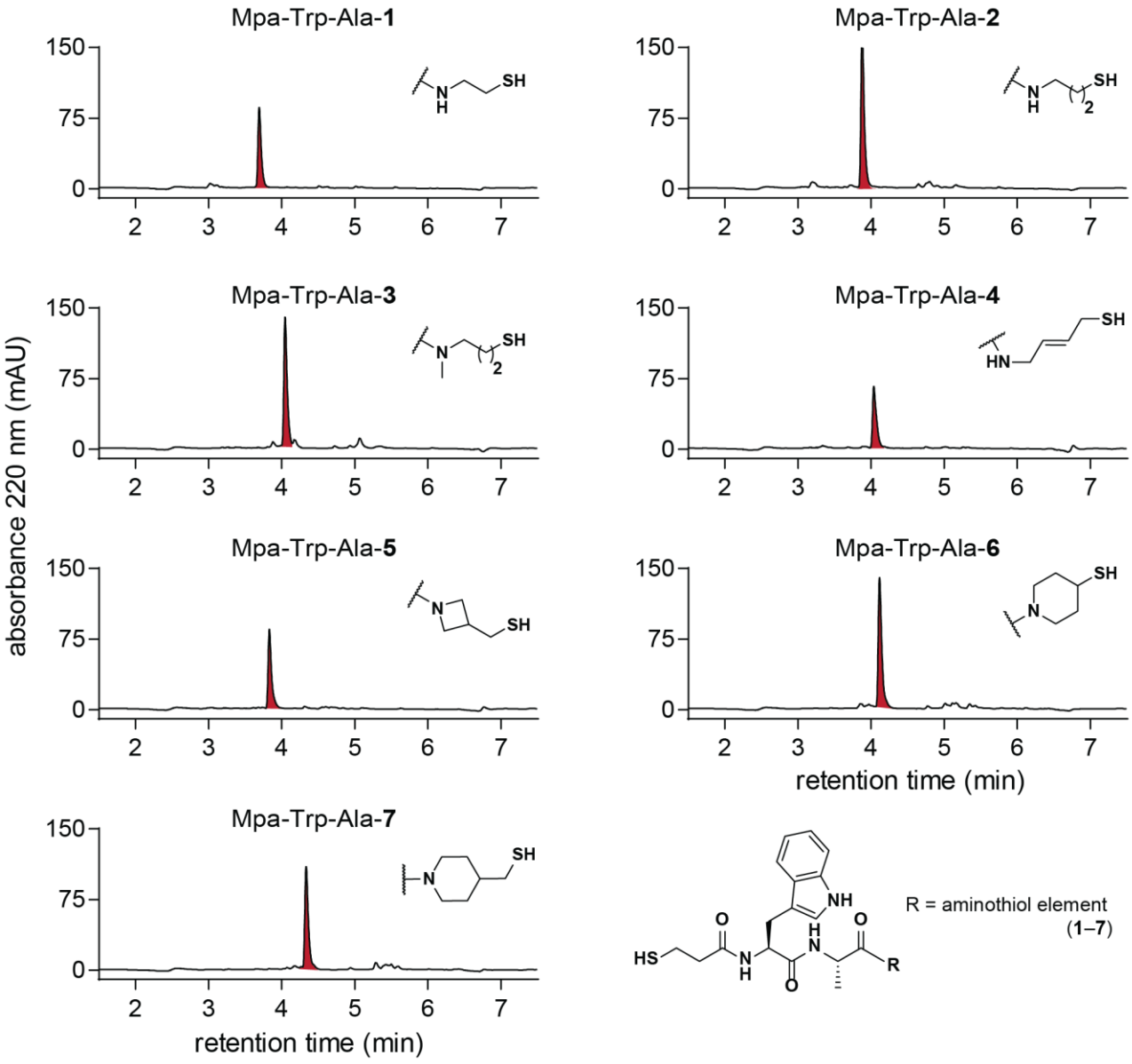

Supporting Figure S2. Quality assessment of linear peptides prepared with resin derivatives. UV_{220} chromatograms of crude peptide controls utilizing different aminothiols (**1**–**7**) after reductive release and RVC from synthesis in 96-well plates (5 µmol scale). Highlighted in red are the desired linear peptide species.

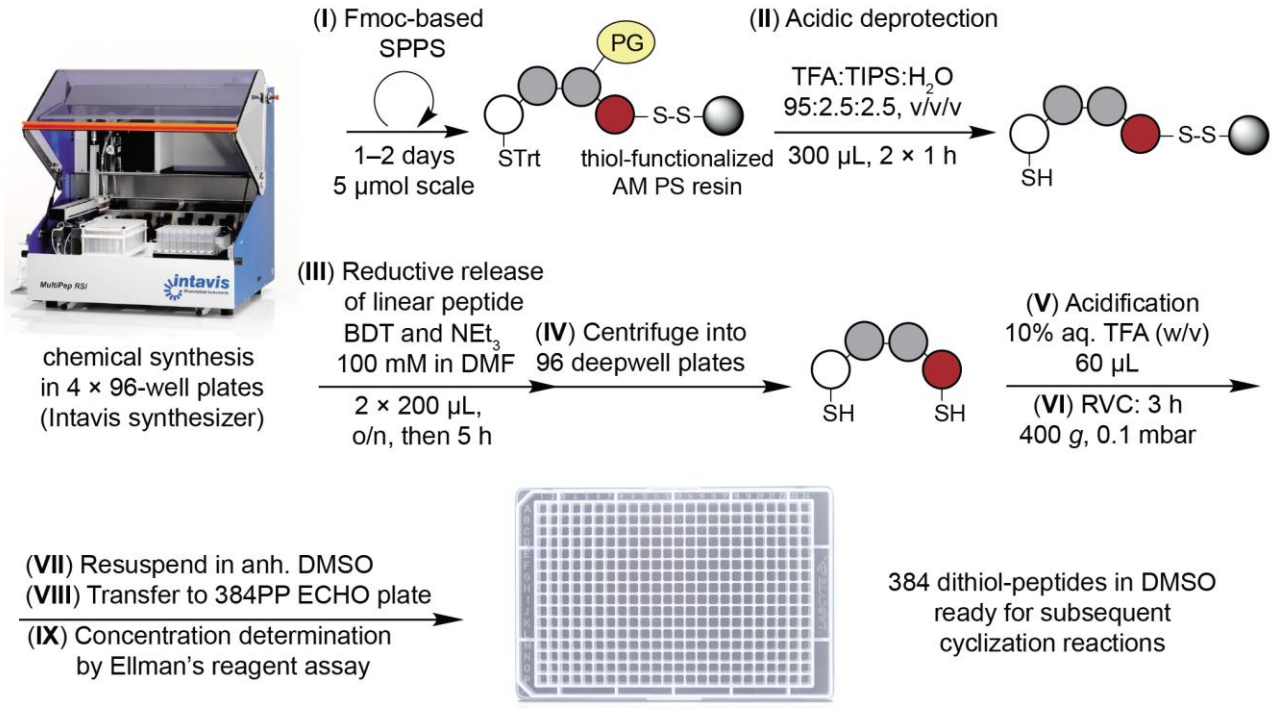

Supporting Figure S3. Workflow of the development of linear peptide libraries in microtiter plates. Simplified visual description for the stepwise synthesis of linear dithiol peptides using the reductive release procedure in microtiter plate format.[24] White circle = 3-mercaptopropionic acid (Mpa); gray = any amino acid, red = aminothiol derivatives (**1**–**7**) covalently attached onto thiol-functionalized aminomethyl polystyrene (AM PS) resin by a disulfide bridge. RVC = rotational vacuum concentration. PG = protecting group.

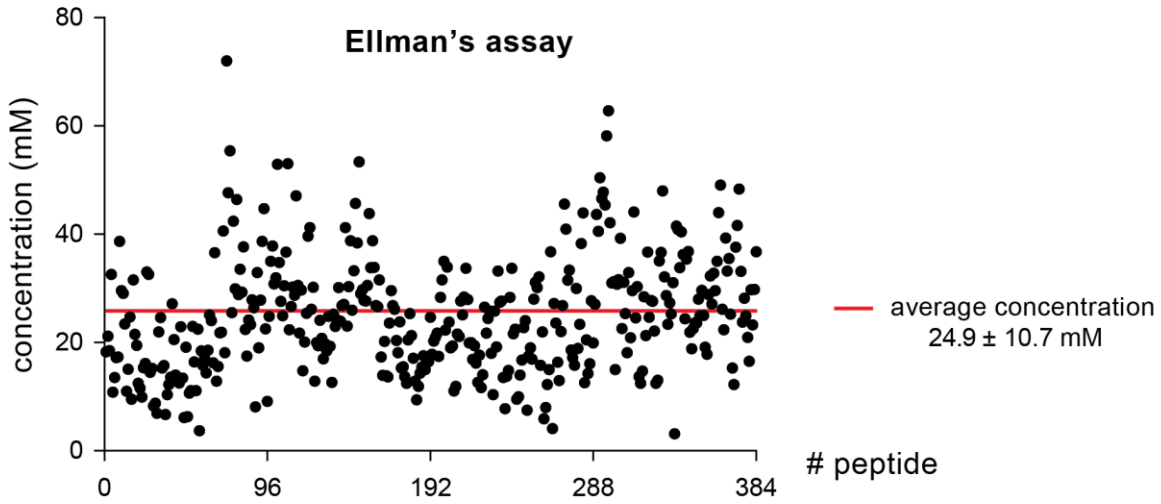

Supporting Figure S4. Concentration determination of the peptide library. Concentration of the individual linear dithiol peptides were determined by solubilizing peptide stock in DMSO (50 µL) and measuring the amounts of free thiols by the Ellman's assay.

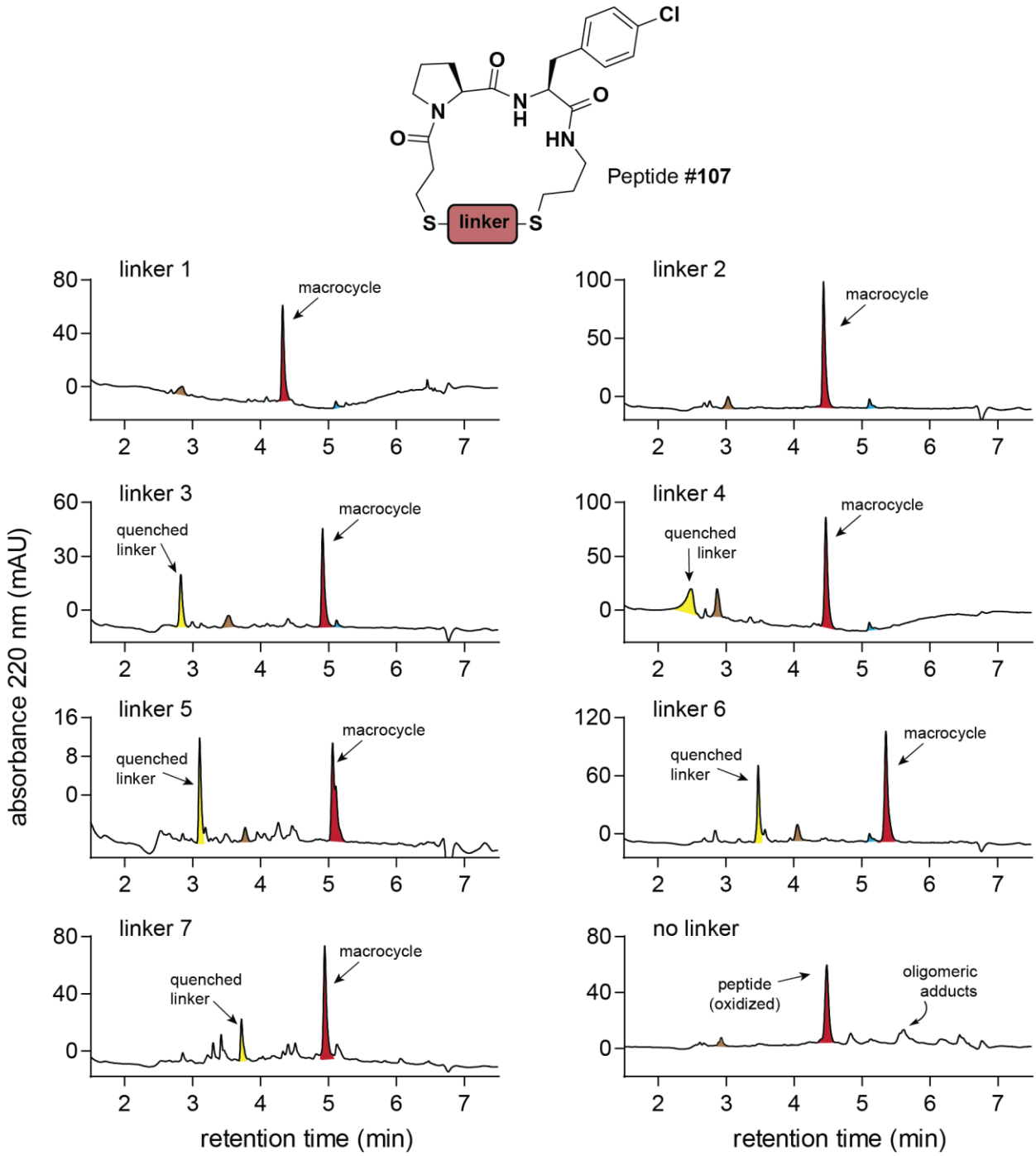

Supporting Figure S5. Quality control of macrocycle library; part I. UV_{220} spectra of randomly picked dithiol peptide (#107 of the 384 synthesized peptides, see Table S1 for full list of sequences) cyclized with the different bis-electrophilic linkers. Highlighted in red are the desired macrocyclic species. Highlighted in yellow, brown and blue is quenched linker adduct, truncated peptide [– 4ClF] and HPLC column impurity, respectively.

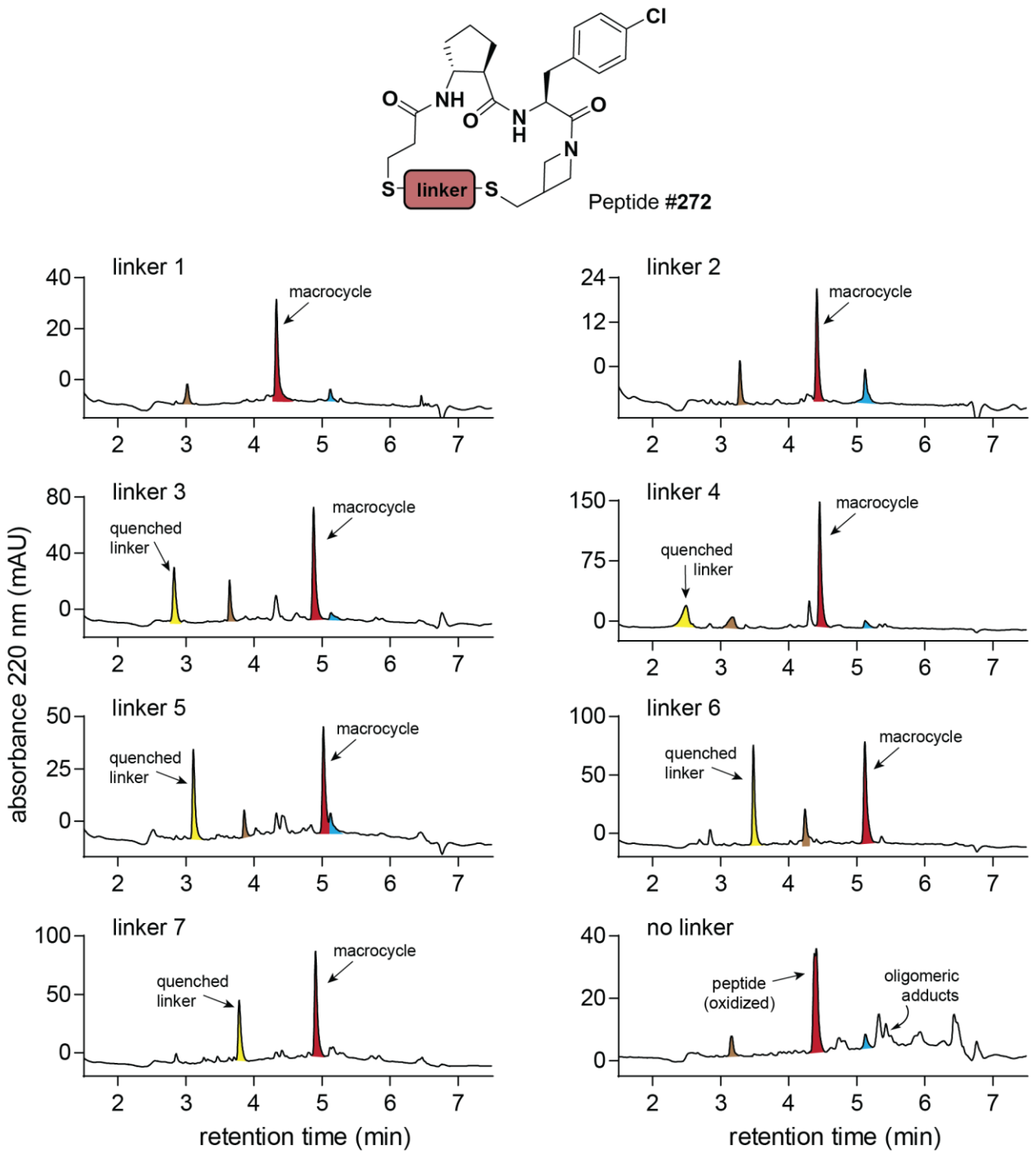

Supporting Figure S5. Quality control of macrocycle library; part II. UV_{220} spectra of randomly picked dithiol peptide (#272 of the 384 synthesized peptides, see Table S1 for full list of sequences) cyclized with the different bis-electrophilic linkers. Highlighted in red are the desired macrocyclic species. Highlighted in yellow, brown and blue is quenched linker adduct, truncated peptide [peptide – 4ClF] and HPLC column impurity, respectively.

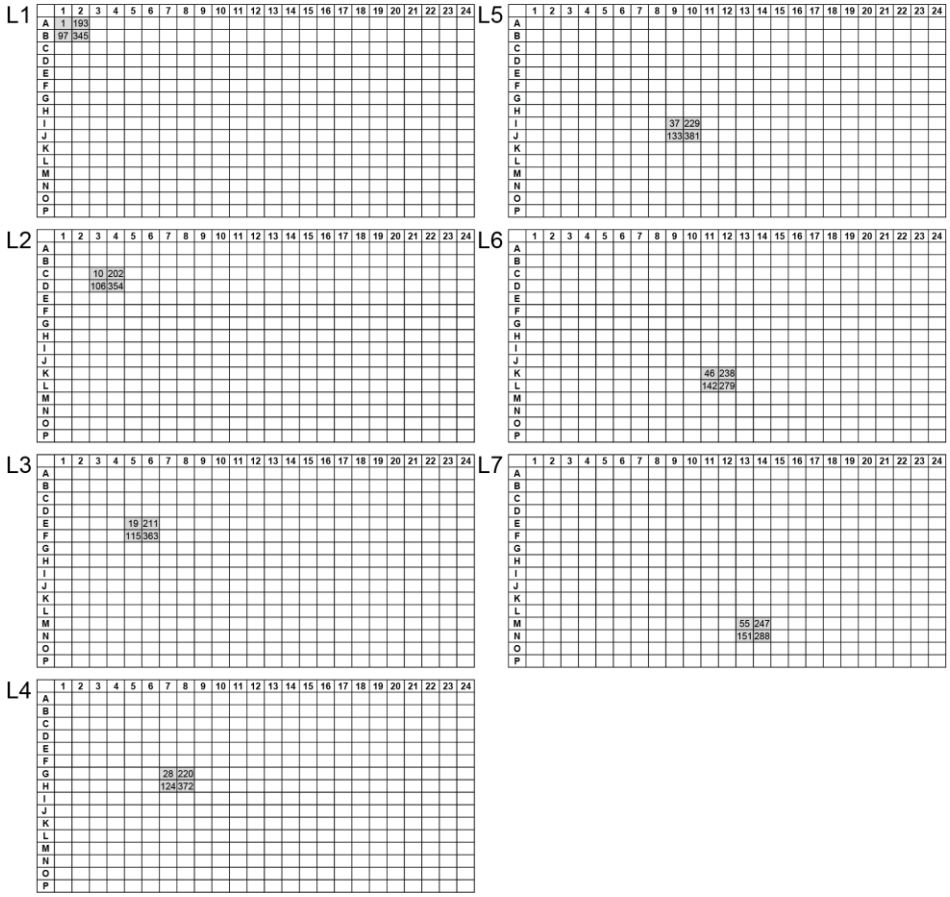

Supporting Figure S5. Quality control of macrocycle library; part III. Scheme used to pick 28 random library compounds. In each one of the seven plates, the dithiol peptides were cyclized with a different linker. Peptides were picked on a diagonal in the plates in different positions to ensure that each peptide sequence is represented only once, and that all seven aminothiol building blocks are equally represented.

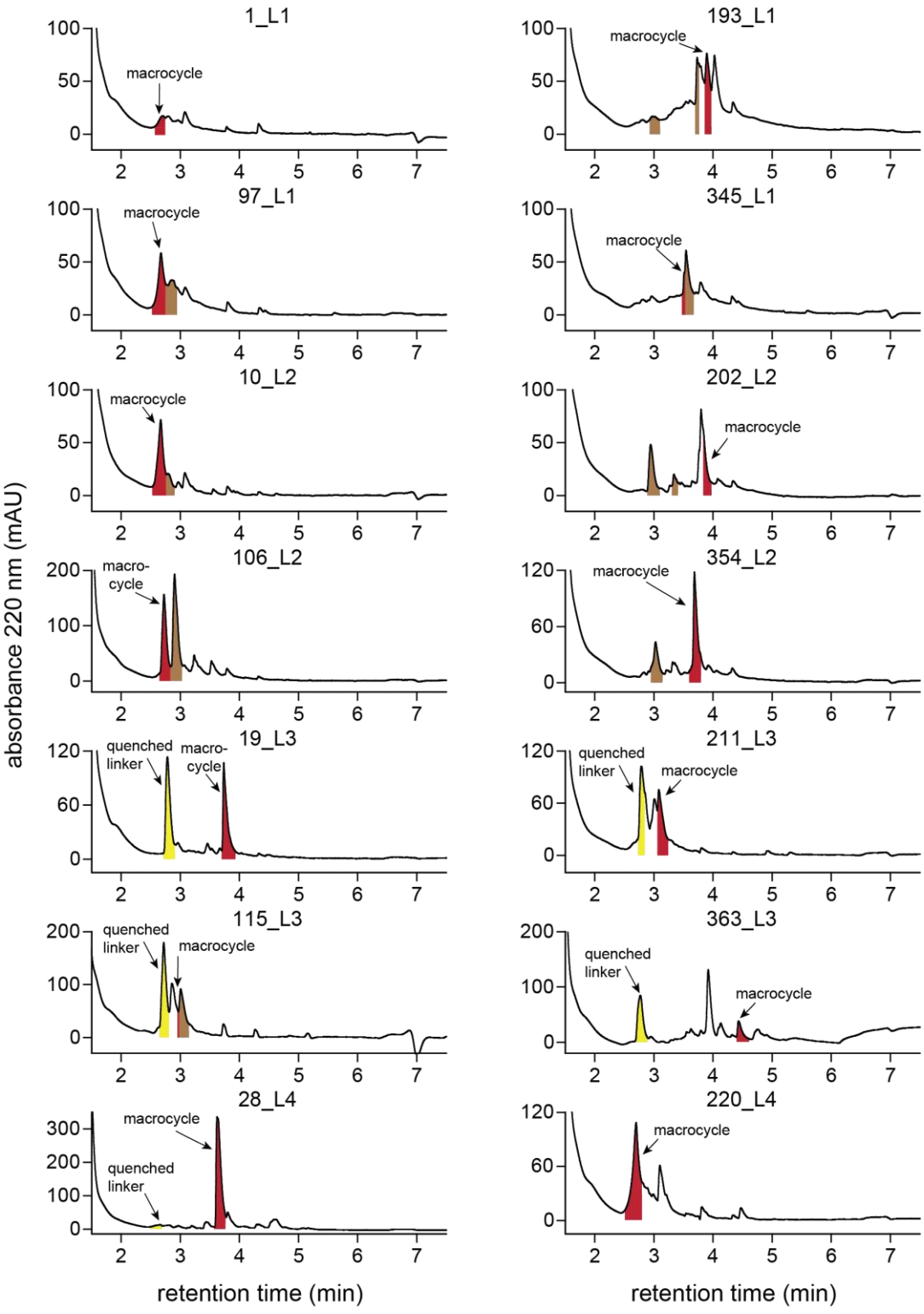

Supporting Figure S5. Quality control of macrocycle library; part VI. UV_{220} spectra of randomly picked library compounds (see scheme on previous page explaining how they were randomly chosen). Highlighted in red are the desired macrocyclic species. Highlighted in yellow and brown are quenched linker adduct and products resulting from truncated peptide, respectively.

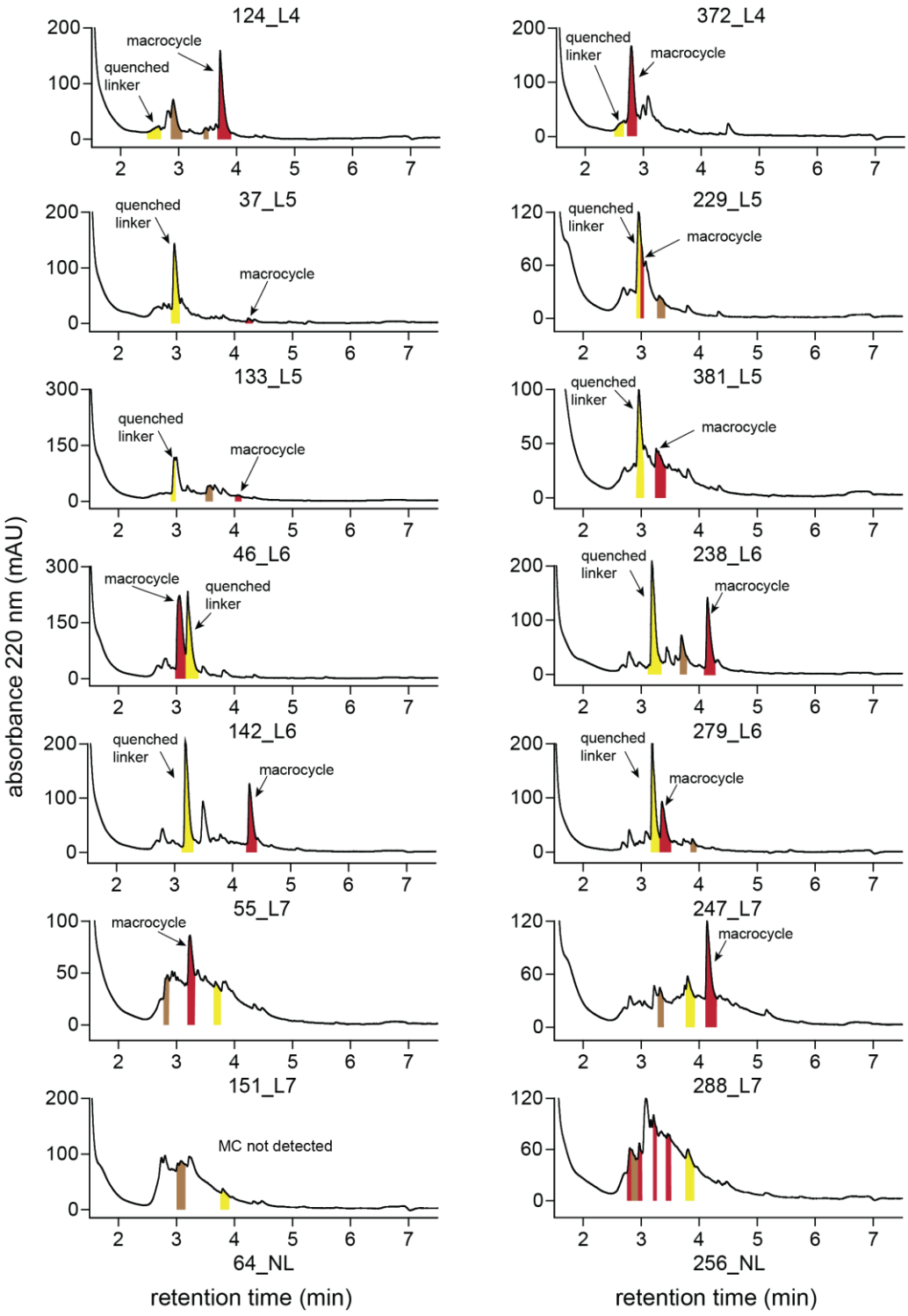

Supporting Figure S5. Quality control of macrocycle library; part V. UV_{220} spectra of randomly picked library compounds (see scheme on previous page explaining how they were randomly chosen). Highlighted in red are the desired macrocyclic species. Highlighted in yellow and brown are quenched linker adduct and products resulting from truncated peptide, respectively.

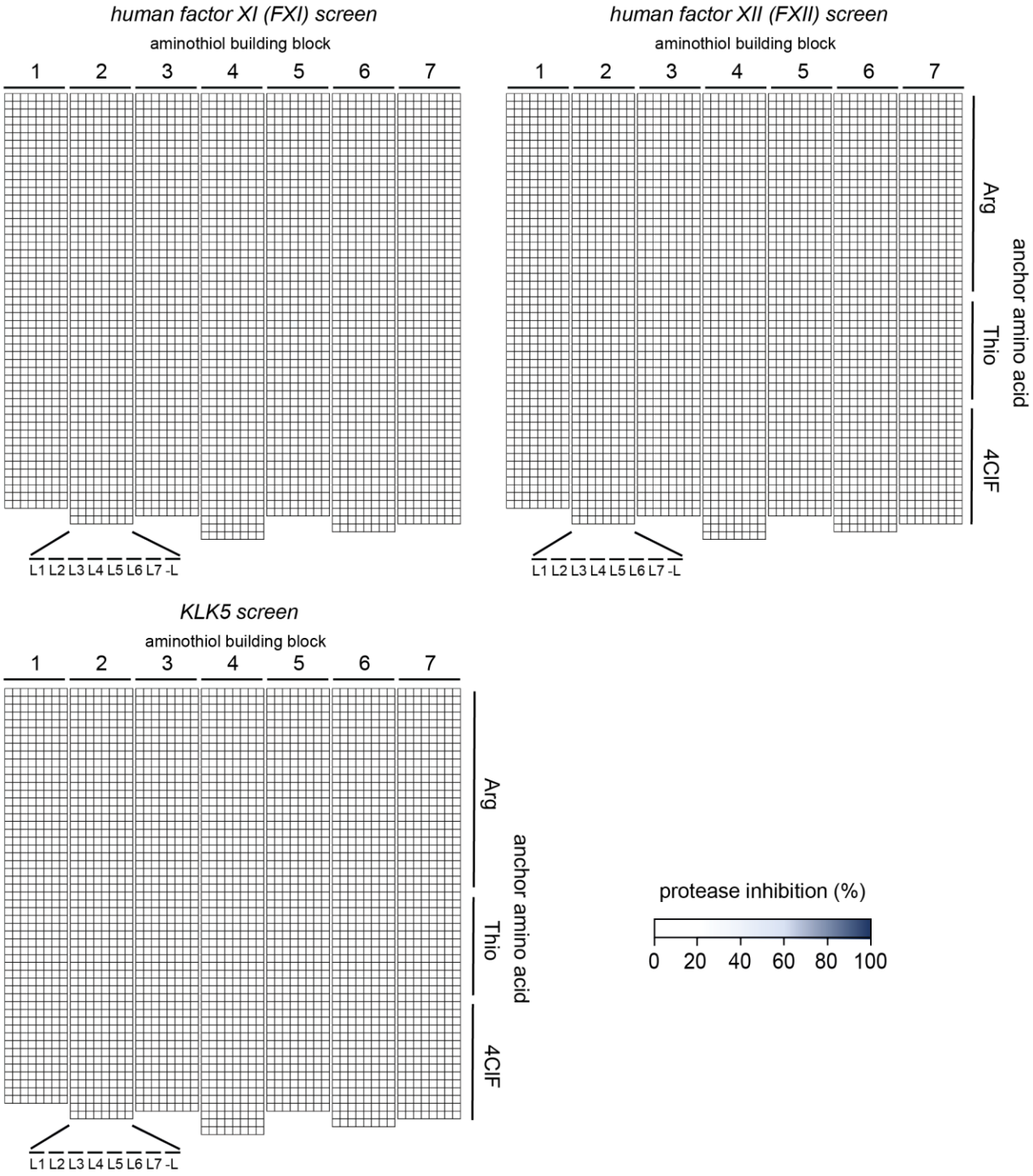

Supporting Figure S6. Screening against other trypsin-like serine proteases. Heatmap depicting residual protease inhibition by the macrocyclic library screened against FXI, FXII and KLK5 at 20 µM crude macrocycle concentration.

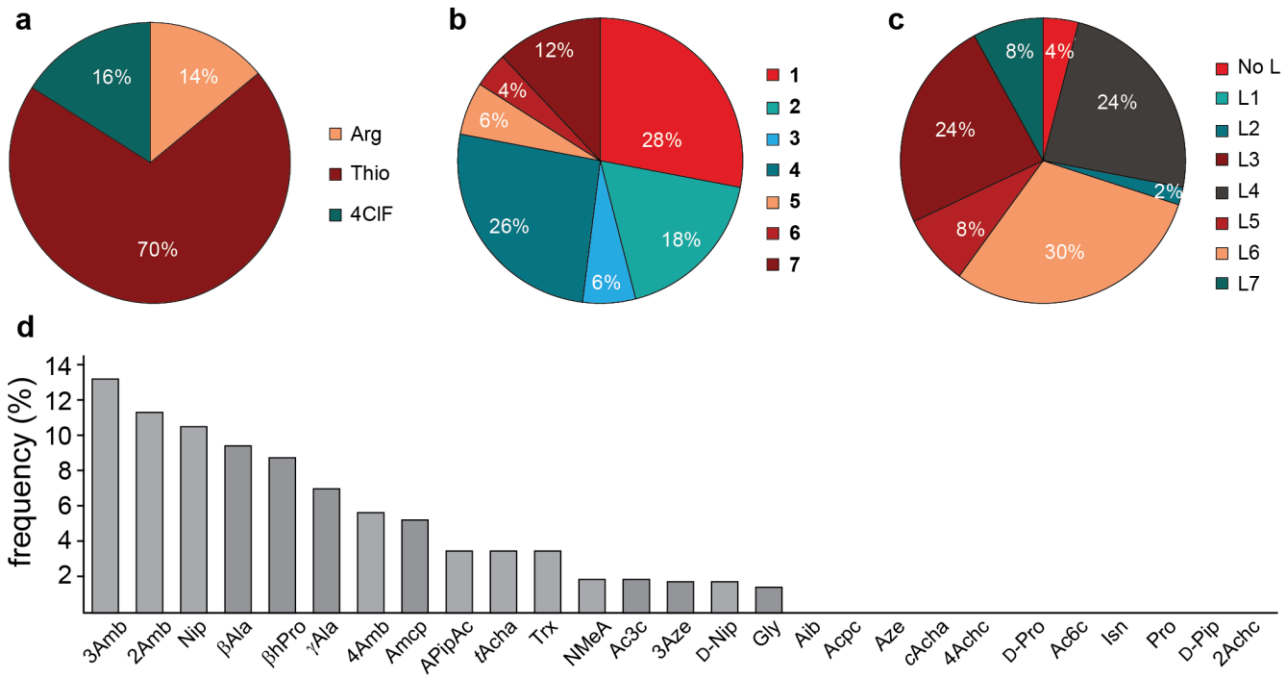

Supporting Figure S7. Molecular properties of hits from thrombin screen. Analysis of the 50 best thrombin inhibitors. a) Pie chart representing the share of hits per S1 pocket binder. b) Pie chart representing the share of each aminothiol derivative. c) Pie chart representing the share per linker. d) Column chart representing the share per amino acid.

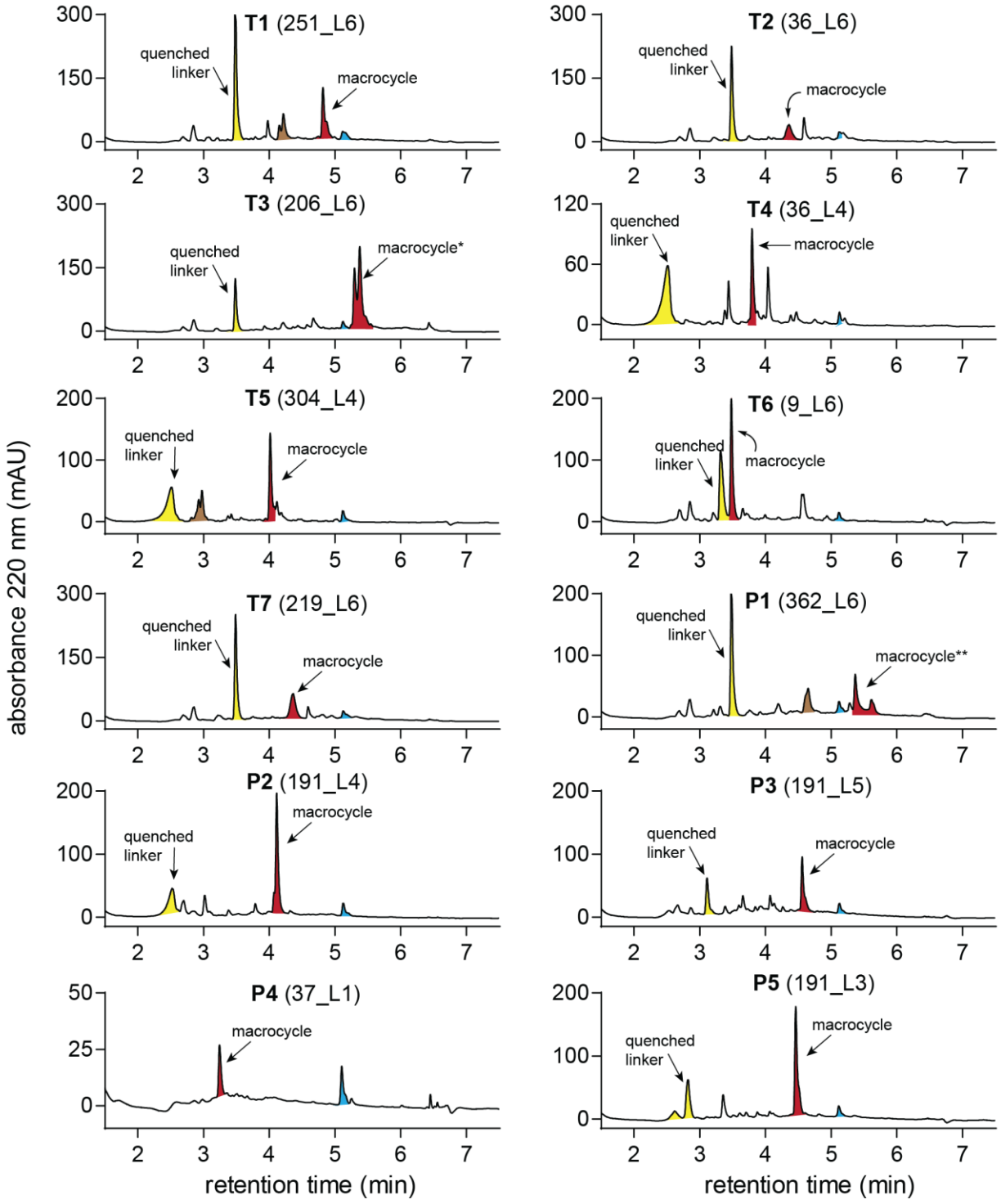

Supporting Figure S8. HPLC spectra of hits from cyclic peptide library screen. UV_{220} spectra of crude cyclic peptide hits from screening against thrombin or PK. Highlighted in red are the desired macrocyclic species. Highlighted in yellow, brown and blue is quenched linker adduct, truncated peptide and HPLC column impurity, respectively. *co-eluting with impurity. **macrocycle exists in two conformers. For chemical structures of the macrocycles, see Figure S9.

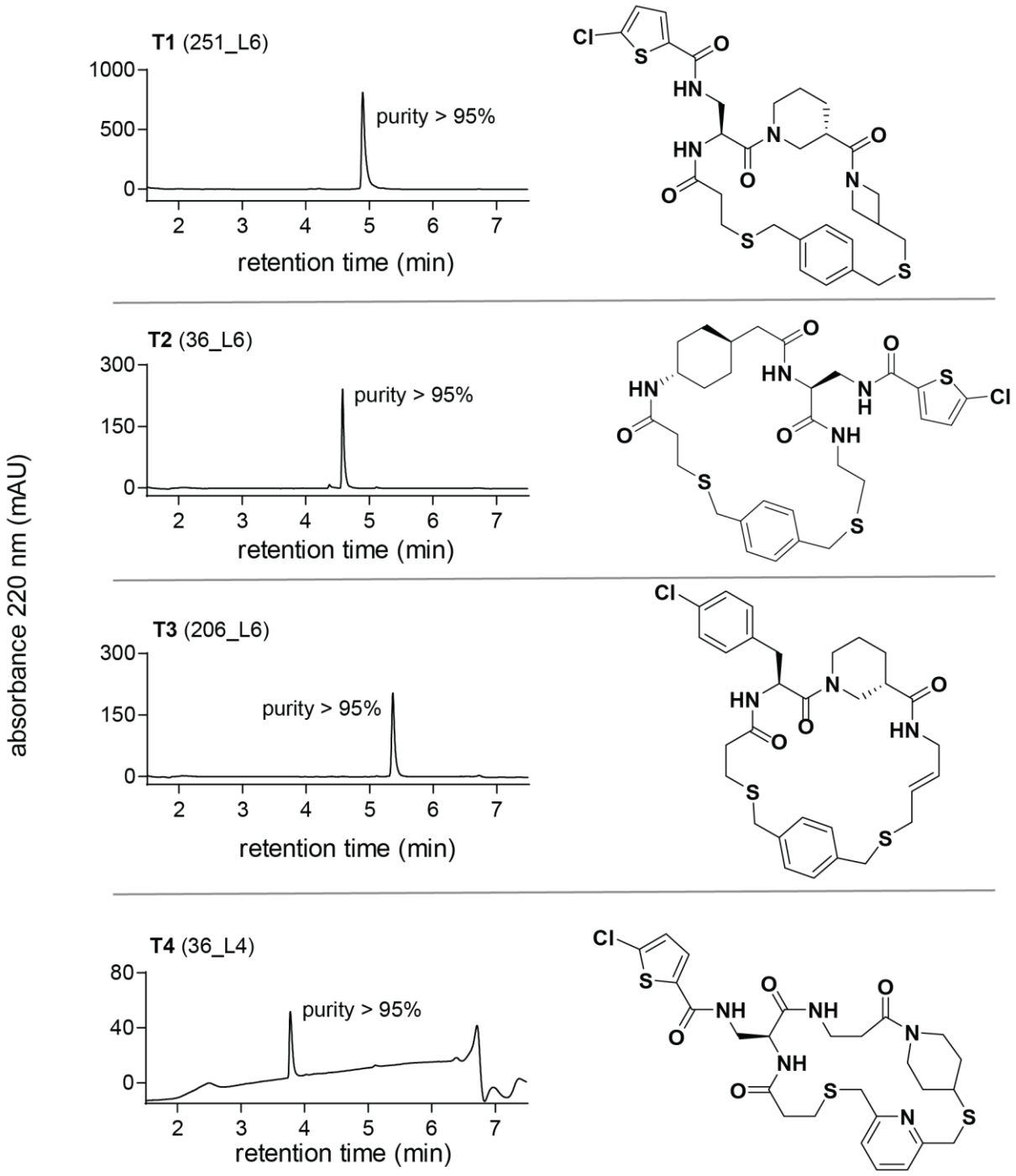

Supporting Figure S9. HPLC spectra of purified macrocyclic species; part I. UV_{220} spectra of purified cyclic peptides obtained after preparative HPLC purification. %-purity is depicted next to the compound peak.

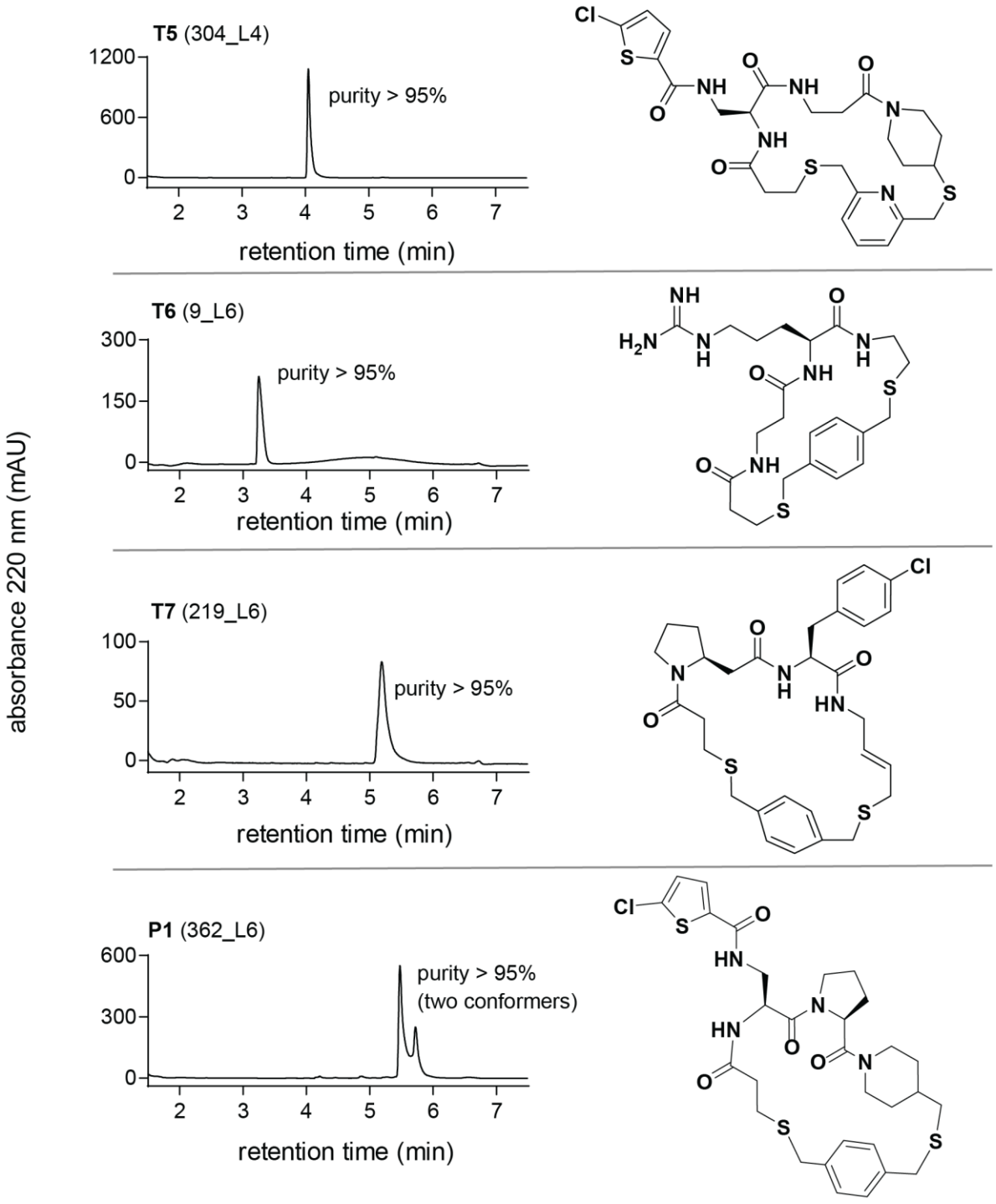

Supporting Figure S9. HPLC spectra of purified macrocyclic species; part II. UV_{220} spectra of purified cyclic peptides obtained after preparative HPLC purification. %-purity is depicted next to the compound peak. Macrocycle **P1** consists in an equilibrium of two conformers. See Figure S10 for variable-temperature HPLC analysis of **P1**.

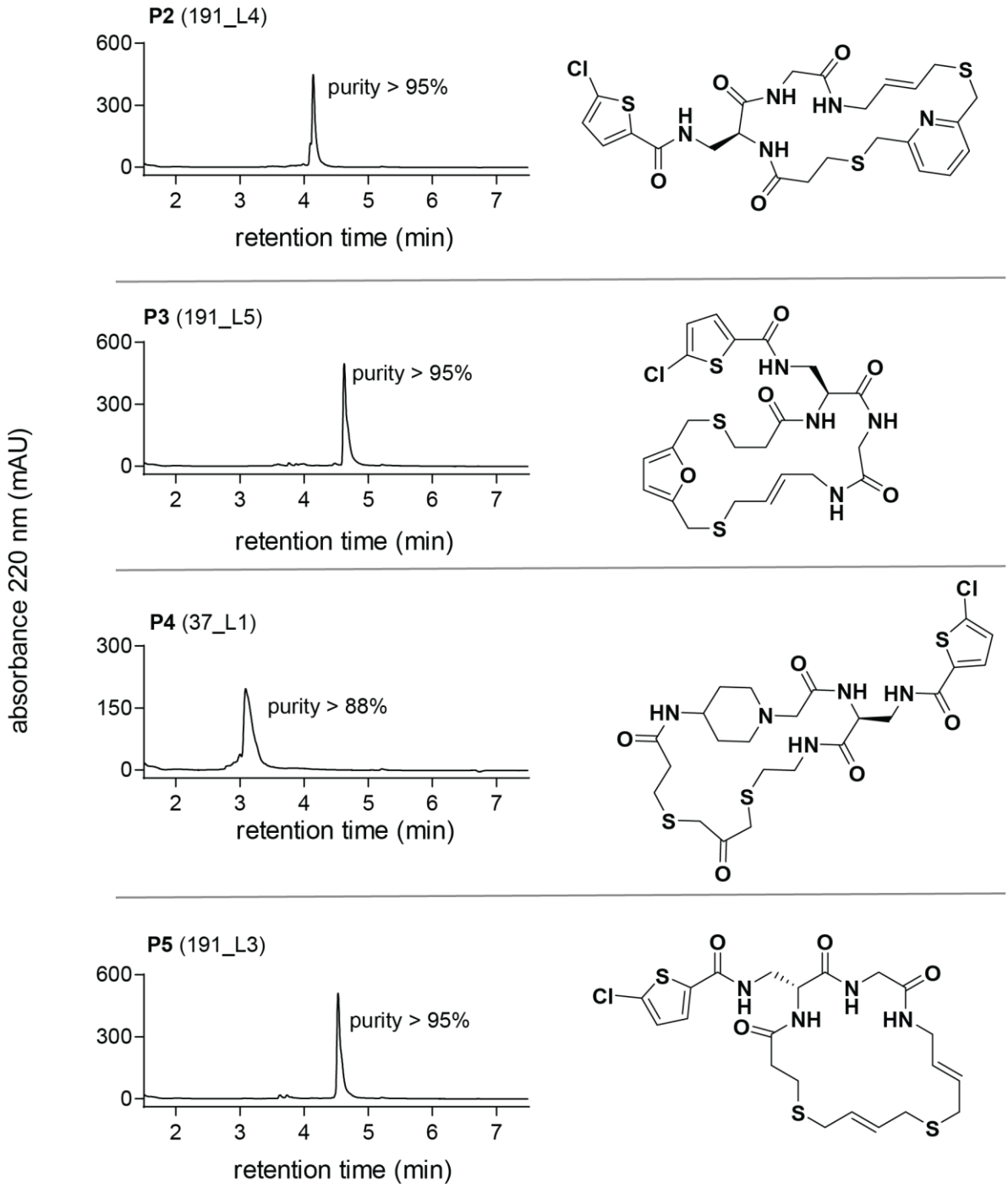

Supporting Figure S9. HPLC spectra of purified macrocyclic species; part III. UV_{220} spectra of purified cyclic peptides obtained after preparative HPLC purification. %-purity is depicted next to the compound peak.

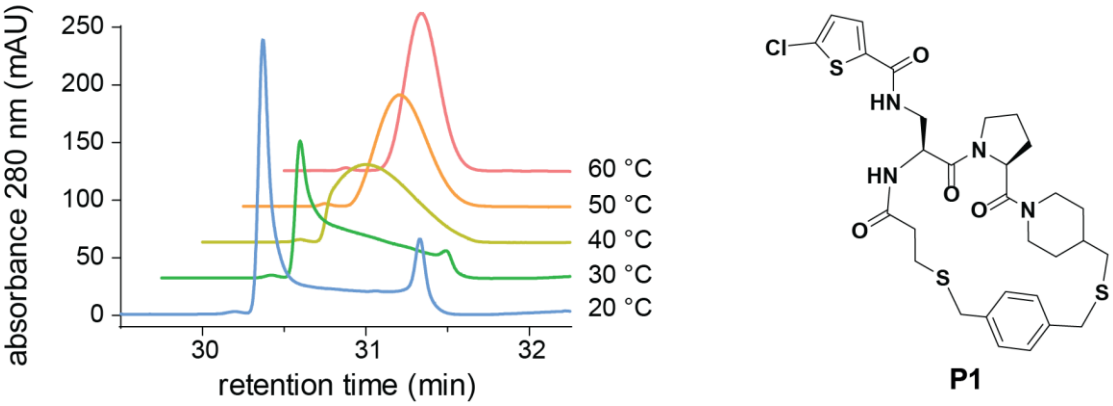

Supporting Figure S10. Variable temperature HPLC spectra. Analytical UV_{280} spectra of purified **P1** run at different column temperature increments. This highlights the presence of multiple conformers at lower temperatures that slowly converges into a single peak at elevated temperatures.

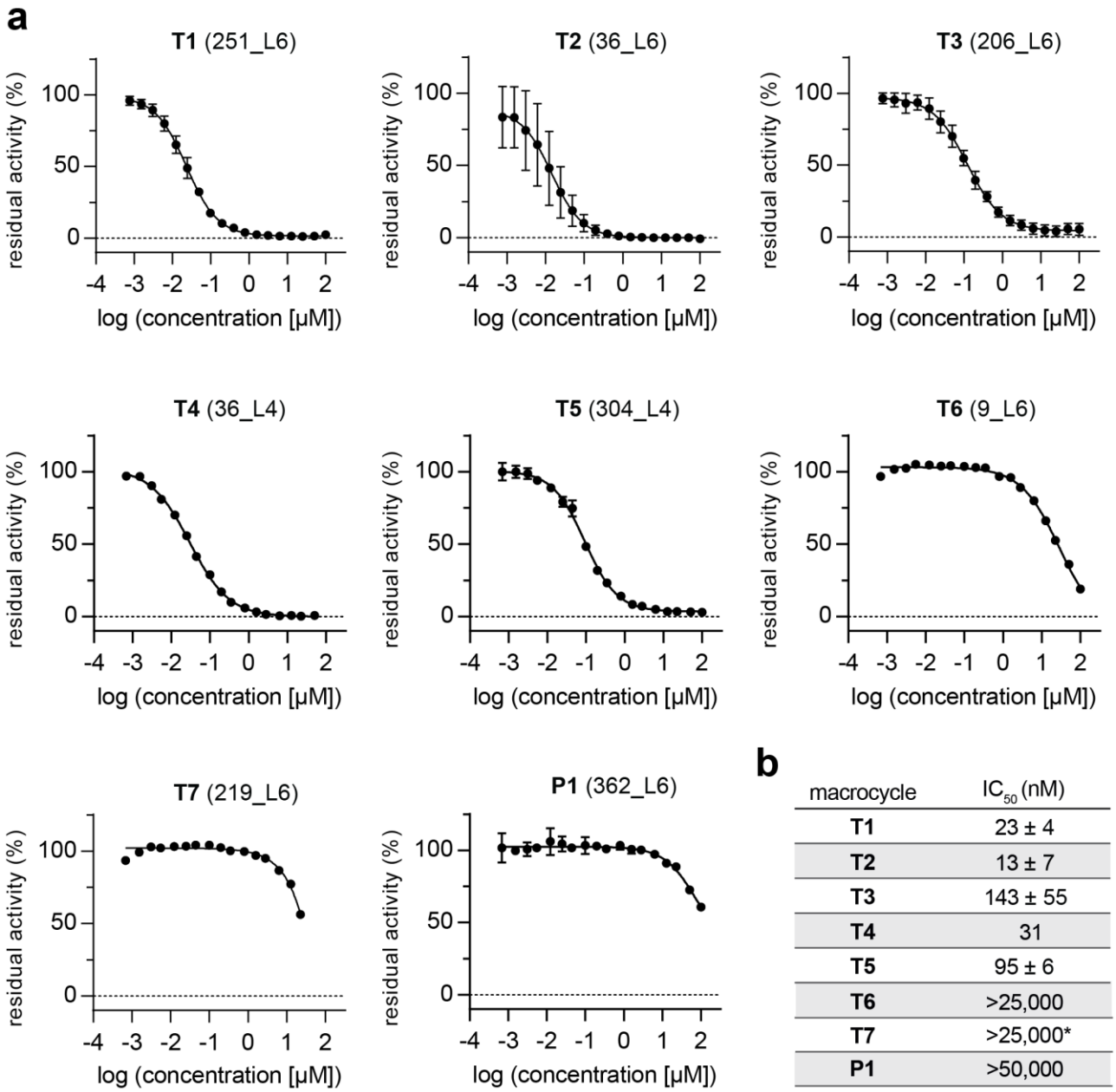

macrocycle	IC_{50} (nM)
T1	23 ± 4
T2	13 ± 7
T3	143 ± 55
T4	31
T5	95 ± 6
T6	>25,000
T7	>25,000*
P1	>50,000

Supporting Figure S11. Dose-response curves for thrombin inhibitors. a) Representative dose-response curves. Data in presented graphs is based on three experiments each performed in one replicate (**T1**–**T3**), or one experiment and two (**T4, T6, T7**) or four replicates (**T5**). b) Potencies for inhibition of the protease activity of recombinant thrombin (4 nM) against Cbz-G-G-R-AMC substrate (50 μM) are given as mean IC_{50} values ± standard deviation (SD). Values were calculated based on data of four independent experiments (**T1**–**T3**; one replicate per experiment), or one experiment and two (**T4, T6, T7**) or four replicates (**T3**). SD values were calculated only for inhibitors for which three or more values were measured. *compound suffers from poor solubility in water and DMSO and IC_{50} determination was difficult.

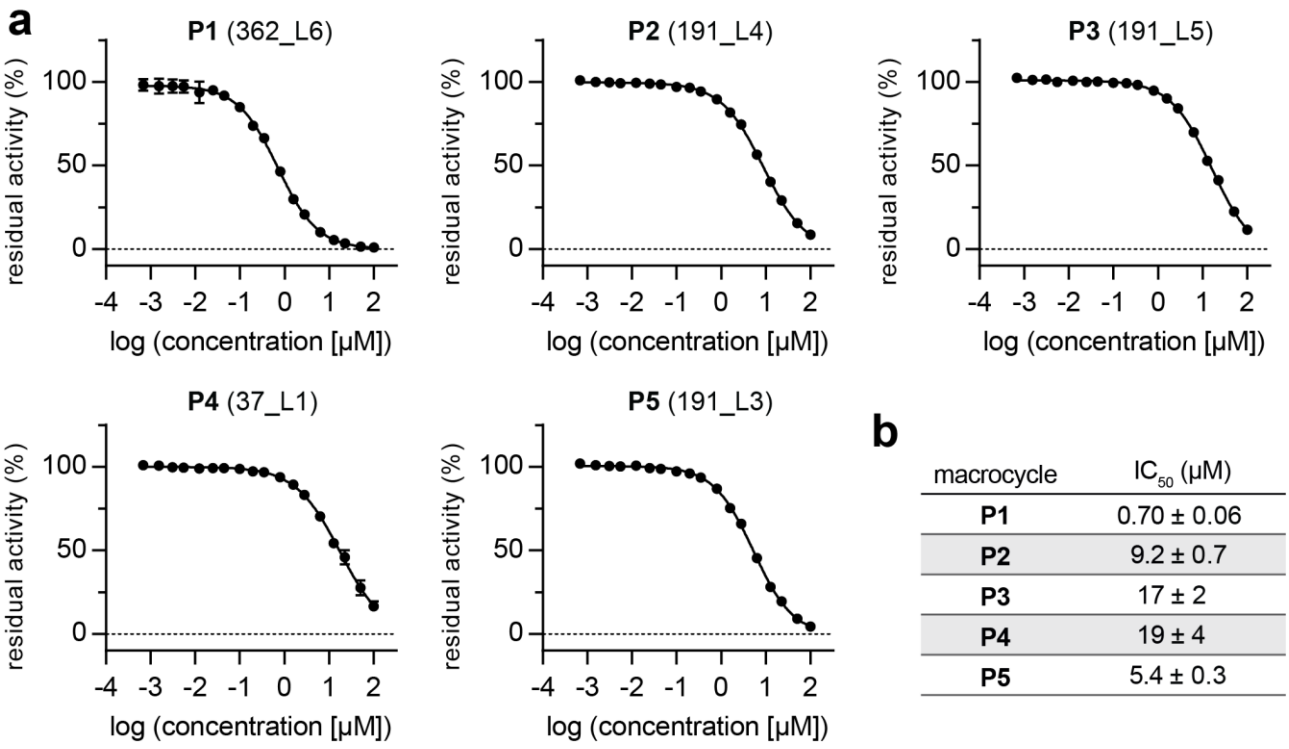

b

macrocycle	IC_{50} (µM)
P1	0.70 ± 0.06
P2	9.2 ± 0.7
P3	17 ± 2
P4	19 ± 4
P5	5.4 ± 0.3

Supporting Figure S12. Dose-response curves for PK. a) Representive dose-response curves. Data in presented graphs is based on one experiment (four replicates per experiment). b) Potencies for inhibition of the protease activity of recombinant PK (0.25 nM) against Cbz-F-R-AMC substrate (50 µM) are given as mean IC_{50} values ± SD. Data are based on 4 replicates performed in parallel.

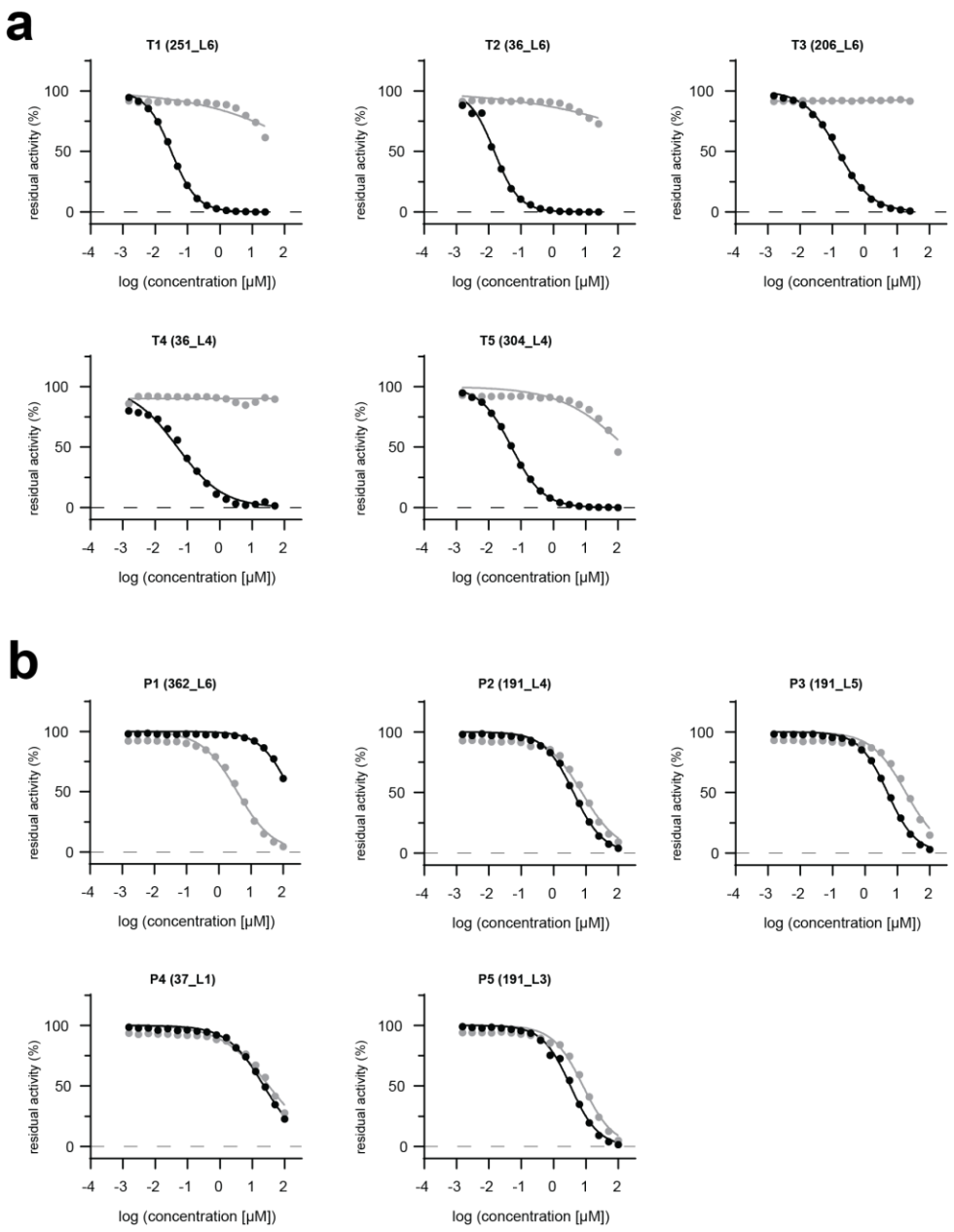

Supporting Figure S13. Inhibitor specificity. Inhibition of thrombin (black) and PK (gray) by inhibitors **T1**–**T5** identified in the thrombin screen (a) and by inhibitors **P1**–**P5** identified in the PK screen (b). The concentration of thrombin was 4 nM and that of PK 0.25 nM. The concentration of the fluorogenic substrates was 50 µM. The dilution series were prepared using acoustic dispensing. Data are based on three replicates performed in parallel (average values are shown but not the SD that were small would not be seen).

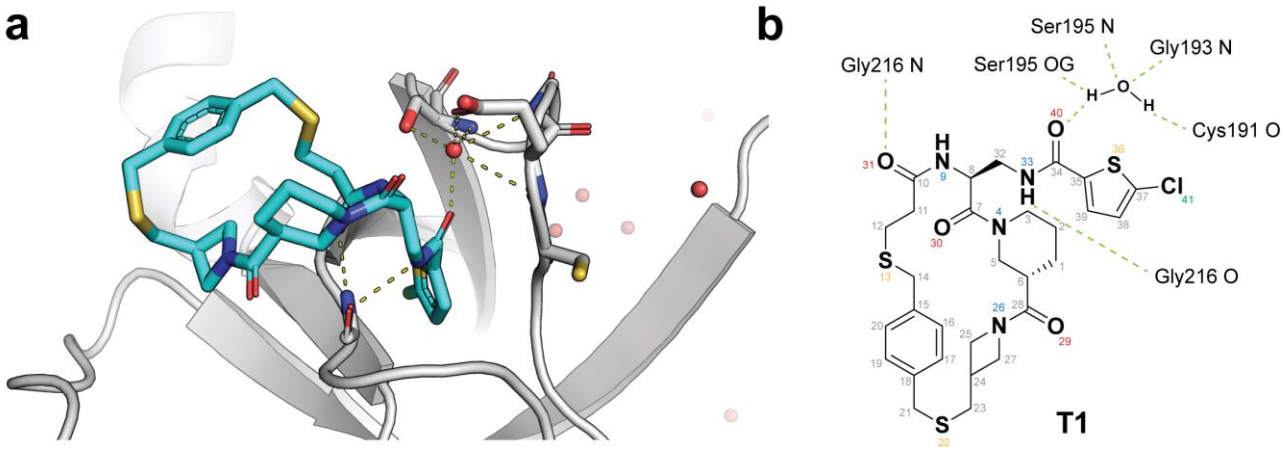

Supporting Figure S14. Structure of thrombin–T1 complex. a) X-ray co-crystal structure of **T1** (cyan) bound to thrombin. **T1** is zoomed in and the H-bond interactions are indicated. b) Chemical structure of **T1** (including X-ray structure numbering) and H-bond interactions formed with thrombin, including those via a water molecule.

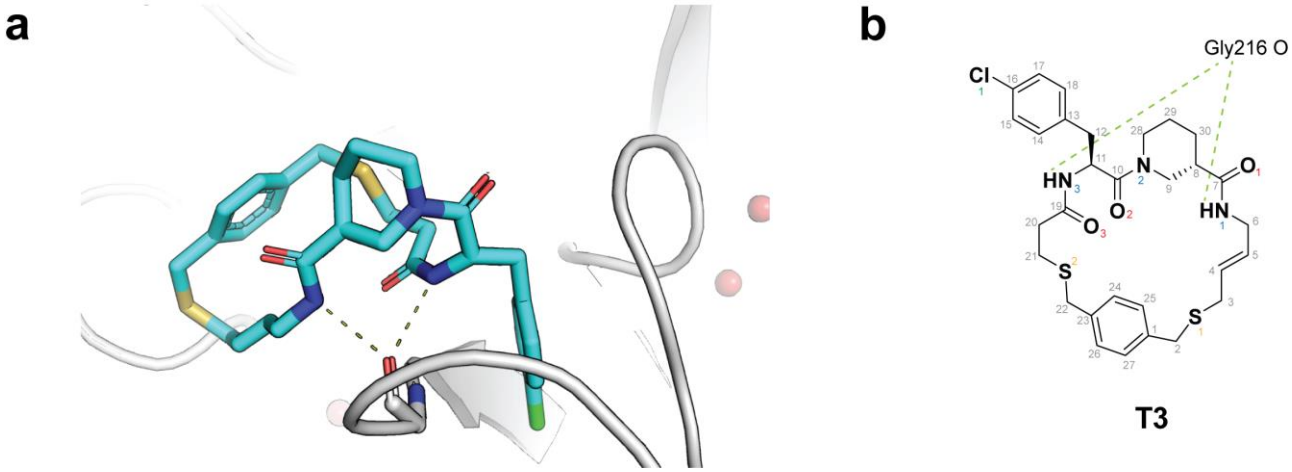

Supporting Figure S15. Structure of thrombin–T3 complex. a) X-ray co-crystal structure of **T3** (cyan) bound to thrombin. **T3** is zoomed in and the H-bond interactions are indicated. b) Chemical structure of **T3** (including X-ray structure numbering) and H-bond interactions formed with thrombin.

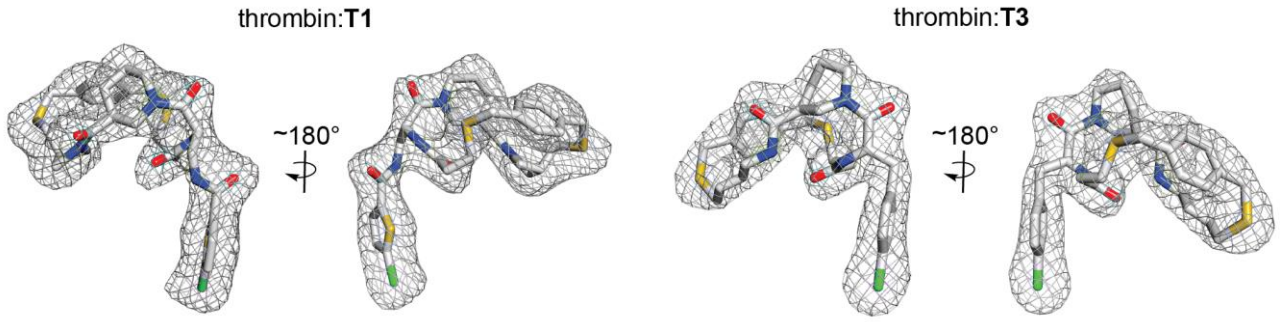

Supporting Figure S16. Electron-density mapping of T1 and T3. Stereo view of compounds **T1** and **T3** (white sticks) when bound to thrombin. The $|F_o|-|F_c|$ omit electron-density map contoured at 3.0 σ (gray mesh) is superimposed.

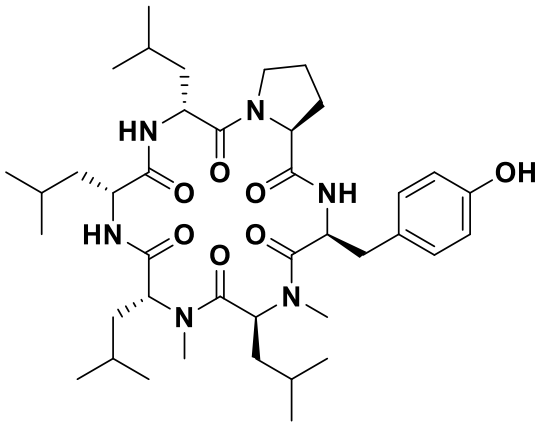

Craik - peptide 15
(Wang *et al.*, 2014)

Carbamazepine

Supporting Figure S17. Chemical structures of PAMPA controls. Compound were purchased or synthesized as previously described: Craik (peptide 15).[25]

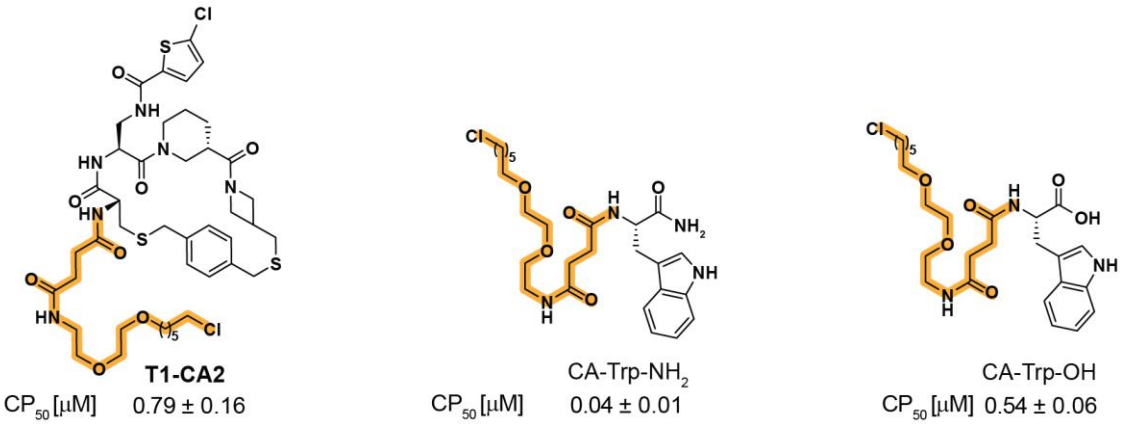

Supporting Figure S18. Additional CAPA data. Structure of additional chloroalkane probes/controls and their mean CP_{50} values ± SD (n = 4).

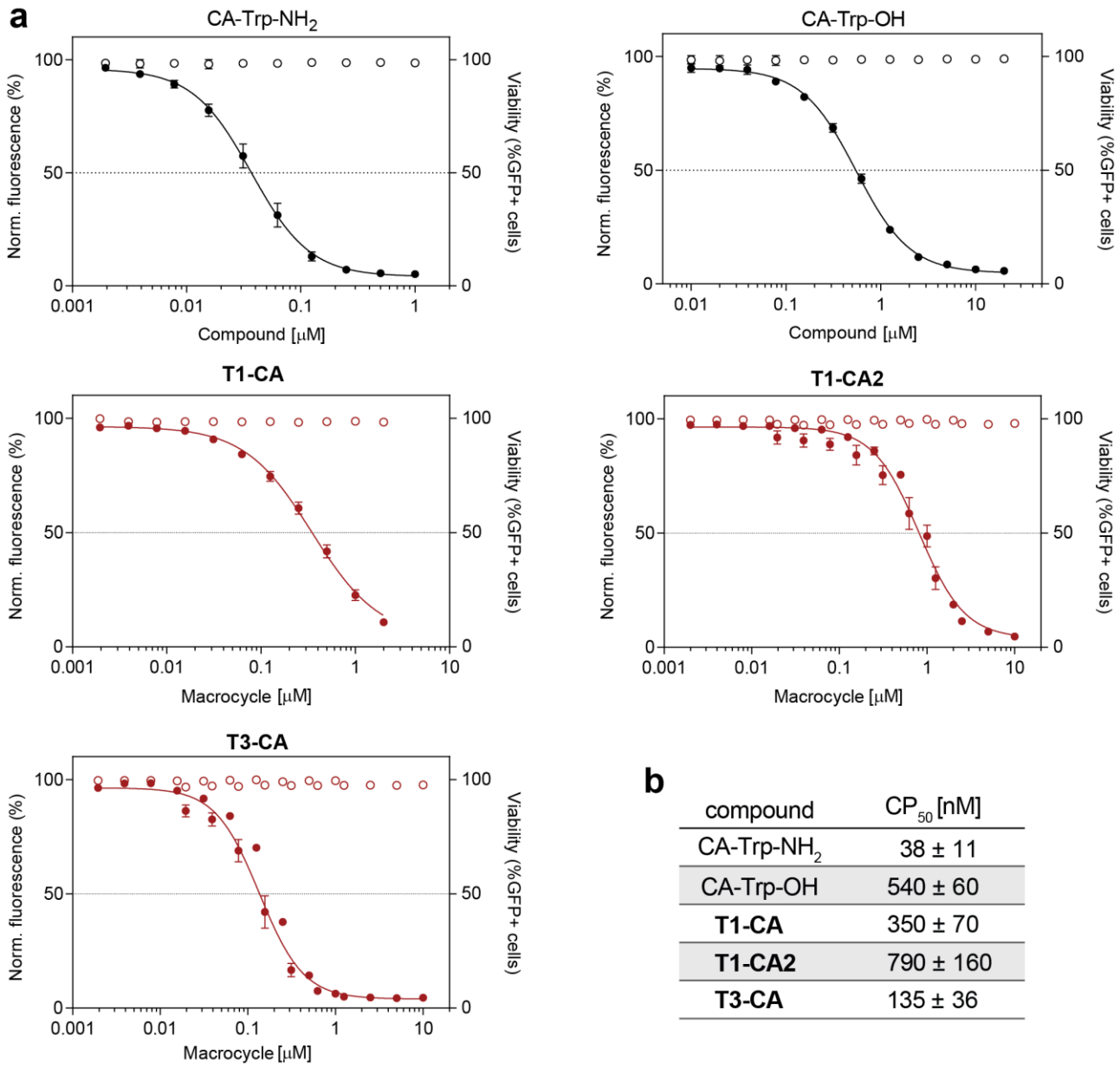

b

compound	CP_{50} [nM]
CA-Trp-NH_2	38 ± 11
CA-Trp-OH	540 ± 60
T1-CA	350 ± 70
T1-CA2	790 ± 160
T3-CA	135 ± 36

Supporting Figure S19. CAPA dose-response curves. a) CAPA results for all tested compound after 4 h treatment with compound/macrocycle at different concentrations. Data in presented graphs are based on four independent experiments performed on different days. White circles represent the cell viability at designated concentrations. b) Calculated CP_{50} values ± SD (n = 4).

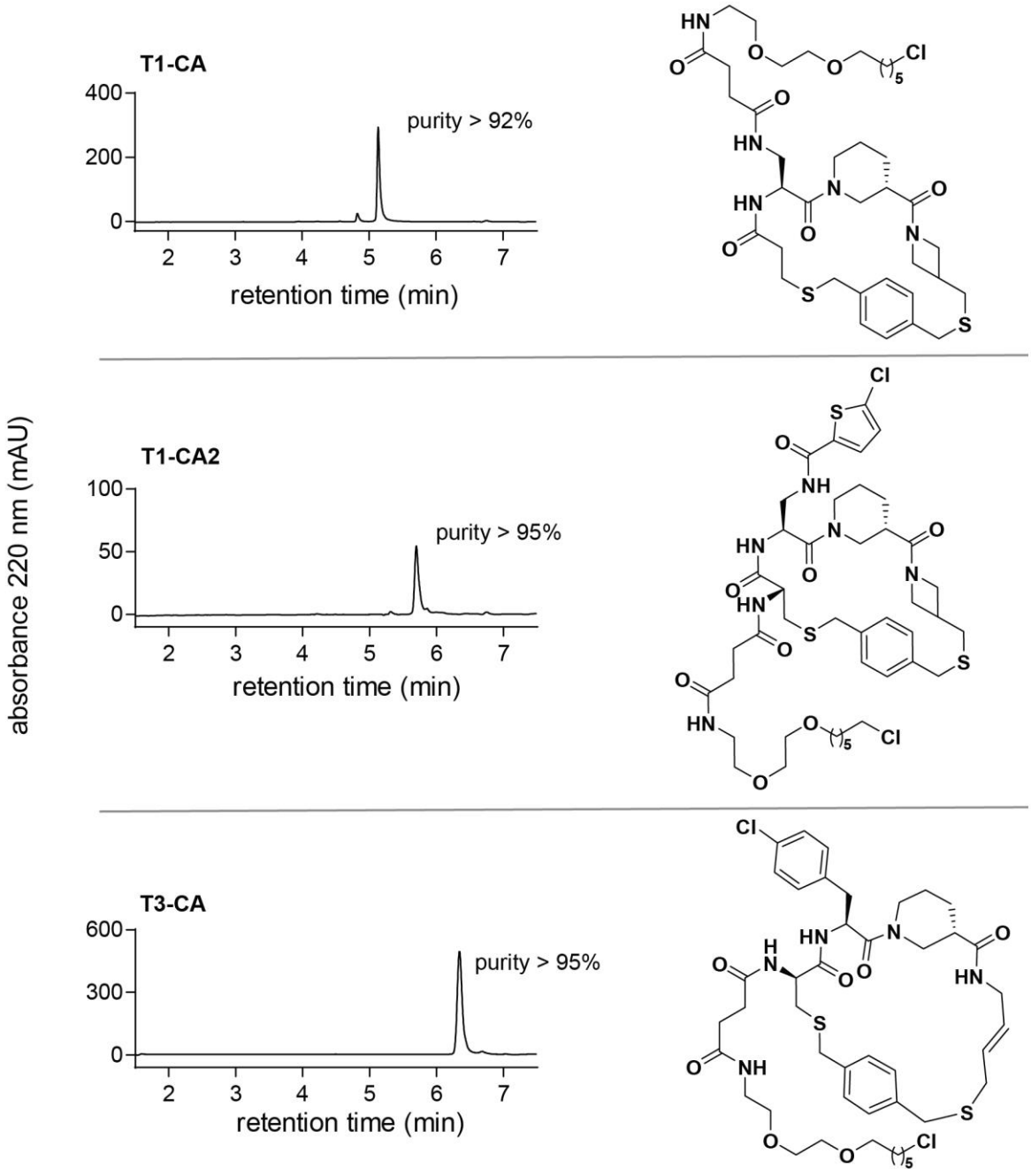

Supporting Figure S20. HPLC spectra and strutures of chloroalkane macrocycles. UV_{220} spectra of purified chloroalkane probes macrocycles obtained after preparative HPLC purification. %-purity is depicted next to the compound peak.

SUPPORTING REFERENCES

[1] A. J. Brockway, C. C. Cosner, O. A. Volkov, M. A. Phillips, J. K. De Brabander, *Synthesis* **2016**, *48*, 2065–2068.

[2] X. Li, X. M. Li, Y. Jiang, Z. Liu, Y. Cui, K. Y. Fung, S. H. E. van der Beelen, G. Tian, L. Wan, X. Shi, C. D. Allis, H. Li, Y. Li, X. D. Li, *Nat. Chem. Biol.* **2018**, *14*, 1140–1149.

[3] S. Habeshian, G. A. Sable, M. Schüttel, M. L. Merz, C. Heinis, *ACS Chem. Biol.* **2022**, *17*, 181–186.

[4] M. Gude, J. Ryf, P. D. White, *Lett. Pept. Sci.* **2002**, *9*, 203–206.

[5] L. Peraro, K. L. Deprey, M. K. Moser, Z. Zou, H. L. Ball, B. Levine, J. A. Kritzer, *J. Am. Chem. Soc.* **2018**, *140*, 11360–11369.

[6] P. Gonschorek, A. Zorzi, T. Maric, M. Le Jeune, M. Schüttel, M. Montagnon, R. Gómez-Ojea, D. P. Vollmar, C. Whitfield, L. Reymond, V. Carle, H. Verma, O. Schilling, A. Hovnanian, C. Heinis, *J. Med. Chem.* **2022**, *65*, 9735–9749.

[7] H. C. Hemker, P. Giesen, R. Al Dieri, V. Regnault, E. De Smedt, R. Wagenvoord, T. Lecompte, S. Béguin, *Pathophysiol. Haemost. Thromb.* **2003**, *33*, 4–15.

[8] S. J. Middendorp, J. Wilbs, C. Quarroz, S. Calzavarini, A. Angelillo-Scherrer, C. Heinis, *J. Med. Chem.* **2017**, *60*, 1151–1158.

[9] I. P. Michael, G. Sotiropoulou, G. Pampalakis, A. Magklara, M. Ghosh, G. Wasney, E. P. Diamandis, *J. of Biol. Chem.* **2005**, *280*, 14628–14635.

[10] V. Baeriswyl, H. Rapley, L. Pollaro, C. Stace, D. Teufel, E. Walker, S. Chen, G. Winter, J. Tite, C. Heinis, *ChemMedChem* **2012**, *7*, 1173–1176.

[11] L. Peraro, Z. Zou, K. M. Makwana, A. E. Cummings, H. L. Ball, H. Yu, Y.-S. Lin, B. Levine, J. A. Kritzer, *J. Am. Chem. Soc.* **2017**, *139*, 7792–7802.

[12] C.R.O. Bartling, F. Alexopoulou, S. Kuschert, Y.K. Chin, X. Jia, V. Sereikaite, D. Özcelik, T.M. Jensen, P. Jain, M.M. Nygaard, K. Harpsøe, D.E. Gloriam, M. Mobli, K. Strømgaard. *J. Med. Chem.* **2023**, *66*, 3045–3057.

[13] E. R. Ballister, C. Aonbangkhen, A. M. Mayo, M. A. Lampson, D. M. Chenoweth, *Nat. Commun.* **2014**, *5*, 5475.

[14] L. Potterton, J. Agirre, C. Ballard, K. Cowtan, E. Dodson, P. R. Evans, H. T. Jenkins, R. Keegan, E. Krissinel, K. Stevenson, A. Lebedev, S. J. McNicholas, R. A. Nicholls, M. Noble, N. S. Pannu, C. Roth, G. Sheldrick, P. Skubak, J. Turkenburg, V. Uski, F. von Delft, D. Waterman, K. Wilson, M. Winn, M. Wojdyr, *Acta Cryst.* **2018**, *D74*, 68–84.

[15] A. J. McCoy, R. W. Grosse-Kunstleve, P. D. Adams, M. D. Winn, L. C. Storoni, R. J. Read, *J. Appl. Crystallogr.* **2007**, *40*, 658–674.

[16] S. Habeshian, M. L. Merz, G. Sangouard, G. K. Mothukuri, M. Schüttel, Z. Bognár, C. Díaz-Perlas, J. Vesin, J. Bortoli Chapalay, G. Turcatti, L. Cendron, A. Angelini, C. Heinis, *Nat. Commun.* **2022**, *13*, 3823.

[17] A. A. Vagin, R. A. Steiner, A. A. Lebedev, L. Potterton, S. McNicholas, F. Long, G. N. Murshudov, *Acta Cryst.* **2004**, *D60*, 2184–2195.

[18] P. D. Adams, P. V. Afonine, G. Bunkóczi, V. B. Chen, I. W. Davis, N. Echols, J. J. Headd, L. W. Hung, G. J. Kapral, R. W. Grosse-Kunstleve, A. J. McCoy, N. W. Moriarty, R. Oeffner, R. J. Read, D. C. Richardson, J. S. Richardson, T. C. Terwilliger, P. H. Zwart, *Acta Cryst.* **2010**, *D66*, 213–221.

[19] P. Emsley, B. Lohkamp, W. G. Scott, K. Cowtan, *Acta Cryst.* **2010**, *D66*, 486–501.

[20] E. Krissinel, K. Henrick, *J. Mol. Biol.* **2007**, *372*, 774–797.

[21] R. A. Laskowski, J. D. Watson, J. M. Thornton, *Nucleic Acids Res.* **2005**, *33*, W89–W93.

[22] R. A. Laskowski, M. B. Swindells, *J. Chem. Inf. Model.* **2011**, *51*, 2778–2786.

[23] Schrodinger LLC. The PyMOL Molecular Graphics System, Version 1.8. (2015).

[24] Z. Bognar, G. K. Mothukuri, A. L. Nielsen, M. L. Merz, P. M. F. Pânzar, C. Heinis, *Org. Biomol. Chem.* **2022**, *20*, 5699–5703.

[25] C. K. Wang, S. E. Northfield, B. Colless, S. Chaousis, I. Hamernig, R.-J. Lohman, D. S. Nielsen, C. I. Schroeder, S. Liras, D. A. Price, D. P. Fairlie, D. J. Craik, *Proc. Natl. Acad. Sci. USA* **2014**, *111*, 17504–17509.

ABBREVIATION LIST

ADE	acoustic droplet ejection
AM PS	amino methyl polystyrene
AUC	area under the curve
BDT	1,4-butanedithiol
BSA	bovine serum albumin
CA	chloroalkane
CAPA	chloroalkane penetration assay
CI	confidence interval
COC	cyclic olefin copolymer
CP_{50}	half-maximal cellular penetration
DCC	*N,N'*-dicyclohexylcarbodiimide
DTNB	Ellman's reagent (5,5-dithio-bis-(2-nitrobenzoic acid)
HATU	1-[Bis(dimethylamino)-methylene]-1*H*-1,2,3-triazolo[4,5-*b*]pyridinium 3-oxide hexafluorophosphate
HBTU	2-(1*H*-benzotriazol-1-yl)-1,1,3,3-tetramethyluronium hexafluorophosphate
HRMS	high-resolution mass spectrometry
IC_{50}	half maximal inhibitor concentration
K_M	Michaelis−Menten constant
LDV	low dead volume
Mpa	3-mercaptopropionic acid
NAG	*N*-acetyl-β-D-glucosamine
NHS	*N*-hydroxysuccinimide
NMM	*N*-methylmorpholine
NMP	*N*-methylpyrrolidone
NMR	nuclear magnetic resonance
n.d.	not determined
PAMPA	parallel artificial membrane permeability assay
PBS	phosphate buffered saline
PDB	the protein data bank
PEG	polyethylene glycol
PG	protecting group
PP	polypropylene
PS	polystyrene
R	mass retention
RP	reversed phase
RVC	rotational vacuum concentration (SpeedVac)
SD	standard deviation
SH PS	thiol-functionalized polystyrene
TLC	thin-layer chromatography
TOF	time-of-flight
β-ME	β-mercaptoethanol

NMR SPECTRA

^{1}H NMR (400 MHz, $CDCl_3$) of **S1** (crude)

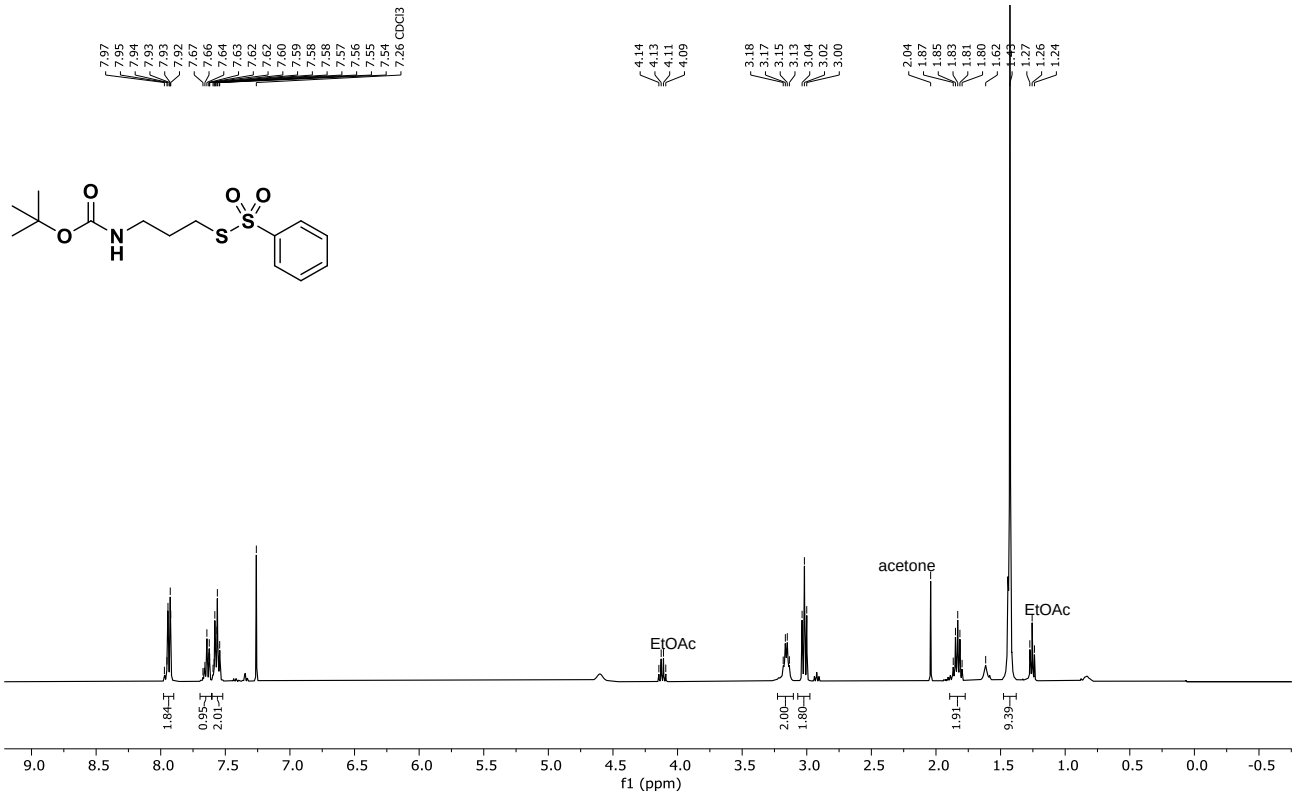

^{1}H NMR (400 MHz, $CDCl_3$) of **S2** (crude)

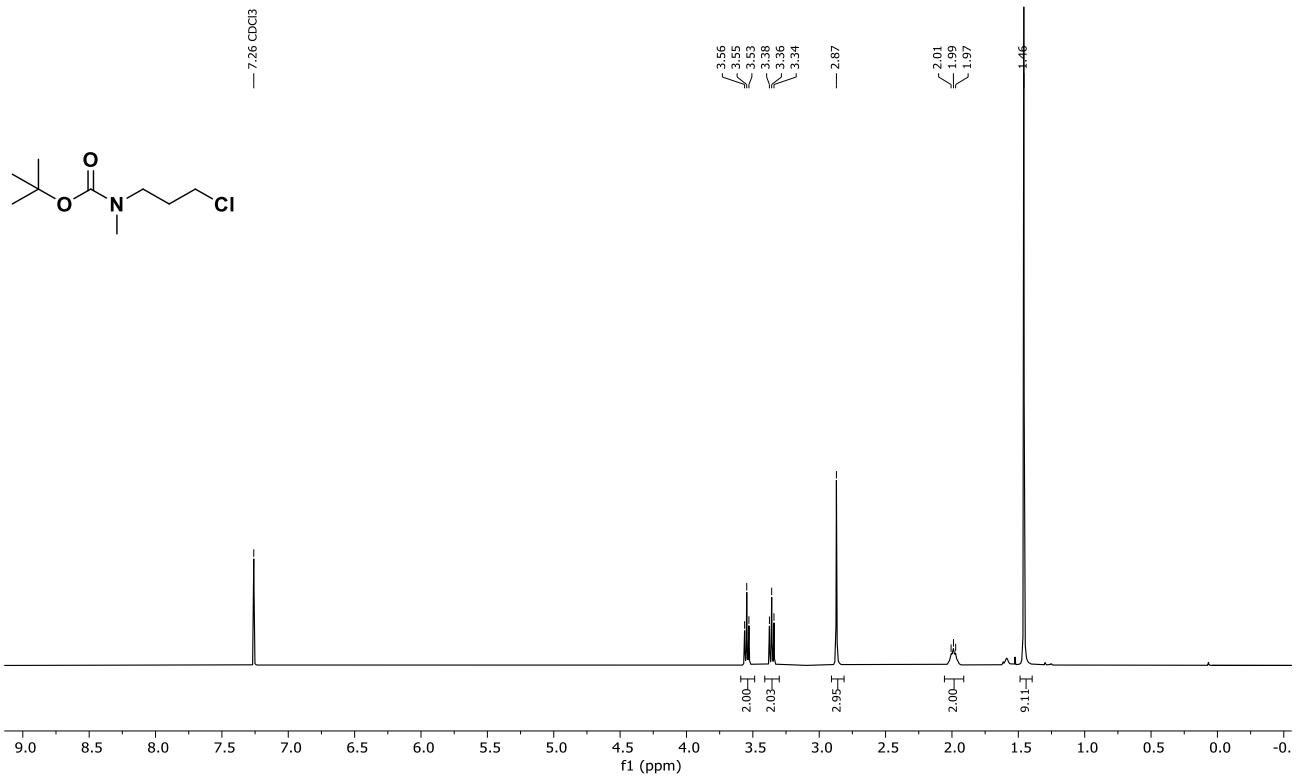

^{1}H NMR (400 MHz, $CDCl_3$) of **S3** (crude)

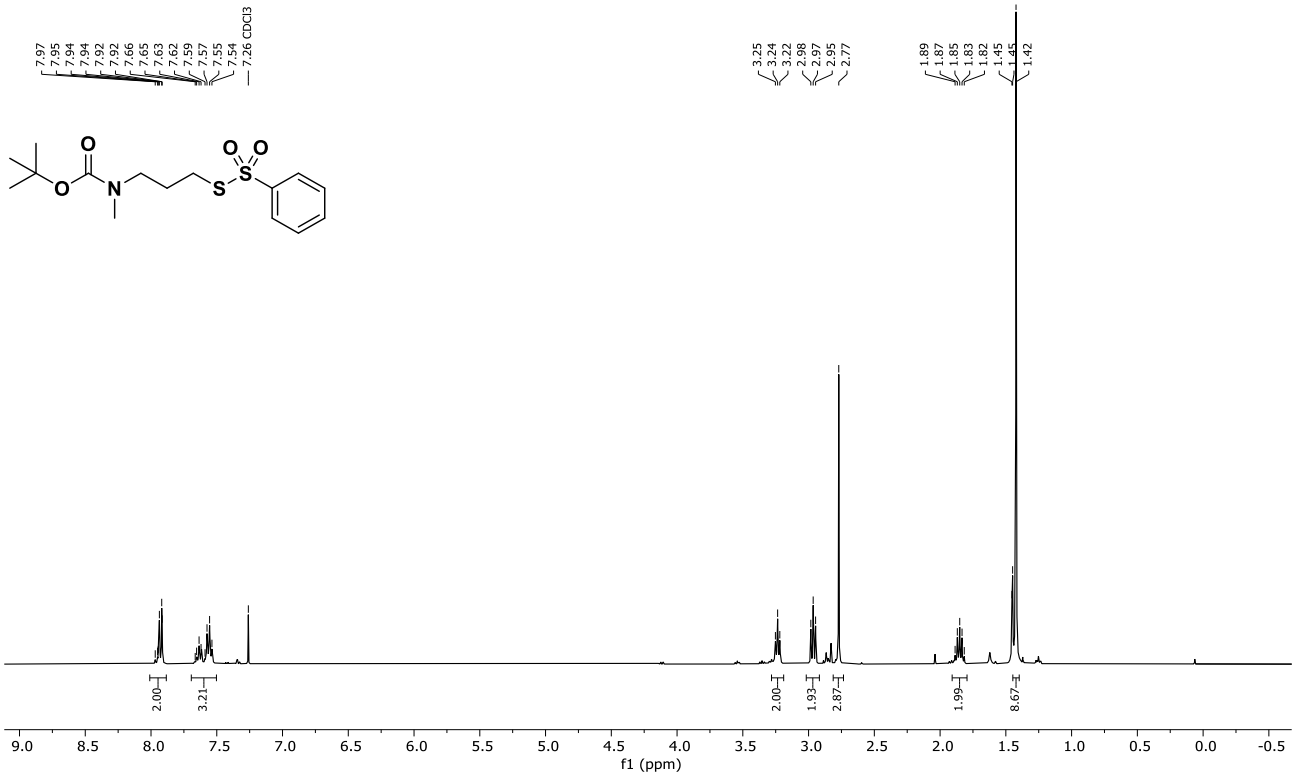

^{1}H NMR (400 MHz, $CDCl_3$) of **S4** (crude)

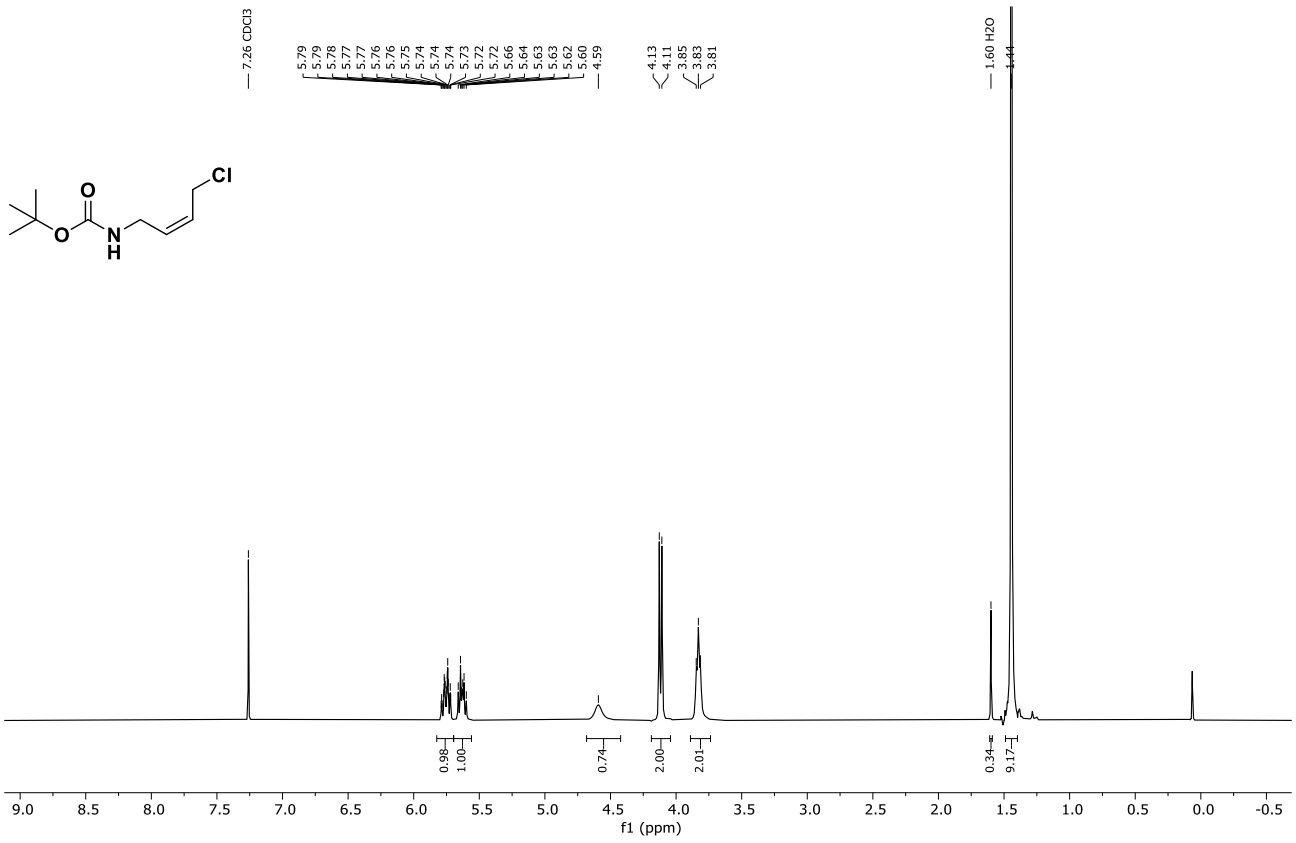

^{1}H NMR (400 MHz, $CDCl_3$) of **S5**

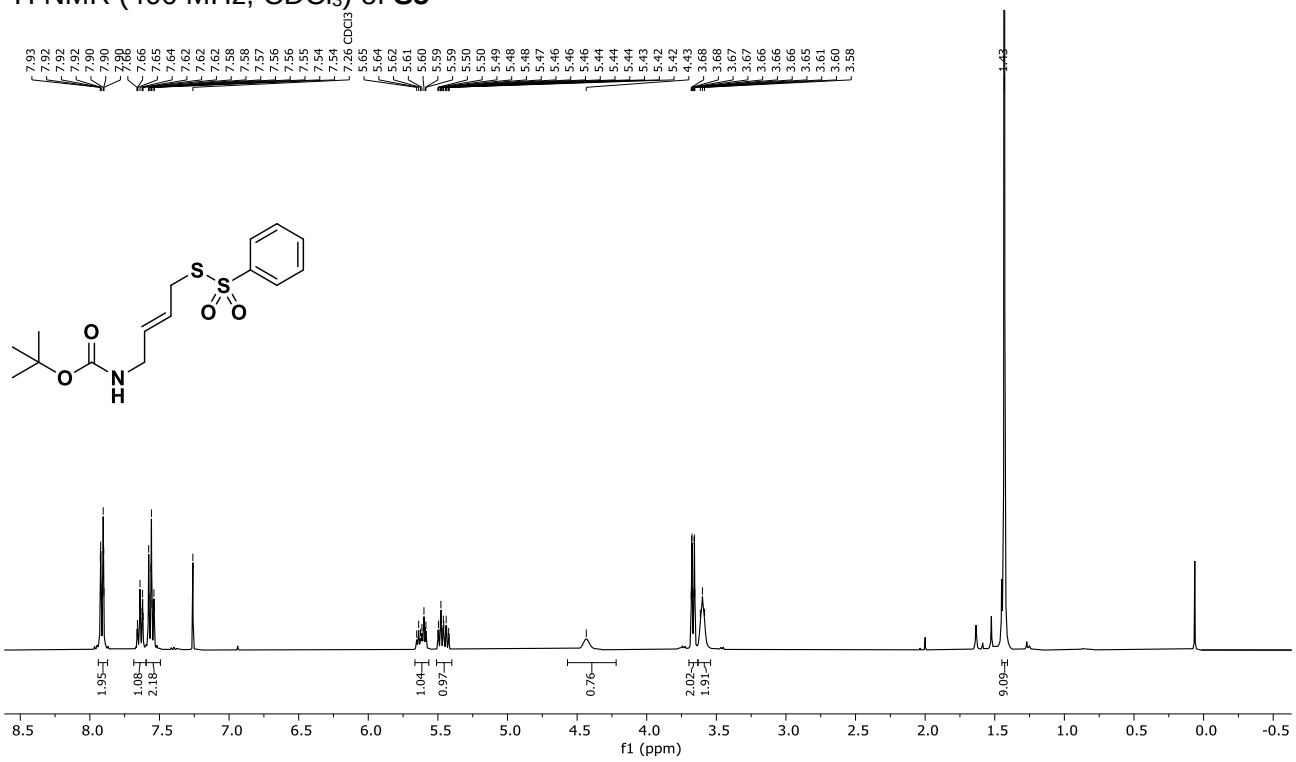

^{1}H NMR (400 MHz, $CDCl_3$) of **S6** (crude)

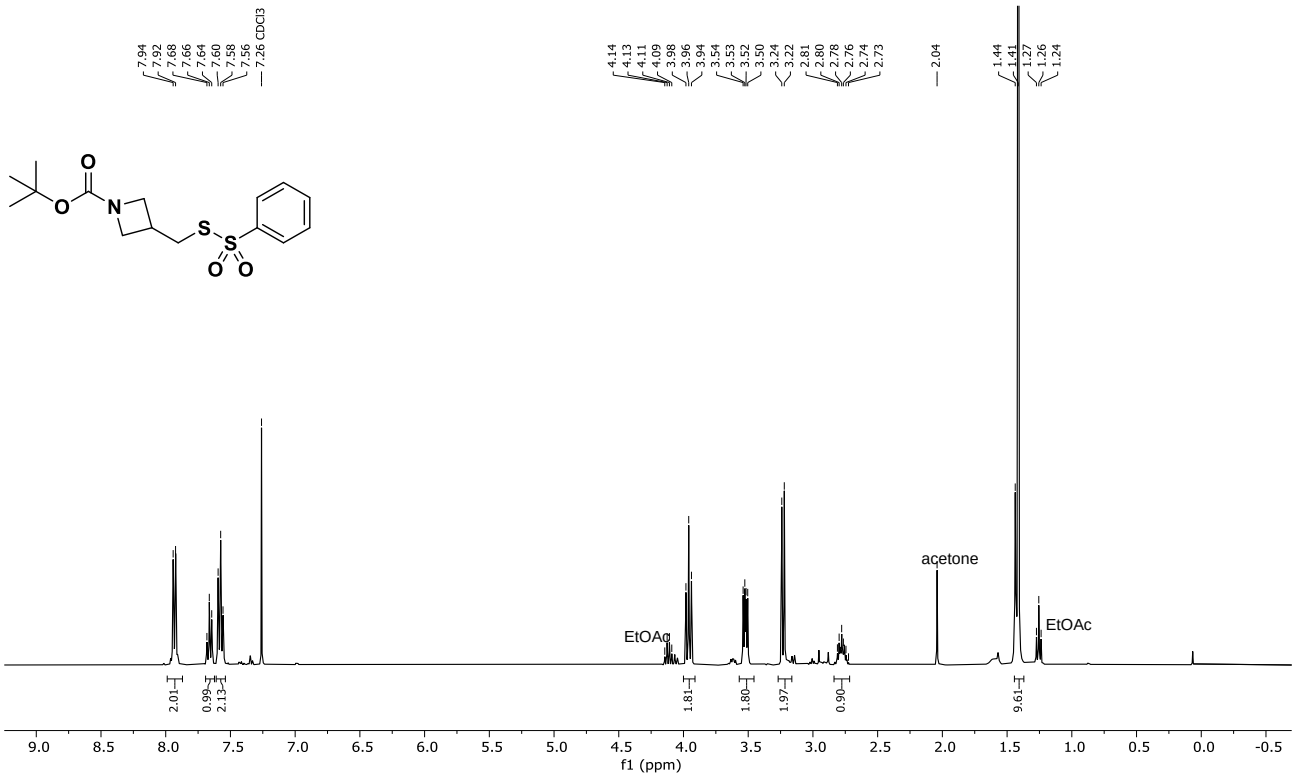

^{1}H NMR (400 MHz, $CDCl_3$) of **S7**

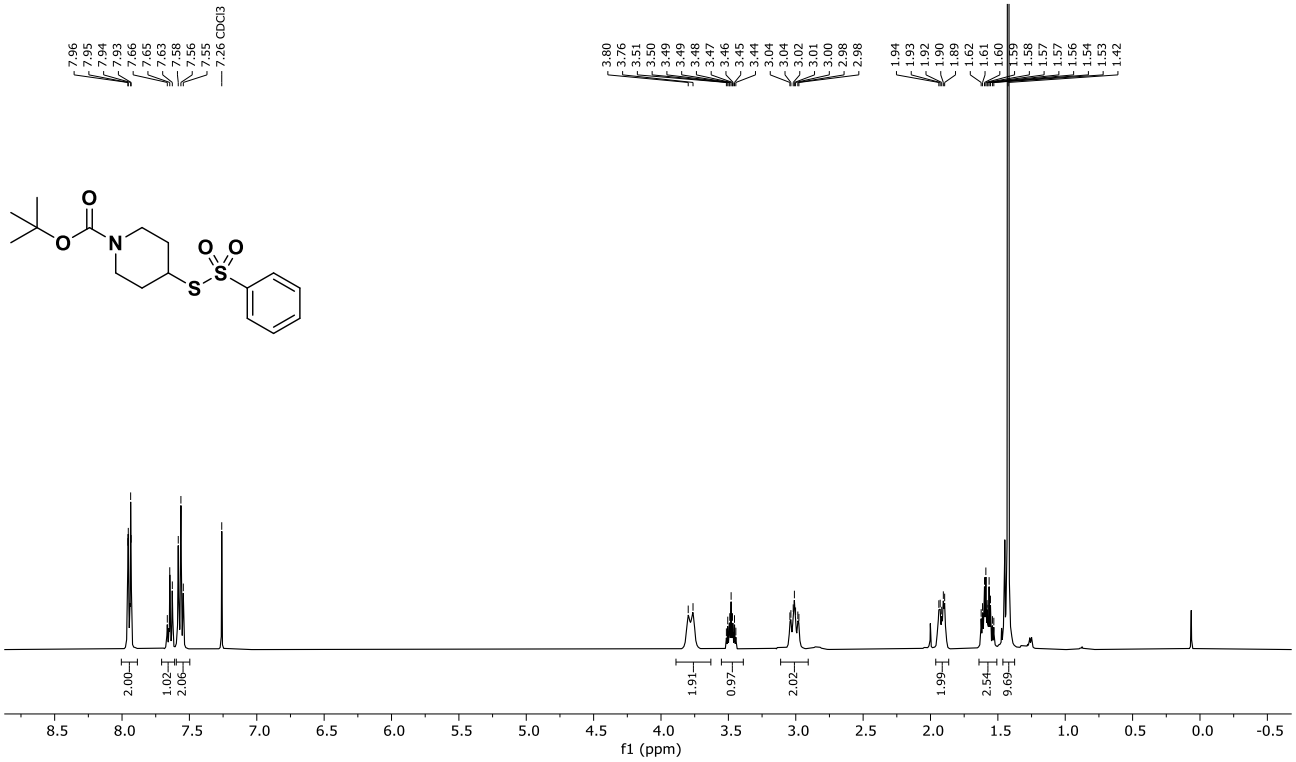

^{1}H NMR (400 MHz, $CDCl_3$) of **S8** (crude)

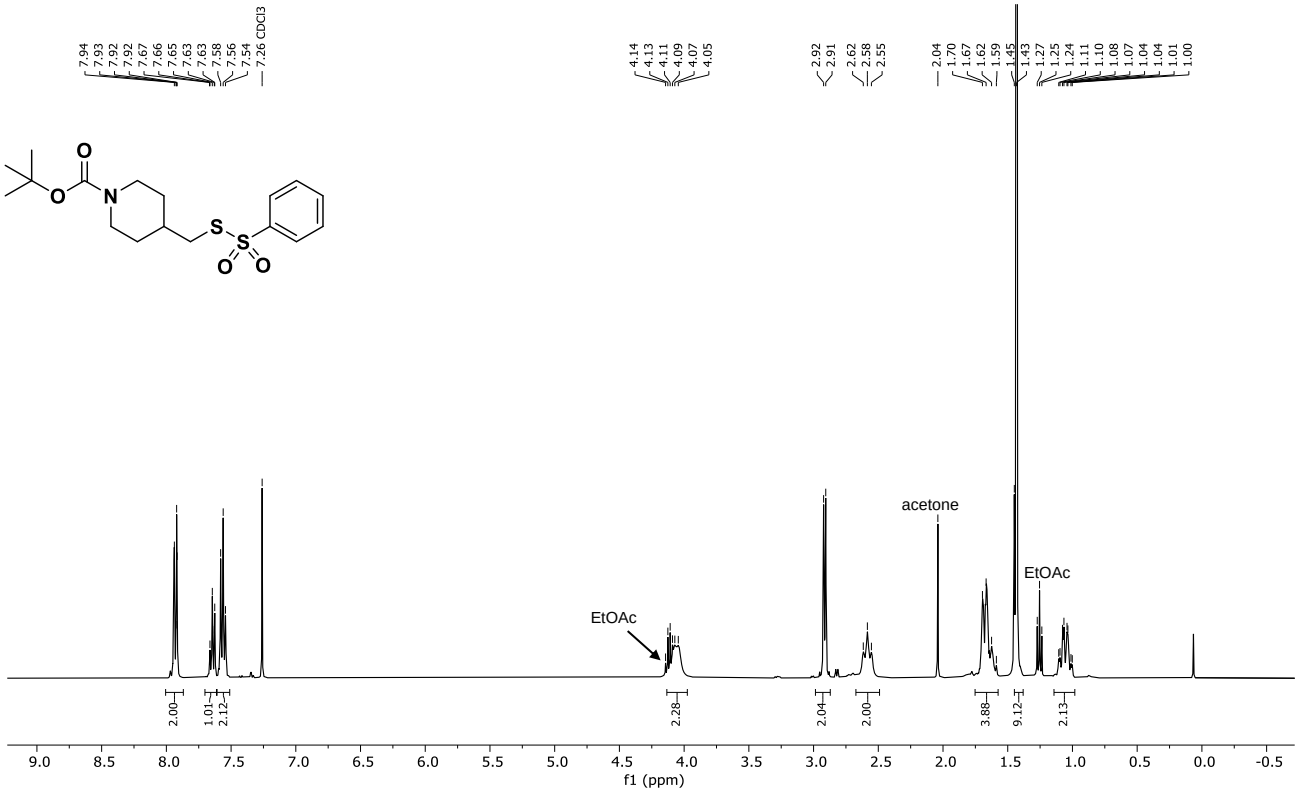

^{1}H NMR (400 MHz, DMSO-d_6) of **Fmoc-Thio-OH**

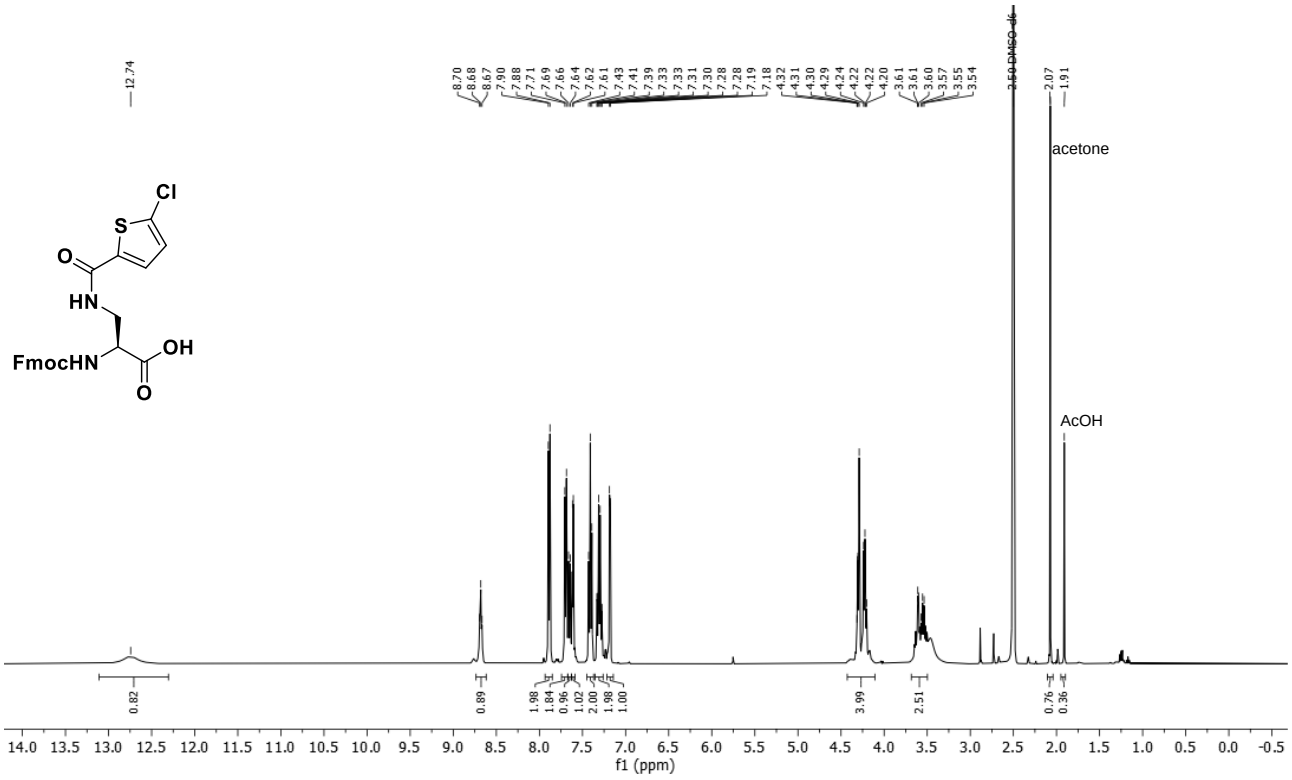

^{13}C NMR (101 MHz, DMSO) of **Fmoc-Thio-OH**